UNIVERSIDAD NACIONAL AUTÓNOMA DE MEXICO

DOCTORADO EN CIENCIAS (FÍSICA)

SHAPES IN QUANTUM MECHANICS

TESIS
QUE PARA OPTAR POR EL GRADO DE:
DOCTOR EN CIENCIAS (FÍSICA)

PRESENTA:
EDUARDO SERRANO ENSÁSTIGA

TUTOR PRINCIPAL
DR. CHRYSSOMALIS CHRYSSOMALAKOS
INSTITUTO DE CIENCIAS NULEARES, UNAM

MIEMBROS DEL COMITÉ TUTOR
DR. DANIEL EDUARDO SUDARSKY SAIONZ
INSTITUTO DE CIENCIAS NUCLEARES, UNAM

DR. PABLO BARBERIS BLOSTEIN
INSTITUTO DE INVESTIGACIONES MATEMÁTICAS APLICADAS
Y EN SISTEMAS, UNAM

CIUDAD DE MÉXICO, MARZO DE 2018

Contents

Abstract

Shapes in Quantum Mechanics is the joint of the two research lines we (my advisor, colleagues and I) work in my PhD studies' period, where the common concept is the *shape* of an object. In the first part of the text, we deal with the shape of a n-body quantum system, its evolution and its consequences on the orientational degrees of freedom. We give the analogy of the classical behavior with coherent states and another purely quantum examples in the three body and four body system. How is it seen the landing of a free falling quantum cat? What if the shape of the cat is in a quantum superposition? What can one expect of an evolution with the less "coherent" shape, an anticoherent shape state? Can we prepare the shape quantum state of a system for a desired orientational behavior? This kind of questions are explored.

The second part of our work is the study of the shape of spin-s states in the projective Hilbert space $\mathbb{P}$. The Majorana stellar representation helps us to associate a physical "shape". More over, it is useful to discover additional information hidden in the usual way to express a spin state. In particular, we concentrate the study in the set of the most "classical" spin states, which are the set of the spin coherent states. It has the property that for all spin s, it is a 2-sphere S^2_{SC}. We address several questions regarding this sphere, in particular its possible intersections with complex lines, which is a criterion to know when a state can be written as a superposition of two coherent states. We also find that, like Dali's iconic clocks, S^2_{SC} extends in all possible directions in $\mathbb{P}$, and plot its image, assuming light in $\mathbb{P}$ propagates along Fubini-Study geodesics. In the last part of the text, we generalize the geometric phase formalism given by Mukunda and Simon to the non-abelian case. We find a realization of a robust non-abelian geometric phase using k-planes of spin states which are anticoherent. Having in mind these applications, we define and characterize the Majorana representation for k-planes of spin states.

Resumen

Shapes in Quantum Mechanics es la conjunción de dos líneas de investigación en las que mi tutor, colegas y yo trabajamos durante el periodo de mis estudios de doctorado, en los cuales el concepto común es el de la *forma* de un objeto. En la primera parte del texto, tratamos con la forma de un sistema cuántico de n-cuerpos, su evolución y sus consecuencias sobre los grados de libertad orientacionales. Damos el análogo del comportamiento clásico con estados coherentes y otros ejemplos puramente cuánticos en el sistema de 3 y 4 cuerpos. ¿Cómo se ve el aterrizaje de un gato cuántico en caída libre? ¿Qué ocurre si la forma del gato está en una superposición cuántica? ¿Qué espera uno de una evolución con el estado de formas menos "coherente", un estado de formas anticoherente? Podemos preparar el estado cuántico de formas de un sistema para un particular comportamiento orientacional? Este tipo de preguntas son exploradas.

La segunda parte de nuestro trabajo consiste en el estudio de las formas de los estados de espín en el espacio proyectivo de Hilbert $\mathbb{P}$. La representación de Majorana nos ayuda a asociar una "forma" física. Más aún, es útil para descubrir información adicional escondida en la forma usual de expresar un estado de espín. En particular, concentramos nuestro estudio en el conjunto de los estados más clásicos permitidos, que son el conjunto de los estados de espín coherentes. Este conjunto tiene la propiedad de que para todo espín forman una 2-esfera S^2_{SC}. Proponemos varias preguntas con respecto a esta esfera, en particular sus posibles intersecciones con líneas complejas, el cual es un criterio para saber cuando un estado puede ser escrito como una superposición de dos estados coherentes. También encontramos que, como los endémicos relojes de Dali, S^2_{SC} se extiende en todas las direcciones posibles en $\mathbb{P}$, y graficamos su imagen, asumiendo que la luz en $\mathbb{P}$ se propaga sobre geodésicas de la métrica de Fubini-Study. En la última parte del texto, generalizamos el formalismo de Mukunda y Simon para la fase geométrica a el caso no-abeliano. Exponemos una realización de una fase geométrica no-abeliana usando k-planos de estados de espín que son anticoherentes. Teniendo en mente este tipo de aplicaciones físicas, definimos y caracterizamos la representación de Majorana para k-planos de estados de espín.

Introduction

A system of n isolating point particles has $3n$ coordinates which can be divided in: three for the position of the center of mass, three to the global orientation of the system and $3n-6$ to describe the shape of the system. The last coordinates are related with the vibrational modes in small oscillations. In general, the coordinates of orientation and shape doesn't evolve independently, which is the origin to many phenomena, since the explanation of how a falling cat, or a diver can re-oriented by himself even with null total angular momentum, to the rovibrational spectre of molecules. Our first contact (and for many people interested in control theory) in this branch of physics relying in the free falling cat problem. Free falling cats, relying on their *feline righting reflex*, manage to land on their feet, even if released upside-down, and with zero initial angular momentum — all they need is a minimal distance of about thirty centimeters to the ground, although claims of much shorter distances exist, including the five centimeters reported by Maxwell [22]. The phenomenon is puzzling, as it seems to violate conservation of angular momentum, but a careful analysis, first carried through by Kane and Scher [49], shows that cats don't rotate *despite* angular momentum conservation, but, rather, *because* of it.

The emergence of geometrical methods in the study of the n-body problem, pioneered by Guichardet [39], revived the interest in the falling cat problem, leading to subsequent refinements and extensions [92], including the influential work of Shapere and Wilczek [90], that embedded the subject in mainstream, application-oriented physics. On the more formal front, the culmination came with the *Falling Cat Theorem*, by Montgomery [75], converting this problem to the prototype of a whole class of classical dynamical systems exhibiting anholonomy. The quantum version of this approach has shed a new, bright light on molecular dynamics (see, *e.g.*, [62, 63, 60, 61]) providing far deeper insights than those accessible to the traditional approaches.

For our goals is sufficient to use systems with three and four point like particles, which have been studied before, both in the classical and the quantum case. Of the recent literature, we single out the treatment in [76], as the most relevant to our own, at the classical level, and that of [47], at the quantum level. A much wider body of work exists related to applications to molecular physics. In this case, the presence of an electron cloud around the nuclei, and its adiabatic treatment in the Born-Oppenheimer scheme, gives rise to another gauge structure, distinct from the one mentioned above, which manifests itself in subtle phase effects — see for example [42, 73] and especially [72] for a review.

The scope of possible applications for the N-body problem is actually considerably wider than molecules. The rotovibrational spectra of more complicated systems, like, for example, the ^{12}C nucleus, can be modelled surprisingly well by triangular configurations of α-particles [15, 68] and the ^{16}O nucleus by a tetrahedral α-particle cluster models of nuclei like [16], which are the configuration that we consider. More over, systems atoms-light can be another scenary to observe the phenomena between orientational degrees of freedom and another internal degrees. For instance, it's already known anticoherent states of light can be produced (see [25]), which are states of interest in our work.

Our first aim we consider is to provide a quantum description of the falling, rotating cat, using the above mentioned geometrical approach. Our cat model is oversimplified: we study a triangular, quasi-rigid cat. But the essence of the phenomenon is captured already by such a simple model. In the quantum case, the system will be described by a superposition of states with non-vanishing probability to have every orientation and every shape in general and, to monitor its evolution, we need to use expectation values of physical quantities. In particular, we can imagine more exotic scenarios purely quantum, and some of them are discussed. In the three body quasi rigid model, shape changes can only induce rotations along one axis, and then this do not capture the non-abelian character of $SO(3)$, so the next step in our work is the study of the four body model, around the tetrahedron as a equilibrium configuration. For this case, we will compare two extreme cases: when its shape wavefunction is described by a coherent state and when it is described by an anticoherent one.

Nowadays, scientists have found and synthesized molecules which act like machines [54, 29, 30], *i.e.*, with some degrees of freedom which can be combined to do an specific motion as a translation, rotation, etc. The motion is described in a semi-classical way, because the

molecules and its constituents of the *machines* are still too big to have a purely quantum behavior. However, we are not far away to have this kind of systems as one could think. One may envisage, in a not-so-distant future, the use of the effect studied here in the manipulation, with extreme accuracy, of the orientation of nanostructures. Suitably large molecular populations could be set to vibrate, causing an entire nanostructure containing them to reorient itself. Some experiments with this flavour have been done [31], but only in orientational degrees. We finish the first part of the text engineering a shape state to obtain a desired orientational evolution, where we choose an axial evolution of the orientational wavefunction in the angle-axis representation of $SO(3)$.

In the second part of the text, we consider a system of s spin 1/2 states, where its degrees of freedom can be separated in: three of global orientation, and the rest to the shape of the state. We just consider totally symmetric pure states. In this case the system is equivalent to a spin-s state, with $2s$ degrees of freedom. In the totally symmetric case, each state of spin s, $|\psi\rangle$ is identified one-to-one with $2s$ indistinguishable points (stars) on the unit sphere (constellation), which is called the Majorana stellar representation [66]. With the constellation of a state, its "shape" can be imagined.

Quantum theory's predominantly algebraic beginnings have given way, in the last decades, to an intense interest in its geometric aspects, including the use of the stellar representation [20, 65, 83]. Although quantum dynamics has also benefited by this trend (see, *e.g.*, [5, 89, 6, 19]), it mostly kinematical considerations are the principal object of study being the space of quantum states, particularly in its finite dimensional incarnation. Properties of states, like entanglement, that are deemed essential for quantum information processing, are seen to admit natural characterizations in purely geometrical terms [27, 55, 78, 95, 45, 7, 23, 69, 69, 9], and the gradual assimilation, by the community, of an ever expanding mathematical arsenal (*e.g.*, [74, 43, 44]) promises to shed a new, bright light on familiar, yet not sufficiently understood concepts.

We are interested in the spin coherent (SC) ones [82], which are the "most classical" ones, just like their harmonic oscillator infinite dimensional counterparts, and generalizations thereof. They are characterized by their vanishing entanglement, yet, they have been shown to serve in classifying that same quantity as it pertains to other symmetric states [67]. In paper, a generic spin state can be expanded in a linear combination of appropriate SC states [67, 87], while in the laboratory, it can be reconstructed by a knowledge of corresponding transition

probabilities [3], the relation between these two statements being less trivial than one might assume. SC states have also appeared in the characterization of the polarization of light [17], and, there too, correspond to maximally classical behavior, that has recently been studied also experimentally [18]. Our study revolves around basic questions about the geometry and topology of quantum state space: going beyond the standard folklore, we aim at an intuitive grasp of what "living in quantum state space" might be like. For example, it is an elementary fact that the SC states form a topological 2-sphere, for any value of the spin of the system, but we feel there is much more to know about this, that is simply absent from the literature: assume one stands on a particular state $|\Psi\rangle$ in quantum state space and looks around, using light that travels along geodesics of the natural Fubini-Study (FS) metric — what does one see? Would the SC sphere look like a distant moon in the sky? Would it look spherical? What part of the sky would it cover? How many times would a light ray intersect its surface, assuming transparency? We do not deny that we would pose these questions in any case for the sheer pleasure of finding out the answer, but it is also true that they have direct physical implications: for example, if looking at the "SC moon" from $|\Psi\rangle$ one can see both a front surface and a rear one, this implies that $|\Psi\rangle$ (a lift of $[\Psi]$ in the overlying Hilbert space) can be written as a linear combination of two SC states. This, in turn, implies that an experimentalist, equipped with a magnetic field and a beam of particles in a SC state (and a picture of the SC moon taken from $|\Psi\rangle$!), can split the beam in two, rotate one component with the magnetic field to produce a second SC state, and then reconstruct $|\Psi\rangle$ by recombining the two SC states and rotating the superposition in its final orientation. The same comment holds true in the case the seemingly esoteric statement that there is a certain complex line going through $|\Psi\rangle$ and intersecting the SC sphere in two points, is valid. Formalizing the above discussion, we are led to consider geodesics of the FS metric, and complex lines, that pass through an arbitrary state $|\Psi\rangle$, and study how they intersect the SC sphere, as $|\Psi\rangle$ is moved around the quantum state space. Others before us have explored quantum state space with a similar geometric/visual point a view (see, *e.g.*, [55, 46, 21]) and an extensive treatment of the subject is in [11].

Berry's discovery of geometric phases, and their description as holonomies in a principal bundle [79], fueled a renaissance of the theory that continues to our days, further impulsed by advances in quantum computing. One of the challenges in quantum computing is the implementation of the fundamental logical operators effectively, where some ideas are englobed and

called geometrical and topological quantum computation [98, 33]. In the last chapter of this text, we explained an idea to solve this aim, using a generalization of a non-Abelian geometric phase, inspired by the work of Mukunda and Simon. It is also used a notion of a Majorana representation, but now for k-planes (vectorial subspaces of dimension k) in the spin Hilbert space $\mathbb{P}$. An idea of the association of a polynomial of one variable to a subspace of $\mathbb{P}$ has been formulated and studied in algebraic geometry [88, 28]. However, its application to quantum mechanics, and moreover, the study of the mapping of a k-plane to a constellation, has not been exploited. We give some advantages to these lines and apply the new results to anticoherent subspaces [80] which has not been studied in a *stellar* way before.

The text consists of four chapters. In chapter one, we give the geometrical framework for the n-body problem in its classical and quantum version. To do the calculations as analytically as possible without missing the phenomena we can studied, we use the quasi-rigid approximation. Also, the tensor operators and the Majorana representation are explained in this chapter. In the last section, we give the classes of quantum states that we will used later. In chapter two we explain the three and four body problem with an equilateral triangle and tetrahedron as the equilibrium configuration, respectively. We study the classical case and implement its analogy in the quantum version using coherent states. Then, we explore another examples in the quantum realm, as the superposition of two coherent shape states. We explore the evolution of the orientation wavefunction when the shape is the less coherent one, which is given by an anticoherent state. Finally, we invent a shape state which produce axial evolution in the orientational part of the system.

In the second part of the text, we expose our results in the Hilbert space of spin states. The chapter three is focused in the set of the spin coherent states. First, we review the Majorana representation, which is our main tool. We give the construction of the Hilbert space as a principal fiber bundle, with fiber diffeomorphic to $SO(3)$, and explained how this construction is useful with a first application: the quantum GPS. The last two sections explain algebraic and geometrical properties of the set of the spin coherent states in the Hilbert space $\mathbb{P}$. In the last chapter, we generalize the Majorana representation for k-planes, *i.e.* linear subspaces of dimension k. To obtain this result, we give the notion of coherent k-planes and an inner product between k-planes, inspired in the usual product for lines. We prove several properties of the constellation of a k-plane, and give several examples. A definition of anticoherent subspaces is

given and it is proved that they are useful for a robust non-abelian geometric phase, inspired by the geometric phase of Mukunda and Simon that is explained in the first section.

Part I

Quantum system of n-point particles

Chapter 1

Geometrical formulation of n-body dynamics

The existence of mysterious relations between all these different domains is the most striking and delightful feature of mathematics.

V. I. Arnold

In this chapter, we introduce the mathematical tools for the n-body problem and for the ro-vibrational phenomena. The geometrical formulation of the classical and quantum n-body problem are discussed in sections 1.1 and 1.2, respectively, following the reference [63]. In section 1.3, we explain the quasi-rigid approximation which simplifies our calculations. For the quantum case, the notions of the tensor operators and the Majorana representation will be useful, which are presented in sections 1.4 and 1.5, respectively. Finally, in section 1.6 we present some classes of quantum states which we use in the next chapter.

1.1 The classical description

We consider an isolated deformable body, modeled by n point-like particles, interacting among themselves through a potential V. The configuration space of the body is $\mathscr{C}_{\text{tot}} = \mathbb{R}^{3n}$ and its Lagrangian is given by

$$L_{\text{tot}} = \frac{1}{2}\sum_{\alpha=1}^{n} m_\alpha |\dot{\mathbf{r}}_{s\alpha}|^2 - V(\mathbf{r}_{s,1}, \ldots, \mathbf{r}_{s,n})\,, \tag{1.1}$$

where $\mathbf{r}_{s\alpha} \in \mathbb{R}^3$ is the α-th particle's position vector with respect to a fixed (or space) frame (hence the s sub-index), and m_α its mass ($\alpha = 1, 2, \ldots, n$), while overdots denote time derivatives. The absence of external forces suggests the elimination of the translational degrees of freedom by introducing relative coordinates, *e.g.*, the mass-weighted Jacobi coordinates,

$$\boldsymbol{\rho}_{s\alpha} = \sqrt{\mu_\alpha} \sum_{\beta=1}^{n} T_{\alpha\beta} \mathbf{r}_{s\beta}, \qquad \alpha = 1, \ldots, n-1, \tag{1.2}$$

where the μ_α are reduced masses and T is a transformation matrix such that

$$T_{n\alpha} = \frac{m_\alpha}{M}\,, \quad \sum_{\beta=1}^{n} T_{\alpha\beta} = 0\,, \quad \alpha = 1, \ldots, n-1\,. \tag{1.3}$$

These conditions in T guarantee the separation of the translational degrees of freedom.

With the coordinate transformation (1.2), the kinetic energy of the center of mass separates from the total kinetic energy, and thus the Lagrangian can be written as $L_{\rm tot} = L_{\rm CM} + L$, with

$$L_{\rm CM} = \frac{1}{2} M |\dot{\mathbf{R}}_s|^2\,, \qquad L = \frac{1}{2} \sum_{\alpha=1}^{n-1} |\dot{\boldsymbol{\rho}}_{s\alpha}|^2 - V(\boldsymbol{\rho}_{s,1}, \ldots, \boldsymbol{\rho}_{s,n-1})\,. \tag{1.4}$$

Likewise, in these coordinates it is clear that the total configuration space can be written as $\mathbb{R}^{3n} = \mathbb{R}^3 \times \mathscr{C}$, where $\mathscr{C} = \mathbb{R}^{3n-3}$ is the translation-reduced configuration space, on which $(\boldsymbol{\rho}_{s,1}, \ldots, \boldsymbol{\rho}_{s,n-1})$ are coordinates. The center of mass dynamics is irrelevant for us, then we assume that $\mathbf{R}_s(t=0) = \dot{\mathbf{R}}_s(t=0) = 0$ and refer to $\mathscr{C}$ simply as *the* configuration space. A point in $\mathscr{C}$ is specified once the body's shape and orientation are given. Now, rigid rotations to the whole system leave the potential invariant. This allows us to factorize $\mathscr{C}$ as a principal fiber bundle with fibers diffeomorphic to $SO(3)$ and base space $\mathscr{S} = \mathbb{R}^{3n-3}/SO(3)$. The base space is called the shape space, and its $3n-6$ coordinates q^μ correspond to independent functions on configuration space, invariant under proper rotations, *i.e.*,

$$q^\mu(\boldsymbol{\rho}_{s,1}, \ldots, \boldsymbol{\rho}_{s,n-1}) = q^\mu(\mathsf{Q}\boldsymbol{\rho}_{s,1}, \ldots, \mathsf{Q}\boldsymbol{\rho}_{s,n-1})\,, \quad \text{for all } \mathsf{Q} \in SO(3)\,. \tag{1.5}$$

The functions q^μ, which we will called *shape coordinates*, are scalar quantities in the sense mentioned above. They are built by a combination of dot and cross products between the weighted Jacobi vectors. Defining the body's orientation, on the other hand, requires (i) an orthonormal frame to compare with the space frame, fixed to the body for each shape, given by relations $\boldsymbol{\rho}_\alpha = \boldsymbol{\rho}_\alpha(q^\mu)$, $\alpha = 1, \ldots, n-1$, and (ii) the rotation $\mathsf{R} \in SO(3)$ that maps the above

body frame to the fixed space frame, parametrized, for example, by Euler angles, $\mathsf{R} = \mathsf{R}(\theta^i)$. The quantities referred to the body frame are written without the sub-index s. Fixing a body frame for each shape is a gauge choice (and section Σ in the fiber bundle), that defines the reference orientation as the one where the body and space frames coincide. This fiber bundle is, in general, non-trivial, so that a section cannot be chosen globally, in other words, there is no smooth assignment of a body frame to all shapes.

In terms of these orientation and shape coordinates, (θ^i, q^μ), and a section $\rho_\alpha(q^\mu)$ as above, a point $(\boldsymbol{\rho}_{s,1}, \ldots, \boldsymbol{\rho}_{s,n-1})$ in $\mathscr{C}$ is defined by

$$\boldsymbol{\rho}_{s,\alpha} = \mathsf{R}(\theta^i)\boldsymbol{\rho}_\alpha(q^\mu), \qquad \alpha = 1, \ldots, n-1. \tag{1.6}$$

The above relation expresses the fact that given a shape of the body q^μ, and a reference orientation $\boldsymbol{\rho}_\alpha(q^\mu)$, any configuration of the body, with that shape, can be reached through a unique rotation $\mathsf{R}(\theta^i)$. For the tangent space $T\mathscr{C}$, it will be convenient to use an anholonomic basis, such that the velocity vector $\mathbf{v}$ of the system has components $v^a = (\boldsymbol{\omega}, \dot{q}^\mu)$, where

$$\omega^i = -\frac{1}{2}\epsilon^{ijk}(\mathsf{R}^T \cdot \dot{\mathsf{R}})_{jk} \tag{1.7}$$

is the i-th component of the angular velocity of the body frame w.r.t. the space frame, referred to the body frame. The corresponding basis vectors satisfy the $\mathfrak{so}(3)$ Lie algebra. In the above expression, and in what follows, we employ the Einstein summation convention for repeated indices.

The Lagrangian (1.4) in the new coordinates and velocities $v(\omega, \dot{q}^\mu)$ is

$$L = \frac{1}{2}G_{ab}v^a v^b - V(q)\,, \qquad (G_{ab}) \equiv \begin{pmatrix} \mathsf{M} & \mathsf{M}\mathbf{A}_\nu \\ \mathbf{A}_\nu^T\mathsf{M} & g_{\mu\nu} + \mathbf{A}_\mu \cdot \mathsf{M} \cdot \mathbf{A}_\nu \end{pmatrix}, \tag{1.8}$$

where (G_{ab}) is the metric in configuration space $\mathscr{C}$, defined by the kinetic energy, and

$$\mathsf{M} = \sum_{\alpha=1}^{n-1} \boldsymbol{\rho}_\alpha \otimes \boldsymbol{\rho}_\alpha - |\boldsymbol{\rho}_\alpha|^2\, \mathbb{1}\,, \tag{1.9}$$

$$\mathbf{A}_\mu = \mathsf{M}^{-1}\sum_{\alpha=1}^{n-1} \boldsymbol{\rho}_\alpha \times \frac{\partial \boldsymbol{\rho}_\alpha}{\partial q^\mu}\,, \tag{1.10}$$

$$g_{\mu\nu} = \sum_{\alpha=1}^{n-1} \frac{\partial \boldsymbol{\rho}_\alpha}{\partial q^\mu} \cdot \frac{\partial \boldsymbol{\rho}_\alpha}{\partial q^\nu} - \mathbf{A}_\mu \cdot \mathsf{M} \cdot \mathbf{A}_\nu\,, \tag{1.11}$$

with M the inertia tensor, $\mathbf{A}_\mu$ the (Coriolis) gauge potential and $g_{\mu\nu}$ the metric on shape space $\mathscr{S}$, respectively.

A velocity vector of the form $v^a = (\boldsymbol{\omega}, 0)$ is purely rotational, or *vertical*, since $\dot{q}^\mu = 0$ implies the body's shape is not changing. A complementary notion of horizontality is furnished by decreeing a velocity vector *horizontal* if the corresponding motion of the system has zero total angular momentum. It turns out that horizontal and vertical vectors are orthogonal according to the above metric G_{ab}. In the anholonomic basis introduced earlier, the angular momentum, referred to the body frame, is given by

$$(\mathsf{R})^{-1}\mathbf{L}_s = \mathbf{L} = \mathsf{M} \cdot (\boldsymbol{\omega} + \mathbf{A}_\mu \dot{q}^\mu)\,, \tag{1.12}$$

and thus, vanishing angular momentum implies

$$\boldsymbol{\omega} dt = \hat{\mathbf{n}} d\omega = -\mathbf{A}_\mu dq^\mu\,, \tag{1.13}$$

where $\hat{\mathbf{n}} d\omega$ is an infinitesimal rotation $d\omega$ along the $\hat{\mathbf{n}}$ axis. In this case, the last equation is a connection, and $\mathbf{A}_\mu$ maps infinitesimal changes in shape space to infinitesimal rotations, so that the horizontal lift in $\mathscr{C}$ of a given path $q^\mu(t)$ in shape space has orientational coordinates given by

$$\mathsf{R}(t) = \mathscr{P} \exp\left(-\int_{q_0}^{q(t)} \mathsf{A}_\mu dq^\mu \right), \tag{1.14}$$

where the space and body frames were assumed in coincidence at $t = 0$, $\mathscr{P}\exp$ is the path-ordered exponential (the composition of rotations is non-abelian), and the antisymmetric matrix A_μ is related to the gauge potential via $(\mathsf{A}_\mu)_{ij} = -\epsilon_{ijk} A^k_\mu$. The acquired rotation for a path on the base space is only independent of the gauge if the path is closed. We obtain that the connection has anholonomy with $n \leq 3$ particles, and therefore the horizontal lift produces open curves.

With the gauge potential, it is possible to define an associated curvature 2-form $\mathbf{B}$, called the *Coriolis tensor*, with components given by

$$\mathbf{B}_{\mu\nu} = \partial_\mu \mathbf{A}_\nu - \partial_\nu \mathbf{A}_\mu - \mathbf{A}_\mu \times \mathbf{A}_\nu\,, \tag{1.15}$$

such that a cyclic deformation in shape space, with $\mathbf{L} = 0$, around the infinitesimal parallelogram spanned by the vectors y^μ and z^μ, produces the gauge-covariant infinitesimal rotation generated by $\boldsymbol{\omega} dt = -\mathbf{B}_{\mu\nu} y^\mu z^\nu$. Note that $\mathsf{R} \neq \mathsf{I}$ requires both a non-zero enclosed area by the closed path $q^\mu(t)$ in shape space and $\mathbf{B} \neq 0$ in at least one point of the enclosed area.

The dynamics of the system can also be described by means of the gauge-covariant Hamiltonian

$$H = \frac{1}{2}\,\mathbf{L}\cdot\mathsf{M}\cdot\mathbf{L} + \frac{1}{2}(p_\mu - \mathbf{A}_\mu\cdot\mathbf{L})g^{\mu\nu}(p_\nu - \mathbf{A}_\nu\cdot\mathbf{L}) + V(q)\,, \tag{1.16}$$

where $p_\mu = g_{\mu\nu}\dot{q}^\nu + \mathbf{A}_\mu\cdot\mathbf{L}$ is the momentum conjugate to the shape coordinate q^μ. For $\mathbf{L}=0$, (1.16) shows that the shape and orientation degrees of freedom decouple and one can solve independently for $q^\mu(t)$, plug it into expression (1.14), and obtain the orientation trajectory in $SO(3)$. For the case of $\mathbf{L}\neq 0$, the total rotation acquires time dependent contribution $(\mathsf{M}^{-1}\mathbf{L})dt$ in addition to the obtained by shape deformations.

1.2 Quantum version

In the quantum case, the configuration of the system doesn't have an specific shape and orientation, instead of that the general quantum state will be described by a wavefunction $\Psi(\mathsf{R},q)$ on $\mathscr{C}$ which codifies the probability to find our system in the configuration (R,q) for each point of $\mathscr{C}$[1]. The closed circuit $q^\mu(t)$ in shape space, considered in the classical case, will be replaced by a similar circuit of the expectation value $\langle\Psi|q^\mu|\Psi\rangle$, while the resulting classical rotation at the end of the cycle will correspond to a vertical shift in the support of Ψ. Similarly, the classical condition $\mathbf{L}=0$ will have to be replaced by the vanishing of the expectation value of each of the components of $\mathbf{L}$. In the last case, we can't restrict the study to the state with quantum number $l=0$ because is homogeneous in all the fiber, and then it is impossible to keep track of a rotation of the state. Also, if $\langle\mathbf{L}_s\rangle = 0$, it is not necessary that $\langle\mathbf{L}\rangle$ is zero. This is understood by the fact that the rotation relating the body frame and space frame for each shape $\mathsf{R}(q^\mu)$, is now an operator.

The quantum Hamiltonian is equal to (1.16), with the same ordering, plus an additional potential

$$V_2(q) = \frac{\hbar^2}{2}D^{-1/4}\frac{\partial}{\partial q^\mu}\left(g^{\mu\nu}\frac{\partial D^{1/4}}{\partial q^\nu}\right)\,, \tag{1.17}$$

with $D = (\det\mathsf{M})(\det g_{\mu\nu})$. With the approximations that we will use, $V_2(q)=0$. The hamiltonian H commutes with $\mathbf{L}^2$ and L_{sz}, so its eigenfunctions can be chosen to be simultaneous

[1] In the case that is considered the center of mass degrees of freedom, the wavefunction has the additional factor $\Psi(\mathbf{R})$. For a potential invariant under rotations and translations, the eigenbasis of $\Psi(\mathbf{R})$ are the wave planes.

eigenfunctions of all three operators, with eigenvalues, say, E, l, m, respectively, which we denote by $\psi_{lm}(\mathsf{R}, q)$, suppressing the index E. From the theory of angular momentum, (see, *e.g.*, [58], §58), if we know the wavefunction over a section Σ

$$\chi^l_k(q) = \frac{1}{\sqrt{2l+1}}\psi_{lk}(\mathsf{I}, q)\,, \tag{1.18}$$

we know the whole wavefunction,

$$\psi_{lm}(\mathsf{R}, q) = \sum_{k=-l}^{l} \chi^l_k(q) D^l_{mk}(\mathsf{R})^*\,, \tag{1.19}$$

where $D^l_{km}(\mathsf{R})$ are the Wigner functions corresponding to the $(2l+1)\times(2l+1)$ irreducible matrix representation of $\mathsf{R} \in SO(3)$. In this way, the orientational part of the problem has been taken care of by group theory — substituting the above ψ_{lm} in (1.16), H becomes a $2l$+1-dimensional matrix, with entries depending on the operators q^μ, p_ν, acting on the column vector (χ^l_k), whose components, indexed by k, depend on q. The resulting eigenvalue equation which, with a slight abuse of notation, we write as $H\chi^l_k = E\chi^l_k$, is still a formidable problem to solve, because M, $\mathbf{A}_\mu$, $g_{\mu\nu}$, V, are all, in general, complicated functions of the q's. However, for our purposes it is unnecessary to solve the eigenvalue equation exactly, instead, we will consider some approximations.

1.3 Quasi-rigid approximation

We imagine now that the interaction potential V is due to elastic, but stiff, rods, that connect the n point masses. At their equilibrium length, the rods give the body the shape q_0, which we assume non-collinear and the body can have small deformations around q_0, $q^\mu = q^\mu_0 + \lambda x^\mu$, with λ a small dimensionless parameter. Expanding the potential V around q_0, we obtain a system of coupled harmonic oscillators, small vibrations of which will provide the cyclic shape change we seek. So far the shape coordinates q^μ have been taken arbitrary, but we now have enough motivation to choose them in a very special way: first, the directions $\partial_\mu \equiv \partial/\partial q^\mu$ will be taken to be those of the normal modes of the system, so that the expansion of V around q_0 is diagonalized,

$$V(q) = \frac{1}{2}\sum_{\mu=1}^{3n-6} \frac{\omega^2_{(\mu)}}{\lambda^2} x_\mu x^\mu\,, \tag{1.20}$$

where we have assumed that $V(q_0) = 0$ and that $\partial^2_\mu V = \omega^2_{(\mu)}/\lambda^4$. This latter assumption simply means that we chose the scale of the masses of the particles so that the resulting oscillation frequencies are of order λ^{-2}. Having fixed the directions ∂_μ, we now extend the q-lines (or, what is the same, the x-lines) so that they be geodesics of the $\mathscr{S}$-metric $g_{\mu\nu}$, obtaining Riemann normal coordinates on $\mathscr{S}$. This latter property of the coordinates guarantees that no linear terms appear in the expansion of the metric around q_0,

$$g_{\mu\nu}(x) = \delta_{\mu\nu} + \frac{1}{3}\lambda^2 R_{\mu\alpha\beta\nu}(0)x^\alpha x^\beta + O(\lambda^3)\,, \tag{1.21}$$

where the zeroth order term was made equal to the unit matrix by suitable normalization of the q's. Expression (1.21) implies that the corresponding Christoffel symbols satisfy $\Gamma^\alpha_{\mu\nu}x^\mu x^\nu = \mathscr{O}(\lambda^2)$.

There is one final simplifying choice we can make, related with the gauge potential $\mathbf{A}_\mu$. We opt for the Poincaré (or, transversal) gauge, centered at q_0, so that

$$\mathbf{A}_\mu(x) = \frac{\lambda}{2}\mathbf{B}_{\mu\alpha}(0)x^\alpha + O(\lambda^2)\,, \tag{1.22}$$

which, on the one hand, makes $\mathbf{A}_\mu(0)$ equal to zero, and, on the other, expresses H in terms of the gauge-covariant tensor $\mathbf{B}$. The above expression for $\mathbf{A}$ in terms of $\mathbf{B}$ can be obtained by applying the Poincaré homotopy operator, appropriately generalized to the non-abelian case [41]. In geometrical terms, the corresponding section Σ is the horizontal lift of radial lines, in the coordinates used, emerging from the equilibrium configuration. When the coordinates are Riemann normal coordinates, as above, the section is flat, and the corresponding choice of body frame is that of Eckart [64].

Finally, we rescale various quantities according to

$$p_\mu \to p_\mu/\lambda\,, \quad H \to \lambda^2 H\,, \quad \mathsf{M} \to \lambda^2\mathsf{M}\,, \quad \mathbf{A}_\mu \to \lambda\mathbf{A}_\mu\,, \quad \mathbf{L} \to \mathbf{L}\,, \tag{1.23}$$

and express $R_{\mu\alpha\beta\nu}$ in terms of $\mathbf{B}_{\mu\nu}$,

$$2R_{\mu\nu\sigma\tau} = \mathbf{B}_{\mu\nu}\cdot\mathsf{M}\cdot\mathbf{B}_{\sigma\tau} + \mathbf{B}_{\mu[\tau}\cdot\mathsf{M}\cdot\mathbf{B}_{\sigma]\nu}\,, \tag{1.24}$$

(*cf.* relation (5.61) from [63]), so that H can be expanded as

$$H = \frac{1}{2}\left(\sum_{\mu=1}^{3n-6} p^\mu p_\mu + \omega^2_{(\mu)}x^\mu x_\mu\right) + \frac{1}{2}\lambda^2(\mathbf{L}-\mathbf{S})\cdot\mathsf{M}^{-1}\cdot(\mathbf{L}-\mathbf{S})\,. \tag{1.25}$$

The metric $g_{\mu\nu}$ implicit in the above expression, as well as M^{-1}, are both evaluated at q_0 (and then numerical quantities), and we have introduced the "internal angular momentum" $\mathbf{S}$, and the "shape angular momentum" S,

$$\mathbf{S} = \frac{1}{4}\mathsf{M}\cdot\mathbf{B}_{\mu\nu}S^{\mu\nu}, \qquad S^{\mu\nu} = x^\mu p^\nu - x^\nu p^\mu\,, \tag{1.26}$$

with $\mathbf{B}_{\mu\nu}$ also evaluated at q_0. The shape and orientation degrees of freedom are only coupled by the cross terms, proportional to $\mathbf{L}\cdot\mathsf{M}^{-1}\cdot\mathbf{S}$ and $\mathbf{S}\cdot\mathsf{M}^{-1}\cdot\mathbf{L}$ in (1.25), which can be interpreted as infinitesimal rotations about the unit vector $\widehat{\mathsf{M}^{-1}\cdot\mathbf{S}}$ by an angle $|\mathsf{M}^{-1}\cdot\mathbf{S}|$, both of the latter quantities being operators in shape space. Spite of that the Hamiltonian (1.25) is valid upto second order of λ, there are systems and models where it is indeed the exact one (for instance, see [16], [68]), and therefore we will consider it exact. We are sure that our results are also observed in more general Hamiltonians, in a more complex manner.

1.3.1 The commutation relations of $[\mathbf{S}_i, \mathbf{S}_j]$

In this subsection, we prove that the vector $\mathbf{S}$ is indeed an angular momentum operator. We start calculating the commutator between the components of $S^{\mu\nu}$,

$$\begin{aligned}
[S^{\mu\nu}, S^{\alpha\beta}] &= [q_\mu p_\nu, q_\alpha p_\beta] - [q_\nu p_\mu, q_\alpha p_\beta] - [q_\mu p_\nu, q_\beta p_\alpha] + [q_\nu p_\mu, q_\beta p_\alpha] \\
&= i\,(q_\alpha p_\nu \delta_{\mu\beta} - q_\mu p_\beta \delta_{\nu\alpha} \\
&\quad + q_\nu p_\beta \delta_{\alpha\mu} - q_\alpha p_\mu \delta_{\beta\nu} \\
&\quad + q_\mu p_\alpha \delta_{\beta\nu} - q_\beta p_\nu \delta_{\alpha\mu} \\
&\quad + q_\beta p_\mu \delta_{\nu\alpha} - q_\nu p_\alpha \delta_{\mu\beta}) \\
&= i\left(S^{\alpha\nu}\delta_{\mu\beta} + S^{\beta\mu}\delta_{\nu\alpha} + S^{\nu\beta}\delta_{\alpha\mu} + S^{\mu\alpha}\delta_{\beta\nu}\right)\,.
\end{aligned} \tag{1.27}$$

And then,

$$\begin{aligned}
[S_i, S_j] &= \left[\tfrac{1}{4}(\mathsf{M}\mathbf{B}_{\mu\nu})_i S^{\mu\nu}, \tfrac{1}{4}(\mathsf{M}\mathbf{B}_{\alpha\beta})_j S^{\alpha\beta}\right] \\
&= \left(\tfrac{1}{4}\right)^2 (\mathsf{M}\mathbf{B}_{\mu\nu})_i (\mathsf{M}\mathbf{B}_{\alpha\beta})_j \left[S^{\mu\nu}, S^{\alpha\beta}\right] \\
&= \tfrac{i}{16}(\mathsf{M}\mathbf{B}_{\mu\nu})_i (\mathsf{M}\mathbf{B}_{\alpha\beta})_j \left(S^{\alpha\nu}\delta_{\mu\beta} + S^{\beta\mu}\delta_{\nu\alpha} + S^{\nu\beta}\delta_{\alpha\mu} + S^{\mu\alpha}\delta_{\beta\nu}\right) \\
&= \tfrac{i}{8}\left[(M\mathbf{B}_{\mu\alpha})_i (\mathsf{M}\mathbf{B}_{\mu\beta})_j - (M\mathbf{B}_{\mu\alpha})_j (\mathsf{M}\mathbf{B}_{\mu\beta})_i\right] S^{\alpha\beta}\,.
\end{aligned} \tag{1.28}$$

The factor of $S^{\alpha\beta}$ is only shape dependent $\{q^\mu\}$, then we can use the classical results to calculate this part. We begin with one identity of the eq.(5.61) of [63], given by the calculation

of one Riemann tensor's component in the configuration space

$$0 = \frac{1}{4}(\mathsf{M}_{;\alpha}\mathsf{M}^{-1}\mathsf{M}_{;\beta})_{ij} - \frac{1}{4}(\mathsf{M}_{;\beta}\mathsf{M}^{-1}\mathsf{M}_{;\alpha})_{ij} + \frac{1}{2}\epsilon_{ijk}(\mathsf{M}\mathbf{B}_{\alpha\beta})_k + \frac{1}{4}\left[(\mathsf{M}\mathbf{B}_{\mu\alpha})_i(\mathsf{M}\mathbf{B}^{\mu}{}_{\beta})_j - (\mathsf{M}\mathbf{B}_{\mu\beta})_i(\mathsf{M}\mathbf{B}^{\mu}{}_{\alpha})_j\right], \tag{1.29}$$

where

$$\mathsf{M}_{;\mu} = \mathsf{M}_{,\mu} - [\mathsf{A}_\mu, \mathsf{M}], \tag{1.30}$$

is the covariant derivative of M, $\mathsf{M}_{,\mu}$ the ordinary derivative, and A_μ is the antisymmetric matrix associated to $\mathbf{A}_\mu$. Taking M, $g_{\mu\nu}$ and A_μ, evaluated in the configuration equilibrium, the inertia tensor and the metric are constants, and A_μ is zero. Therefore $\mathsf{M}_{;\mu} = 0$, $\mathsf{M}\mathbf{B}^{\mu}{}_{\alpha} = \mathsf{M}\mathbf{B}_{\mu\alpha}$ and

$$[(\mathsf{M}\mathbf{B}_{\mu\alpha})_i(\mathsf{M}\mathbf{B}_{\mu\beta})_j - (\mathsf{M}\mathbf{B}_{\mu\beta})_i(\mathsf{M}\mathbf{B}_{\mu\alpha})_j] = -2\epsilon_{ijk}(\mathsf{M}\mathbf{B}_{\alpha\beta})_k\,. \tag{1.31}$$

And finally, eq. (1.28) is equal to

$$[S_i, S_j] == -\frac{i}{4}\epsilon_{ijk}(\mathsf{M}\mathbf{B}_{\alpha\beta})_k S^{\alpha\beta} = -i\epsilon_{ijk}S_k\,, \tag{1.32}$$

which are the commutation relations for an angular momentum operator in the body frame.

1.4 Tensor operators

Let us consider the Hilbert space generated by spin-s states. A *tensor (multipolar) operator* of range σ [1, 14, 36] consists of elements of an irreducible set of linear operators $\{T_{\sigma\mu} : \mu = \sigma, \sigma-1, \ldots, -\sigma\}$ transforming under the action of $SU(2)$ according to the σ irreducible matrix representation $R^{(\sigma)}(g)$,

$$\begin{aligned} R(g)T_{\sigma\mu}R(g)^{-1} &= \sum_{\mu'=-\sigma}^{\sigma} R^{(\sigma)}(g)_{\mu'\mu}T_{\sigma\mu'}\,, \\ R(g)T^{\dagger}_{\sigma\mu}R(g)^{-1} &= \sum_{\mu'=-\sigma}^{\sigma} R^{(\sigma)}(g)^{-1}_{\mu\mu'}T^{\dagger}_{\sigma\mu'}\,. \end{aligned} \tag{1.33}$$

Under infinitesimal rotations, the transformation laws are

$$\begin{aligned} [S_+, T_{\sigma\mu}] &= [(\sigma-\mu)(\sigma+\mu+1)]^{1/2}T_{\sigma,\mu+1}\,, \\ [S_-, T_{\sigma\mu}] &= [(\sigma+\mu)(\sigma-\mu+1)]^{1/2}T_{\sigma,\mu-1}\,, \\ [S_3, T_{\sigma\mu}] &= \mu T_{\sigma\mu}\,. \end{aligned} \tag{1.34}$$

The explicit expression of $T_{\sigma\mu}$ can be given in terms of the 3j-symbols or the Clebsh-Gordan coefficients,

$$T_{\sigma\mu} = \sqrt{2\sigma+1}\sum_{m,m'}(-1)^{s-m}\begin{pmatrix} s & \sigma & s \\ -m & \mu & m' \end{pmatrix}|s^m\rangle\langle s^{m'}| = \sqrt{\frac{2\sigma+1}{2s+1}}\sum_{m,m'}C^{sm'}_{sm\sigma\mu}|s^m\rangle\langle s^{m'}|\,. \tag{1.35}$$

From the latter expression, it is easy to deduce $0 \leq \sigma \leq 2s$, and the following properties of $T_{\sigma\mu}$:

$$\mathrm{Tr}(T^\dagger_{\sigma_1\mu_1}T_{\sigma_2\mu_2}) = \delta_{\sigma_1\sigma_2}\delta_{\mu_1\mu_2}\,, \quad T^\dagger_{\sigma\mu} = (-1)^\mu T_{\sigma,-\mu}\,. \tag{1.36}$$

The set $\{T_{\sigma\mu} : 0 \leq \sigma \leq 2s,\, -\sigma \leq \mu \leq \sigma\}$ is an orthogonal basis for the $(2s+1)\times(2s+1)$ matrices with the property (1.33). In other words, the $T_{\sigma\mu}$ are the matrix analogs of the spherical harmonic functions $Y_{lm}(\theta,\,\phi)$, which span the space of real functions valued on the sphere $f(\theta,\phi)$. We write the expressions of $T_{\sigma\mu}$, for small values of σ, in terms of the components of the operator $\mathbf{S}$,

$$T_{10} = \left(\frac{3}{s(s+1)(2s+1)}\right)^{1/2}S_3\,, \quad T_{1,\pm1} = \pm\left(\frac{3}{2s(s+1)(2s+1)}\right)^{1/2}S_\pm\,, \tag{1.37}$$

$$T_{20} = \left(\frac{5}{(2s+3)(s+1)(2s+1)(2s-1)}\right)^{1/2}(3S_3^2 - \mathbf{S}^2)\,. \tag{1.38}$$

The operators $T_{\sigma\mu}$ can be obtained recursively from the top component $T_{\sigma\sigma}$ the operator S_-

$$T_{\sigma\mu} = \left[\frac{(\sigma+\mu)!}{(2\sigma)!(\sigma-\mu)!}\right]^{1/2}[S_-, T_{\sigma\sigma}]_{\sigma-\mu}\,. \tag{1.39}$$

Furthermore, by (1.34), $T_{\sigma\sigma}$ must be proportional to the product of σ times S_+, and $T_{\sigma\mu}$ can be written as a linear combination of operators of the form $S_{a_1}S_{a_2}\ldots S_{a_\sigma}$, where S_{a_i} is a component of $\mathbf{S}$. This result allows us to define a *parity* property for $T_{\sigma\mu}$; with the transformation $\mathbf{S}\to-\mathbf{S}$, $T_{\sigma\mu}$ is mapping to $(-1)^\sigma T_{\sigma\mu}$.

Scalar operators under rotations have well defined expansions in terms of tensor operators. For our problem, we are interested in two types of them, $(\hat{\mathbf{n}}\cdot\mathbf{S})^k$ and $(\mathbf{L}\cdot\mathbf{S})^k$, for an arbitrary value of k, where $\hat{\mathbf{n}}$ is the unit vector in direction (θ,ϕ), and $\mathbf{B}$ and $\mathbf{S}$ are angular momentum operators of spin b and s, respectively. Their expansions must be of the form

$$(\hat{\mathbf{n}}\cdot\mathbf{S})^k = \sum_{\sigma=0}^{2s}A^{(k)}_\sigma(s)\sum_{\mu=-\sigma}^{\sigma}Y^*_{\sigma\mu}(\theta,\,\phi)T^{(s)}_{\sigma\mu}\,, \tag{1.40}$$

$$(\mathbf{B}\cdot\mathbf{S})^k = \sum_{\sigma=0}^{2j}\alpha^{(k)}_\sigma(b,s)\sum_{\mu=-\sigma}^{\sigma}T^{(b)\dagger}_{\sigma\mu}\otimes T^{(s)}_{\sigma\mu}\,, \tag{1.41}$$

where $j = \min(b, s)$, $A_\sigma^{(k)}(s)$ and $\alpha_\sigma^{(k)}(b, s)$ depends only of s and b. In the appendix C we deduce recursive expressions for these constants and include a closed formula to calculate $A_\sigma^{(k)}$ found in [25].

1.5 Majorana Representation

In a relatively little known 1932 paper [66], E. Majorana showed how to characterize, up to an overall phase, a normalized spin-s state $|\Psi\rangle$ by a set of $2s$ points (*stars*) on the unit sphere, the latter known as the *Majorana constellation* corresponding to $|\Psi\rangle$. The construction generalizes the well known characterization of a spin-1/2 state, up to phase, by a single point on the Bloch sphere. The precise statement is that points in the projective Hilbert space $\mathbb{P} = \mathbb{C}P^N$ of a spin-s system ($N \equiv 2s$) are in one-to-one correspondence with unordered sets of (possibly coincident) $2s$ points on the unit sphere. Here we explain the original construction of the Majorana constellation. There are additional ways to understand this construction, another more intuitive that we will expose in the second part of the thesis. In this part, it is only used as a mathematical tool to observe rotations in simple quantum states.

Given an arbitrary spin-s state, expressed in the S_z-eigenbasis,

$$|\Psi\rangle = \sum_{m=-s}^{s} c_m |s, m\rangle \,, \tag{1.42}$$

we associate to it its *Majorana polynomial* $p_{|\Psi\rangle}(\zeta)$,

$$p_{|\Psi\rangle}(\zeta) = \sum_{m=-s}^{s} (-1)^{s-m} \sqrt{\binom{2s}{s-m}} c_m \, \zeta^{s+m} \,, \tag{1.43}$$

where ζ is an auxiliary complex variable. The N roots $\zeta_i \in \mathbb{C}$, $i = 1, \ldots, N$, of $p_{|\Psi\rangle}$ can be mapped to N points $\hat{\mathbf{n}}_i$ on the 2-sphere via stereographic projection from the south pole. The resulting constellation, made up of the N stars, is the *stellar representation* of the state $|\Psi\rangle$. If the polynomial turns out of a lower degree, *i.e.*, if $c_m = 0$ for $m = s, s-1, \ldots, s-k$, then $\zeta = \infty$ is considered a root of multiplicity $k+1$, resulting in the appearance of $k+1$ stars at the south pole of S^2. The particular choice of coefficients in (1.43) results in that a transformation $D(\mathsf{R})$ of $|\Psi\rangle$ in Hilbert space, where $D(\mathsf{R})$ is the spin-s irreducible representation of $\mathsf{R} \in SU(2)$, corresponds to a rotation R of the corresponding constellation on S^2 (see figure 1.1). In the next section we plot the constellation of several states.

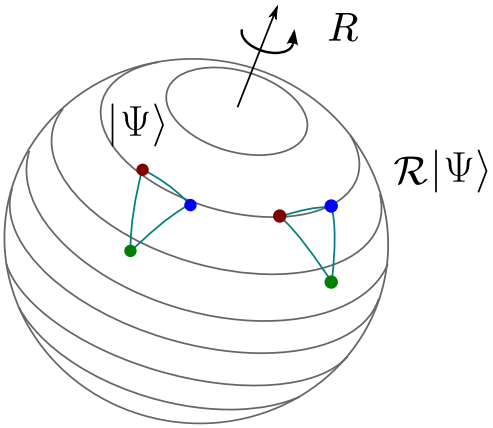

Figure 1.1: A rotation $D(\mathsf{R})$ of state $|\psi\rangle$ corresponds to a rotation R of its constellation.

1.6 Some quantum states classes

In the thesis, we will mostly use three types of states: the canonical coherent states, the spin coherent states and the anticoherent states. In the second part of the thesis, the spin coherent states are extensively studied. To this part, we use the references [35, 82, 48].

1.6.1 Canonical coherent states

We start with a brief description of the canonical coherent states generated by the annihilation and creation operators a and $a^\dagger$. The canonical coherent states are defined, for each complex number $z \in \mathbb{C}$, by a unitary transformation of the vacuum state,

$$|z\rangle = D(z)|0\rangle = e^{za^\dagger - \bar{z}a}|0\rangle = e^{-|z|/2}\sum_{n=0}^{\infty}\frac{1}{\sqrt{n!}}z^n|n\rangle\,, \tag{1.44}$$

with $|n\rangle$ the eigenstate of the number operator $N|n\rangle = n|n\rangle$ and D the displacement operator. These states are eigenvectors of the annihilation operator (it is proved with the latter equation)

$$a|z\rangle = z|z\rangle\,. \tag{1.45}$$

Between the properties of the canonical coherent states are the following: Two coherent states are never orthogonal,

$$\langle z_1|z_2\rangle = e^{-\frac{1}{2}\left(|z_1|^2+|z_2|^2\right)+z_1\bar{z}_2}\,. \tag{1.46}$$

There exists a resolution of the identity with the coherent states

$$\pi^{-1}\int |z\rangle\langle z| d^2z = \mathsf{I}\,, \tag{1.47}$$

Finally, they are the most localized states in some point of the phase space. They minimize the uncertainty relation with isotropic dispersion $\Delta x = \Delta p = 1/\sqrt{2}$.

In the next chapter, we will consider coherent states in at most a 3-dimensional space, then they will be labeled with three complex numbers $\vec{\alpha} = (\alpha_1, \alpha_2, \alpha_3)$, and its wavefunction $\psi(x) = \psi_{\vec{\alpha}}(x_1, x_2, x_3)$ will be given by

$$\psi_{\vec{\alpha}}(x_1, x_2, x_3) = \langle x_1\,, x_2\,, x_3|D_1(\alpha_1)D_2(\alpha_2)D_3(\alpha_3)|0\,, 0\,, 0\rangle = \frac{1}{\pi^{3/4}}\prod_{i=1}^{3} e^{-\frac{1}{2}(x_i - \langle x_i\rangle)^2} e^{i\langle p_i\rangle(x_i - \frac{1}{2}\langle x_i\rangle)}\,, \tag{1.48}$$

with $D_i(\alpha)$ the displacement operator associated of the i-th coordinate. The expectation values of the position and momentum are

$$\langle \vec{x}\rangle = \sqrt{2}\mathrm{Re}(\vec{\alpha})\,, \qquad \langle \vec{p}\rangle = \sqrt{2}\mathrm{Im}(\vec{\alpha})\,. \tag{1.49}$$

The state (1.48) has an expectation value of the angular momentum operator $\langle \mathbf{L}\rangle = 2\mathrm{Re}(\vec{\alpha}) \times \mathrm{Im}(\vec{\alpha})$.

1.6.2 Spin coherent states

The spin coherent states (also called Bloch coherent states) are similar to the canonical coherent states, but now their definition uses the angular momentum operators. Let us consider a spin state with spin s and the eigenstates of S_z, $S_z|s, m\rangle = m|s, m\rangle$ for $m = -s, -s+1, \ldots, s$. The set of the spin coherent states is the orbit of the eigenstate of maximal projection, $\mathsf{R}|s, s\rangle$ under the action of the rotation $SO(3)$ group. We characterize every spin coherent state with the direction $\hat{\mathbf{n}}$ where its expectation value of the operator $\hat{\mathbf{n}} \cdot \mathbf{S}$ is maximal, $|\hat{\mathbf{n}}\rangle$. A canonical rotation to obtain $|\hat{\mathbf{n}}\rangle$ starting in $|\hat{\mathbf{z}}\rangle = |s, s\rangle$ is

$$|\hat{\mathbf{n}}\rangle = e^{zS_-} e^{-\ln(1+|z|^2)S_z} e^{-\bar{z}S_+}|s, s\rangle\,, \tag{1.50}$$

with $z = \tan(\theta/2)e^{i\phi}$ the stereographic projection of $\hat{\mathbf{n}}$. From the calculations we obtain

$$|\hat{\mathbf{n}}\rangle = (1 + |z|^2)^s \sum_{m=-s}^{s} z^{s-m}\sqrt{\binom{2s}{s+m}}|s, m\rangle\,. \tag{1.51}$$

The square of the overlap between two spin coherent states $|\hat{\mathbf{n}}\rangle$ and $|\hat{\mathbf{n}}'\rangle$ is

$$|\langle\hat{\mathbf{n}}'|\hat{\mathbf{n}}\rangle|^2 = \frac{1}{2}\left(1+\cos\theta\cos\theta'+\sin\theta\sin\theta'\cos\left(\phi-\phi'\right)\right)^{2s} = \left(\cos\frac{\Phi}{2}\right)^{4s}, \tag{1.52}$$

with Φ the angle between $\hat{\mathbf{n}}$ and $\hat{\mathbf{n}}'$. The set of the spin coherent states has a resolution of the identity

$$\mathbb{1} = \frac{2s+1}{4\pi}\int |\hat{\mathbf{n}}\rangle\langle\hat{\mathbf{n}}|\sin\theta d\theta d\phi\,. \tag{1.53}$$

The Majorana representation of the spin coherent states is just one star with multiplicity $2s$ (see figure 1.2) and therefore they are the spin states with the more *compact* constellation. In the second part of the thesis, we study several geometrical properties of the set of the spin coherent states in the Hilbert space.

1.6.3 Anticoherent states

An spin-s state is q-anticoherent [99] if the expectation values of $(\hat{\mathbf{n}}\cdot\mathbf{S})^k$, seen as functions $f_k(\hat{\mathbf{n}})$, satisfy

$$f_k(\hat{\mathbf{n}}) = \langle(\hat{\mathbf{n}}\cdot\mathbf{S})^k\rangle = \text{const.}\,, \tag{1.54}$$

for every $k \leq q$. The l.h.s.of condition (1.54) can be written in terms of tensor operators (section 1.4) as

$$\langle(\hat{\mathbf{n}}\cdot\mathbf{S})^k\rangle = \sum_{\sigma=0}^{2s} A_\sigma^{(k)}(s)\sum_{\mu=-\sigma}^{\sigma} Y_{\sigma\mu}^*(\hat{\mathbf{n}})\rho_{\sigma\mu}\,, \tag{1.55}$$

with $\rho_{\sigma\mu} = \langle T_{\sigma\mu}\rangle$. The anticoherence condition (1.54) is translated into $\rho_{\sigma\mu} = 0$ for $0 < \sigma \leq q$ and $-\sigma \leq \mu \leq \sigma$, *cf.* [38]. The value of ρ_{00} only depends on s: $\rho_{00} = 1/\sqrt{2s+1}$. The q-anticoherence property is invariant under rotations, and therefore states with same *shape* constellation have the same order of anticoherence. Opposite to the spin coherent states, the stars in the Majorana representation for the anticoherent states tend to spread uniformly on the 2-sphere [99]. In the figure 1.2 we plot the constellation of a spin coherent state and the 1-anticoherent state for $s = 1$ (2 stars), $|1,0\rangle$. The latter has a constellation formed by two antipodal stars. For $s = 1$ there is not q-anticoherent states with $q \leq 2$. On the other hand, for each value of spin $s \geq 1$, there exists a 1-anticoherent state. An example is the GHZ states defined for each spin s as

$$|GHZ_s\rangle = \frac{1}{\sqrt{2}}\left(|s,s\rangle + |s,-s\rangle\right)\,. \tag{1.56}$$

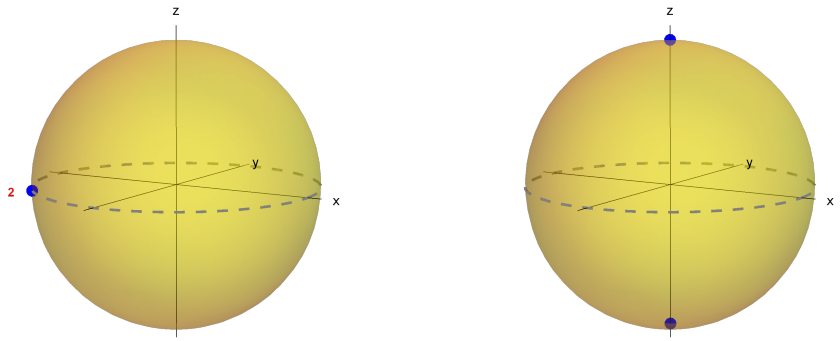

Figure 1.2: The constellation of the spin coherent state (left) of $s = 1$ in the direction $(\theta, \phi) = (\pi/2, 5\pi/4)$ and the $1-$anticoherent state (right) $|s, m\rangle = |1, 0\rangle$

.

Their constellations are regular polygons (see figure 1.3) on the Equator. Adding a relative phase between the states $|s, s\rangle$ and $|s, -s\rangle$ corresponds to a rotation along the $\hat{\mathbf{z}}$, and therefore it has the same shape constellation. For $s = 1$, the GHZ state is the state $|1, 0\rangle$ rotated.

The platonic solids have an important place in the anticoherent states [99]. For instance, the first 2-anticoherent state (in increasing order of the spin s) appears in $s = 2$, which is the state with constellation like tetrahedron $|\psi_{tet}\rangle = (-|2, 2\rangle + \sqrt{2}|2, -1\rangle)/\sqrt{3}$. In the same way, the first 3-anticoherent state is found in $s = 3$ and has a constellation with octahedron's shape, $|\psi_{oct}\rangle = (|3, 2\rangle - |3, -2\rangle)/\sqrt{2}$. And so on for the next platonic states. On the other hand, we can build spin states inspired of geometrical objects. For instance, a triangular prism defines a $s = 3$ spin state, and a state with this shape is given by $|\psi_{PT}\rangle = (\sqrt{2}|3, 3\rangle + \sqrt{5}|3, 0\rangle + \sqrt{2}|3, 3\rangle)/3$, which by the particular choice of ratio between the lengths of the triangular prism, is a 2-anticoherent state. In the figure 1.4, we plot the constellation of $|\psi_{tet}\rangle$, $|\psi_{oct}\rangle$ and $|\psi_{TP}\rangle$. The octahedron and triangular prism state will be used in the subsection 2.5.2.

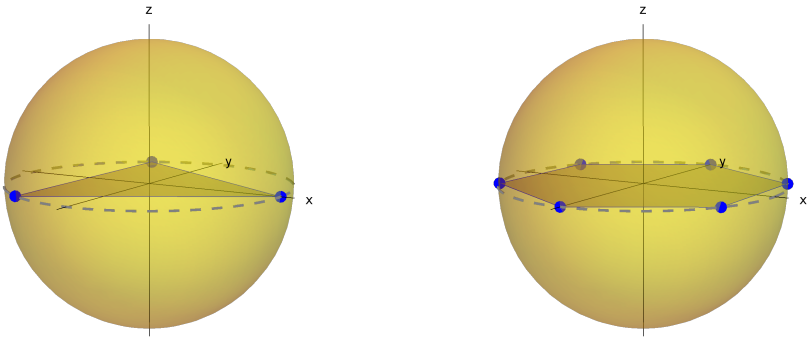

Figure 1.3: The constellation of the GHZ states for $s = 3/2, 3$ which are the equilateral triangle and the regular hexagon on the Equator, respectively.

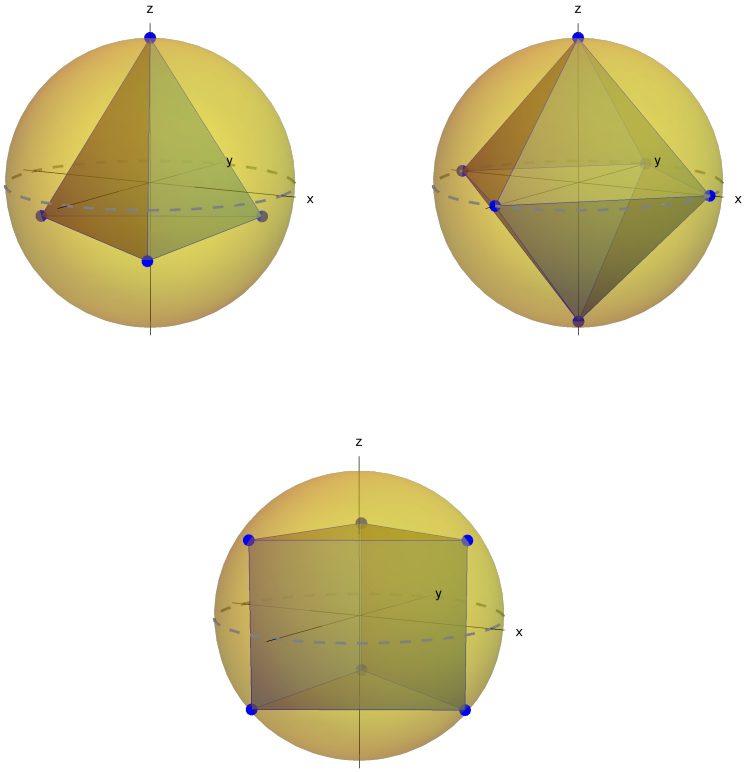

Figure 1.4: The constellations of the states $|\psi_{tet}\rangle$, $|\psi_{oct}\rangle$ and $|\psi_{TP}\rangle$.

Chapter 2

Three and four body quantum systems

What we observe as material bodies and forces are nothing but shapes and variations in the structure of space.

E. Schrödinger

In this chapter, we study the three and four body systems. In the first two sections, we explain the three body model and its quasi-rigid approximation. In section 2.3 we discuss the quantum case and give several examples. In sections 2.4 and 2.5 we give the four body model, in its classic and quantum version respectively. We study several examples in the last section.

2.1 Three-body model

Let us consider three particles with masses $\{m_\alpha\}_{\alpha=1}^3$ and position vectors $\{\mathbf{r}_{s\alpha}\}_{\alpha=1}^3$, respectively. In this case the shape space has dimension $3n-6=3$ and we can define $n-1=2$ Jacobi vectors as

$$\boldsymbol{\rho}_{s1}=\sqrt{\mu_1}(\mathbf{r}_{s2}-\mathbf{r}_{s1})\,,\qquad \boldsymbol{\rho}_{s2}=\sqrt{\mu_2}(\mathbf{r}_{s3}-\mathbf{R}_{s,12})\,, \tag{2.1}$$

where

$$\mu_1=\frac{m_1m_2}{m_1+m_2}\,,\qquad \mu_2=\frac{m_3(m_1+m_2)}{m_1+m_2+m_3}\,,\qquad \mathbf{R}_{s,12}=\frac{m_1\mathbf{r}_{s1}+m_2\mathbf{r}_{s2}}{m_1+m_2}\,, \tag{2.2}$$

are the reduced masses and the center of mass of each particles' cluster. The hamiltonian (1.16) of the three body system can be found exactly [63] with a particular set of coordinates in shape space (*shape coordinates*).

$$q_1 = \rho_{s1}^2 - \rho_{s2}^2\,, \quad q_2 = 2\boldsymbol{\rho}_{s1}\cdot\boldsymbol{\rho}_{s2}\,, \quad q_3 = 2|\boldsymbol{\rho}_{s1}\times\boldsymbol{\rho}_{s2}| \geq 0\,, \tag{2.3}$$

mapping $\mathscr{S}$ to the upper half of $\mathbb{R}^3$. The q_3 coordinate measures the area of the (triangular) body, so that the plane $q_3 = 0$ corresponds to collinear shapes. In the q_3 axis are the equilateral triangular shapes (whose inertia tensor is degenerate) and when $q_2 \neq 0$ and $q_1 = 0$, are the isosceles triangle's shape. In the figure 2.1 is plotted the shape space and in some particular points and we draw the respective triangle. In the last equation, we switch to lower indices for typographical convenience. In the literature, there are many, even radically different coordinates in the space of triangles, see *e.g.*, [13]. In the principal-axis gauge, $\mathbf{A}$ is given by

$$\mathbf{A}_\mu dq^\mu = \frac{q_1 dq_2 - q_2 dq_1}{2q(q_1^2+q_2^2)}\,\hat{\mathbf{z}}\,, \tag{2.4}$$

with $q = \rho_{s1}^2 + \rho_{s2}^2 = (q_1^2+q_2^2+q_3^2)^{1/2}$, while $\mathbf{B}_{\mu\nu}$ turns out to be

$$\mathbf{B}_{\mu\nu} = \frac{1}{2q^3}\epsilon_{\mu\nu\alpha}q^\alpha\,\hat{\mathbf{z}}\,. \tag{2.5}$$

The last two expressions show that $\mathbf{A}$ has a string singularity along the q_3-axis, while $\mathbf{B}$ resembles a magnetic monopole located at the origin of $\mathscr{S}$. The string singularity of $\mathbf{A}$ is related to the fact that, on the q_3-axis, the principal axis frame is itself singular, that is, the functions $\boldsymbol{\rho}_\alpha(q^\mu)$ that define the body frame are not differentiable there [60]. In fact, it is easy to show that in going around the q_3 axis once in a circle the principal axes in the plane of the triangle reverse their direction, and this holds true regardless of the radius of the circle, a classical fact that is echoed in the sign change of the wavefunction in going around "diabolical points" in the spectrum of multiparametric hamiltonians (see, *e.g.*, [42, 13]). This singularity is relevant because the section wavefunction $\chi_k^l(q^\mu)$ is itself singular at the same places the gauge potential is, but can be relocated by changing the gauge (it cannot be eliminated though). One of these gauges is the so-called "north-regular gauge",

$$\rho_1 = \frac{1}{2\sqrt{q+q_3}}\,(q+q_3+q_1, q_2, 0)\,, \qquad \rho_2 = \frac{1}{2\sqrt{q+q_3}}\,(q_2, q+q_3-q_1, 0)\,, \tag{2.6}$$

which its gauge potential is

$$\mathbf{A}_\mu dq^\mu = \frac{q_1 dq_2 - q_2 dq_1}{2q\,(q+q_3)}\hat{\mathbf{z}}\,. \tag{2.7}$$

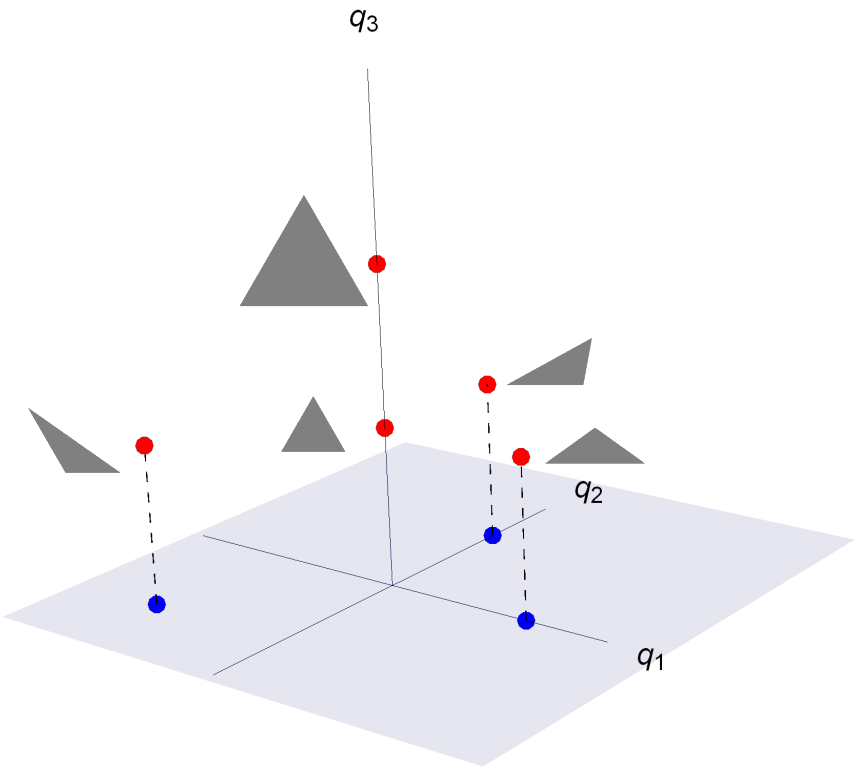

Figure 2.1: Shape space of the three body system. The gray triangles are the shapes of the system in the red points $(q_1, q_2, q_3) = (0, 0, 1), (0, 0, 2), (1, 0, 1), (0, 1, 1), (-1, -1, 1)$, respectively, when the particle masses are equal. The blue points and the dashed lines mark the position of the red points.

The singularity is relocated to the negative q_3 axis, which is not part of $\mathscr{S}$ [63]. On the other hand, the singularity of $\mathbf{B}$ is immune to gauge transformations. With the shape coordinates and gauge, it may be calculated the other quantities of interest,

$$\mathsf{M} = \begin{pmatrix} \frac{q-q_1}{2} & -\frac{q_2}{2} & 0 \\ -\frac{q_2}{2} & \frac{q+q_1}{2} & 0 \\ 0 & 0 & q \end{pmatrix}, \quad \mathsf{M}^{-1} = \begin{pmatrix} \frac{2(q+q_1)}{q_3^2} & \frac{2q_2}{q_3^2} & 0 \\ \frac{2q_2}{q_3^2} & \frac{2(q-q_1)}{q_3^2} & 0 \\ 0 & 0 & q^{-1} \end{pmatrix}, \quad g^{\mu\nu} = 4q(dq_1^2 + dq_2^2 + dq_3^2)\,. \tag{2.8}$$

The final Hamiltonian for the three-body system is the following,

$$H = \left(\frac{q+q_1}{q_3^2}\right) L_x^2 + \left(\frac{q-q_1}{q_3^2}\right) L_y^2 + \left(\frac{1}{q+q_3}\right) L_z^2 + \left(\frac{2q_2}{q_3^2}\right) L_x L_y - \frac{2L_z}{q+q_3} \left(-q_2 p_1 + q_1 p_2\right) + 2q(p_1^2+p_2^2+p_3^2) + V(q)\,. \tag{2.9}$$

2.2 Quasi-rigid three body system

In this section, let's consider the masses of the particles equal $m_\alpha = m = 1$. The singular behavior of the wavefunction can be avoided in this case by adopting the north regular gauge, which is also an Eckart, and Poincaré gauge, centered on the equilibrium point $q_0 = (q_0^1, q_0^2, q_0^3) = (0, 0, 1)$ (an equilateral triangle shape of unit distance between the masses).

We make a linear coordinate transformation,

$$\tilde{q}_1 = -\frac{1}{3} q_1 + \frac{\sqrt{2}}{3} q_2\,, \quad \tilde{q}_2 = -\frac{\sqrt{2}}{3} q_1 - \frac{1}{3} q_2\,, \quad \tilde{q}_3 = -\frac{1}{2} q_3\,, \tag{2.10}$$

so that $\tilde{q}_0 = (0, 0, -1/2)$, and the x's, defined in the standard way by $\tilde{q}^\mu = \tilde{q}_0^\mu + \lambda x^\mu$, are normal modes. x_3 corresponds to the (highest frequency) breathing mode with $\omega_3 = \sqrt{2}$ (in natural units), while x_1 and x_2 are degenerate orthogonal modes of frequency $\omega_1 = \omega_2 = 1$. The corresponding patterns of oscillation are illustrated in Fig. 2.2. The moment of inertia tensor for the equilibrium shape is

$$\mathsf{M} = \begin{pmatrix} 1/2 & 0 & 0 \\ 0 & 1/2 & 0 \\ 0 & 0 & 1 \end{pmatrix}, \tag{2.11}$$

while the only non-trivial component of the Coriolis tensor is $\mathbf{B}_{12} = 2\hat{\mathbf{z}}$ and therefore the internal angular momentum reduces to $\mathbf{S} = S_{12}\hat{\mathbf{z}}$, where $S_{12} = x_1 p_2 - x_2 p_1$ is the shape angular momentum in the x_1-x_2 plane. Accordingly, the Hamiltonian takes the form

$$H = \frac{1}{2}\left(p_1^2 + p_2^2 + x_1^2 + x_2^2\right) + \frac{1}{2}\left(p_3^2 + 2x_3^2\right) + \lambda^2 \left(\mathbf{L}^2 - \frac{1}{2} L_z^2 - L_z S_{12} + \frac{1}{2} S_{12}^2\right). \tag{2.12}$$

2.2.1 Three-body classic model

As mentioned before, in the classical case the condition of vanishing angular momentum makes it possible to find the solutions of the equations of motion for the shape coordinates independently

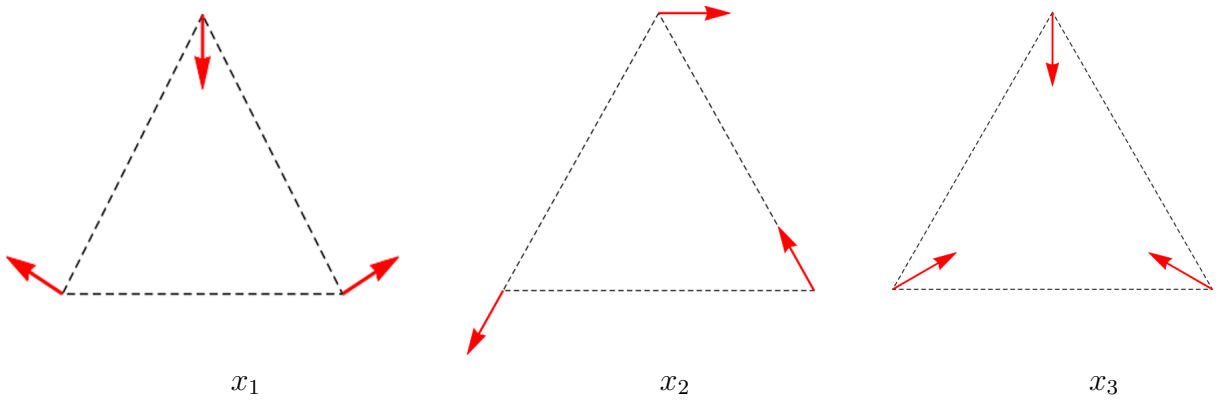

Figure 2.2: The normal modes of oscillation of the three body system when the equilibrium shape corresponds to an equilateral triangle. From left to right, the breather (or *symmetric stretching*) mode x_3, the *bending* mode x_2, and the *asymmetric stretching* mode x_1, the latter two being degenerate in frequency.

of the orientation ones. For the above hamiltonian, S_{12} is a constant of the motion, with $x^\mu(t)$ being harmonic oscillators, to leading order in λ,

$$x^\mu(t) = x_0^\mu \cos\omega_\mu t + \frac{p_0^\mu}{\omega_\mu}\sin\omega_\mu t, \tag{2.13}$$

with frequencies $\omega_\mu = (1, 1, \sqrt{2})$ and $p^\mu(t) = \dot{x}^\mu(t)$. In fact, the degeneracy of the normal modes x_2, x_3 implies that $\mathbf{S}(t)$ is a constant of motion and therefore both, the rotation axis $\hat{\mathbf{n}} = \hat{\mathbf{S}}$ and the angular velocity $\dot{\phi} = \lambda^2\sqrt{\mathbf{S}\cdot\mathbf{S}}$, do not change as a function of time. This result is valid whenever the evolution of the shape coordinates is given by degenerate normal modes. Eq. (1.14) then gives

$$\mathsf{R}(t) = \begin{pmatrix} \cos\left(\lambda^2 S_{12} t\right) & \sin\left(\lambda^2 S_{12} t\right) & 0 \\ -\sin\left(\lambda^2 S_{12} t\right) & \cos\left(\lambda^2 S_{12} t\right) & 0 \\ 0 & 0 & 1 \end{pmatrix}, \tag{2.14}$$

which represents a rotation about $\hat{\mathbf{z}}$ by an angle $\alpha(t) = -\lambda^2 S_{12} t$, so that the cyclic shape change (2.13) with $x_3(t) = 0 = p_3(t)$ gives rise to $\alpha(2\pi) = -2\pi\lambda^2 S_{12}$. In Fig. 2.3 we show the cyclic deformation sequence that produces the rotation (2.14), for $S_{12} = 4$, and a total time interval of one period, $0 \le t \le T = 2\pi/\omega_1$. Note that the triangle is deformed, w.r.t. the equilateral

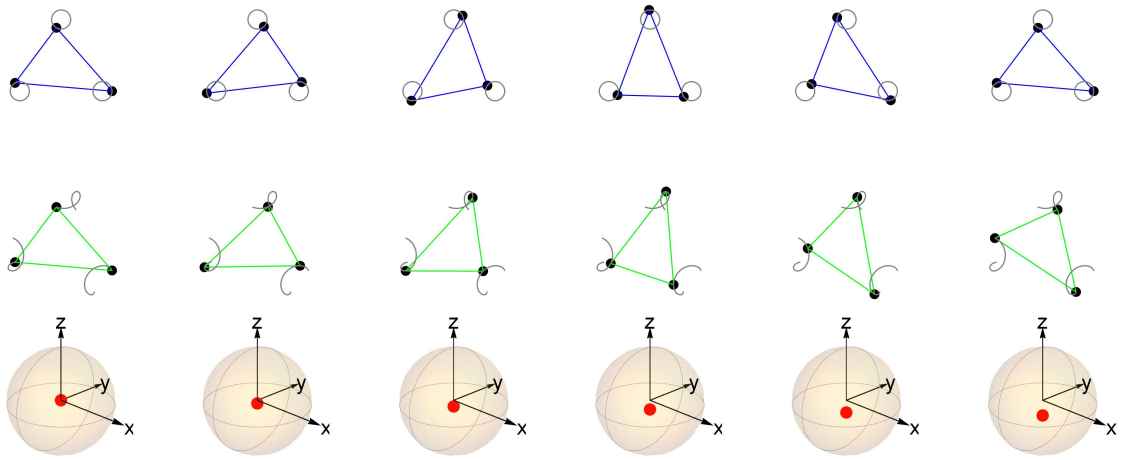

Figure 2.3: Sequence of the orientation change produced by a cyclic deformation in the x_1-x_2 plane of shape space, for the three body problem. The top row and middle row are the snapshots of the deformation in the body (blue) and space (green) frames in $t = 0, 2\pi/5, \ldots, 2\pi$, for $S_{12} = 4$ and $\lambda = 0.5$. In each snapshot we plot the whole trajectory of each particle. Each particle rotates counterclockwise around a certain point, and to preserve the vanishing total angular momentum, the whole system must rotate clockwise, as it is observed in the space frame. For purposes of illustration, the deformation w.r.t. the equilibrium equilateral configuration, has been visually exaggerated by a factor of 4. The ball on the bottom row is $SO(3)$ in the axis-angle representation. The red dot close to the origin of $SO(3)$ represents the rotation that connects the (blue) body frame with the (green) space frame. The downwards motion of the dot signals a clockwise rotation of the body frame around the z-axis.

configuration, at all times, since its trajectory in shape space is a circle *centered* on (and, hence, never passing through) that configuration. Flipping the sign of S_{12} gives rise to a rotation in the opposite sense.

2.3 Quantum case

Turning now to the quantum case, we define the annihilation and creation operators for excitations along the three coordinate axes in shape space ($\hbar = 1$, $\mu = 1, 2, 3$),

$$a_\mu = \frac{1}{\sqrt{2}} \left(\sqrt{\omega_{(\mu)}}\, x_\mu + \frac{i}{\sqrt{\omega_{(\mu)}}}\, p_\mu \right) , \qquad a_\mu^\dagger = \frac{1}{\sqrt{2}} \left(\sqrt{\omega_{(\mu)}}\, x_\mu - \frac{i}{\sqrt{\omega_{(\mu)}}}\, p_\mu \right) , \tag{2.15}$$

as well as the circular analogues of the first two,

$$a_\pm = \frac{1}{\sqrt{2}} \left(a_1 \mp i a_2 \right) , \qquad a_\pm^\dagger = \frac{1}{\sqrt{2}} \left(a_1^\dagger \pm i a_2^\dagger \right) , \tag{2.16}$$

and the associated number operators

$$N_\mu = a_\mu^\dagger a_\mu \, , \qquad N_\pm = a_\pm^\dagger a_\pm \, . \tag{2.17}$$

In terms of these operators, the hamiltonian (2.12) takes the form ($\omega_{1,2} = 1$)

$$H = (N + 1) + \omega_3 \left(N_3 + \frac{1}{2} \right) + \lambda^2 \left(\mathbf{L}^2 - \frac{L_z^2}{2} - S L_z + \frac{S^2}{2} \right) , \tag{2.18}$$

with $N = N_+ + N_-$ and $S = N_+ - N_-$, acting on the Hilbert space $L^2(\mathscr{C}, d^3q \; d\mathsf{R})$, where $d\mathsf{R}$ is the normalized Haar measure in $SO(3)$. A complete set of mutually compatible operators, commuting with the hamiltonian, is $\{N, S, N_3, \mathbf{L}^2, L_{sz}, L_z\}$ (see [58]), so the hamiltonian eigenstates are labeled as $|n, s, n_3, l, m, k\rangle$, with $n_3, n, l \in \{0, 1, 2, \ldots\}$, $m, k = -l, -l+1, \ldots, l-1, l$ and $s = -n, -n+2, \ldots, n-2, n$. We are now ready to see the re-orientation of a system by a cyclic shape deformation, which it can be thought as the quantum version of the falling cat problem (a feline who changes its shape to re-orient its body).

2.3.1 Rotations with the Majorana's stellar representation

We take as initial state of the system,

$$|\Psi\rangle = \frac{1}{\sqrt{2}} \Big(|n, s, n_3, 1, 0, 1\rangle + |n, s, n_3, 1, 0, -1\rangle \Big) \equiv |n, s, n_3\rangle \otimes |\Phi\rangle \, , \tag{2.19}$$

where $|\Phi\rangle \equiv (|1, 0, 1\rangle + |1, 0, -1\rangle)/\sqrt{2}$ is the rotational state of the triangle, with Majorana polynomial[1]

$$p_{|\Phi\rangle}(\zeta) = \frac{1}{\sqrt{2}} \Big(\zeta^2 + 1 \Big) , \tag{2.20}$$

[1] Formally, the states of the orientational part do not have the Majorana representation. However, in the case when the state is an eigenstate of L_{sz} (or L_z) with $m = 0$ ($k = 0$), the states are equivalent to spin states (see, *e.g.*, [58], §58).

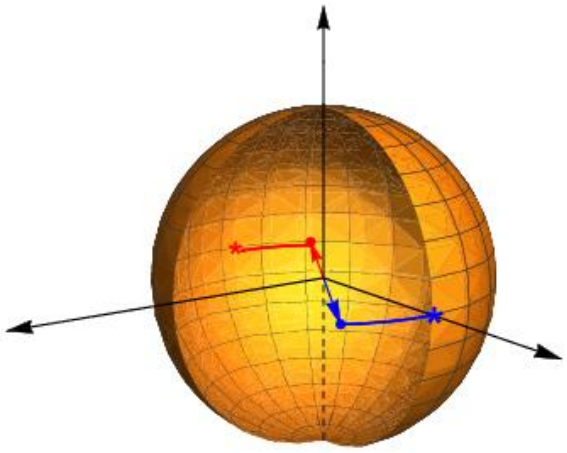

Figure 2.4: The stellar representation of the state $|\Phi(t)\rangle$. The asterisk correspond to $t = 0$ while the dots to $t = \pi/6$.

the roots of which are $\zeta_\pm = \pm i$, and is therefore represented on S^2 by the pair of points $(x_\pm, y_\pm, z_\pm) = (0, \pm 1, 0)$ (see Fig. 2.4). It is easily seen that $\langle\phi|\mathbf{L}|\phi\rangle = \langle\phi|\mathbf{L}_s|\phi\rangle = 0$ holds, and that the only non-trivial time evolution of $|\Psi(t)\rangle \equiv |n, s, n_3\rangle \otimes |\Phi(t)\rangle$ comes from the term $-\lambda^2 L_z S$ in the hamiltonian, resulting in the Majorana polynomial for $|\Phi(t)\rangle$

$$p_{|\Phi(t)\rangle}(\zeta) \sim \zeta^2 + e^{-2i\lambda^2 st}\,, \tag{2.21}$$

the roots of which are $\zeta_\pm = \pm i e^{-i\lambda^2 st}$, with the corresponding stars at $(x_\pm, y_\pm, z_\pm) = \pm\big(\sin(\lambda^2 st), \cos(\lambda^2 st), 0\big)$ (Fig. 2.4). Thus, the state $|\Psi(t)\rangle$ rotates with time about $\hat{\mathbf{z}}$ by an angle $-\lambda^2 st$, in complete agreement with what we found classically. Even so, the correspondence with the example in subsection 2.2.1 is incorrect because $|\Psi(t)\rangle$ is not a state of well defined shape or orientation, nor is it obvious that the rotation found can be somehow associated with a cyclic change of the body's shape. We can do better, in this respect, by considering coherent states in shape space.

2.3.2 Coherent state

Now we will reproduce the simplified free falling quantum cat case. We consider now the state ($\alpha_\pm \in \mathbb{C}$)

$$\Psi(\mathsf{R}, q) = \psi_{\alpha_+,\alpha_-}(x_1, x_2)\psi_0(x_3)\Phi(\mathsf{R})\,, \tag{2.22}$$

where $\psi_{\alpha_+,\alpha_-}(x_1, x_2)$ is a coherent state with

$$\langle x_i\rangle = \sqrt{2}\,\mathrm{Re}(\alpha_i)\,, \qquad \langle p_i\rangle = \sqrt{2}\,\mathrm{Im}(\alpha_i)\,, \quad i = 1, 2\,, \tag{2.23}$$

$$\alpha_1 = \frac{1}{\sqrt{2}}(\alpha_+ + \alpha_-)\,,\ \alpha_2 = \frac{i}{\sqrt{2}}(\alpha_+ - \alpha_-)\,, \tag{2.24}$$

$\psi_0(x_3)$ is the breathing mode ground state ($\alpha_3 = 0$), and $\Phi(\mathsf{R})$ a wavefunction in $SO(3)$. An orientation wavefunction localized in some point of $SO(3)$ is given by $\Phi(\eta) = \Phi(\mathsf{R}_{\hat{\mathbf{n}}}(\eta)) = N_\Phi e^{\cos\eta}$ in the axis-angle representation $(\hat{\mathbf{n}}, \eta)$. The orientation wavefunction probability density $P_\Phi = |\Phi(\eta)|^2$ has a maximum at the origin ($\eta = 0$) and decays monotonically and isotropically with increasing η. $\Phi(\eta)$ itself describes a superposition of various orientations of the body frame, the amplitude for each of which depends only on the rotation angle η, and is independent on the axis of rotation $\hat{n}$ between the two frames (body and space). In appendix B, we prove that any wavefunction on $SO(3)$ that does not depend of the rotation axis can be written as a superposition of the characters of $SU(2)$ $\chi^l(\eta)$ [94], $\Phi(\mathsf{R}) = \sum_l c_l\chi^l(\eta)$, where

$$\chi^l(\mathsf{R}) = \sum_{m=-l}^{l} D^l_{mm}(\mathsf{R}) = \chi^l(\eta) = \frac{\sin[(2l+1)\frac{\eta}{2}]}{\sin\frac{\eta}{2}}\,, \tag{2.25}$$

Compared to the quantum state considered in the previous subsection, Ψ provides localization in both shape and orientation space, and is thus more appropriate for recovering the classical behavior.

We compute now the time evolution of the wavefunction (2.22). The hamiltonian (2.18) can be separated into three mutually commuting terms, $H_S = (N+1) + \omega_3(N_3 + 1/2) + \lambda^2 S^2/2$, acting on the shape variables q, $H_O = \lambda^2(\mathbf{L}^2 - L_z^2/2)$, acting on the orientation variables R, and $H_I = -\lambda^2 SL_z$, that couples q and R. The time evolution operator factorizes accordingly to compute the action of $e^{-iH_O t}$ on Φ, we expand the latter in the H_O eigenfunctions $\{D^l_{km}\}$,

$$\Phi(\eta(\alpha,\beta,\gamma)) = \sum_{lkm} c^l_{km} D^l_{km}(\alpha,\beta,\gamma)\,, \tag{2.26}$$

with

$$c^l_{km} = \frac{2l+1}{8\pi^2}\int_0^{2\pi}\int_0^{\pi}\int_0^{2\pi} d\alpha d\beta d\gamma\, \sin\beta D^l_{km}(\alpha,\beta,\gamma)^*\Phi(\eta(\alpha,\beta,\gamma))\,, \tag{2.27}$$

and $\cos(\eta/2) = \cos\frac{\beta}{2}\cos\frac{\alpha+\gamma}{2}$. When the orientation wavefunction Φ doesn't depend of the rotation axis, $c^l_{km} = c^l\delta_{km}$ holds. This result is proved in the Appendix B and characterize all the orientational wavefunctions of the type $\Phi(\eta)$. The time-evolved orientation wavefunction then becomes

$$\Phi_t(\alpha,\beta,\gamma) = \sum_{lkm} c^l_{km} e^{-i\lambda^2\left(l(l+1)-k^2/2\right)t} D^l_{km}(\alpha,\beta,\gamma)\,. \tag{2.28}$$

Next we easily find for $\psi_{\alpha_+,\alpha_-,t}(x_1,x_2) \equiv e^{-iH_St}\psi_{\alpha_+,\alpha_-}(x_1,x_2)$,

$$\psi_{\alpha_+,\alpha_-,t}(x_1,x_2) = e^{-i\lambda^2 t(\alpha_+\tilde{\partial}_{\alpha_+}-\alpha_-\tilde{\partial}_{\alpha_-})^2/2}\psi_{\alpha_+e^{-it},\alpha_-e^{-it}}(x_1,x_2)\,, \tag{2.29}$$

since the action of the λ-independent part of H_S simply multiplies the α's by e^{-it}, while it is easily shown that $N_\pm|\alpha_\pm\rangle = \alpha_\pm\tilde{\partial}_{\alpha_\pm}|\alpha_\pm\rangle \equiv \alpha_\pm(\partial_{\alpha_\pm} + \alpha^*_\pm/2)|\alpha_\pm\rangle$.

The third coupling term is the most interesting. Using the identity $e^{\mu N_\pm}f(a_\pm) = f(e^\mu a_\pm)e^{\mu N_\pm}$, where f is an arbitrary analytic function, we find

$$\Psi_t(\alpha,\beta,\gamma,x_1,x_2,x_3) = \psi_0(x_3,t)\sum_{lkm} c^l_{km}(t)\psi^{(k)}_{\alpha_+,\alpha_-}(x_1,x_2,t)D^l_{km}(\alpha,\beta,\gamma)\,, \tag{2.30}$$

where

$$\psi_0(x_3,t) = e^{-i\omega_3 t/2}\psi_0(x_3) \tag{2.31}$$

$$c^l_{km}(t) = c^l_{km}e^{-i\lambda^2\left(l(l+1)-k^2/2\right)t} \tag{2.32}$$

$$\psi^{(k)}_{\alpha_+,\alpha_-}(x_1,x_2,t) = e^{-i\lambda^2 t(\alpha_+\tilde{\partial}_{\alpha_+}-\alpha_-\tilde{\partial}_{\alpha_-})^2/2}\psi_{\alpha_+e^{-i(1+k\lambda^2)t},\alpha_-e^{-i(1-k\lambda^2)t}}(x_1,x_2)\,. \tag{2.33}$$

Eq. (2.30) is valid, with the appropriate coefficients c^l_{km}, for an arbitrary initial orientation wavefunction. Taking into account the particular form of these coefficients for the $\Phi(\eta)$ we assumed above, the expression for Ψ_t simplifies to (omitting the arguments of functions)

$$\Psi_t = \psi_0\sum_{lk} c^l e^{-i\lambda^2\left(l(l+1)-k^2/2\right)t}\psi^{(k)}_{\alpha_+,\alpha_-}D^l_{kk}\,. \tag{2.34}$$

To be able to monitor visually the system's evolution, we start from the probability density $P_t(\mathsf{R},q) = |\Psi_t(\mathsf{R},q)|^2$ and compute marginal (reduced) densities

$$P^S_t(q) = \int P_t(\mathsf{R},q)d\mathsf{R}\,, \qquad P^O_t(\mathsf{R}) = \int P_t(\mathsf{R},q)\sqrt{g}\,d^{3n-6}q\,, \tag{2.35}$$

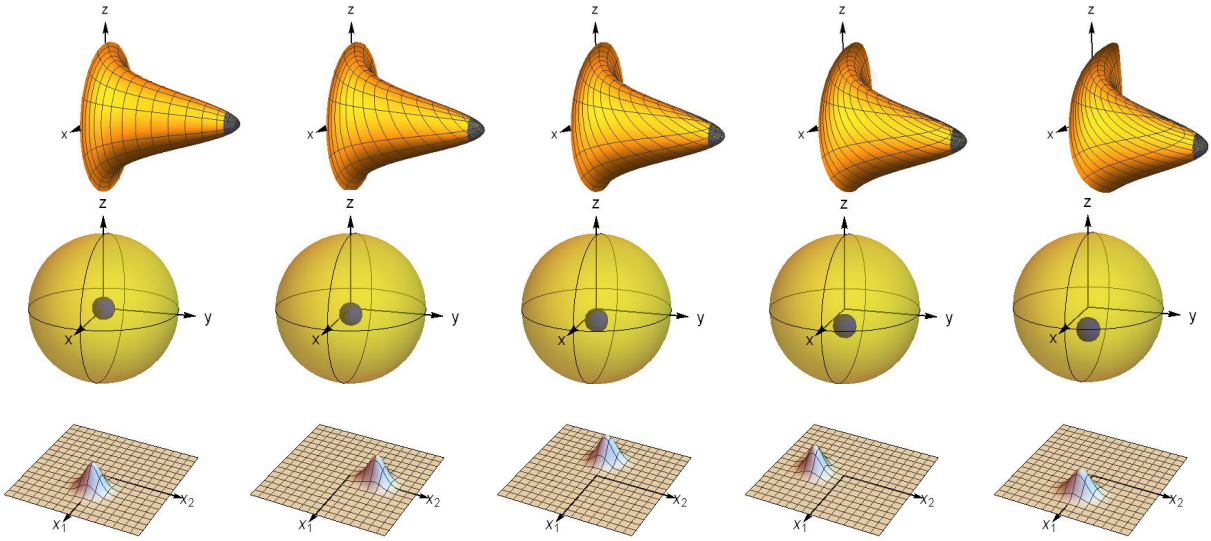

Figure 2.5: Sequence of the orientation change produced by a cyclic deformation in the x_1-x_2 plane in shape space for the three body problem, in the quantum case. The middle row depicts $SO(3)$, as in Fig. 2.3, while the top row contains plots of the reduced orientation probability density $P_t^O(\mathsf{R})$, restricted to the xz plane of $SO(3)$ (elsewhere in $SO(3)$, P_t^O is obtained by rotation around the z-axis). Shown is the time evolution of the probability density associated with the initial wavefunction $\Psi(\mathsf{R}, q)$, given by (2.22), for $t = 2\pi n/4$, $n = 0, 1, \ldots, 4$, $\lambda = 0.2$, and $(\alpha_+, \alpha_-) = (2, 0)$. The little dark spot in the top and middle rows is the $P_t^O(\mathsf{R}) = .90 \max(P_t^O)$ surface. The plots in the bottom row are of the reduced shape probability density $P_t^S(x_1, x_2)$. As the gaussian wavefunction rotates in the x_1x_2 plane of shape space, the orientation wavefunction gets displaced along the z-axis — this is the quantum analogue of the classical cat rotation.

in shape space and $SO(3)$, respectively. In Fig. 2.5 we show the quantum version of the cyclic deformation and the corresponding rotation sequence, as time increases, for $(\alpha_+, \alpha_-) = (2, 0)$, which implies that $\langle S \rangle = 4$, just as in the classical situation shown in Fig. 2.3. The system rotates clockwise as its shape changes, in a fashion similar to its classical counterpart. We note as well that the surface of constant $P_t^O(\mathsf{R})$ (the little dark spot in the top and middle rows) and the width of $P_t^S(q)$ increase their size with time. Both effects are related to the dispersion of the wavefunction, the latter one due to the term $\lambda^2 S^2/2$ of H_S. Let us imagine that the three body system is a *living* being, as a quantum, quasi-rigid, triangular cat that is left to free fall with

its "feet" upwards (imagine the triangle with its plane vertical, and one of its vertices pointing upwards, marking the position of the "feet"), should change its shape cyclically (oscillating in the x_1-x_2 plane) enough times for the little dark spot in Fig. 2.5 to reach the surface of the ball, which corresponds to a rotation (in the average sense) of π, allowing it to land safely on its feet.

2.3.3 Quantum righting reflex and Schroedinger cats

More exotic scenarios are of course imaginable in the quantum realm. For example, as mentioned before, if the cat oscillates in shape space in the opposite sense, then its rotation in physical space will also be in the opposite sense. Imagine then a cat that starts free falling as above, but executes a quantum superposition of the above two oscillations in shape space. In other words, its shape space wavefunction consists of two gaussians that rotate in the x_1-x_2 plane in opposite senses (Fig. 2.6, bottom row). During the fall, the cat will be in a superposition of orientation states, as it rotates both, say, clockwise and anticlockwise in physical space. As we see in the top and middle rows of Fig. 2.6, there will be two little dark spots inside the $SO(3)$ ball, moving in opposite directions. If lucky, the cat can still land on its feet, if the two "copies" rotate by $\pm\pi$.

Something slightly more interesting will happen if the cat does exactly as above, but is released with its feet pointing sideways (horizontally), and only has half the time available before landing. Then one copy in the quantum superposition lands on its feet, and survives the fall, while the other lands on its back, and gets killed, instantly converting the falling feline into a Schroedinger cat.

We could also fix as our initial state a wavefunction like (2.22), with $(\alpha_+, \alpha_-) = (\sqrt{2}, \sqrt{2})$ or, equivalently, with $(\alpha_1, \alpha_2) = (2, 0)$, which corresponds to a coherent state oscillating along x_1, with $\langle S \rangle = 0$. Also, we put $\lambda = 0.35$ to observe only the dispersion effects. Then, comparing with the analogous classical case, the system would not be expected to rotate. Contrary to the classical case though, if left oscillating long enough, the system manages to access, with significant probability, orientations quite distinct from its initial one — see the ellipsoidal-shaped surface inside the $SO(3)$ ball in Fig. 2.7 at $t = 2\pi$. Of course, wavefunctions tend to disperse with time, but what distinguishes this case is that the spreading out is somehow channeled along the z-axis. The term S^2 of the Hamiltonian tends to split the initial gaussian of $P_t^S(x_1, x_2)$ (bottom row of Fig. 2.7). To end this section, we mention that the effects studied here ought to be

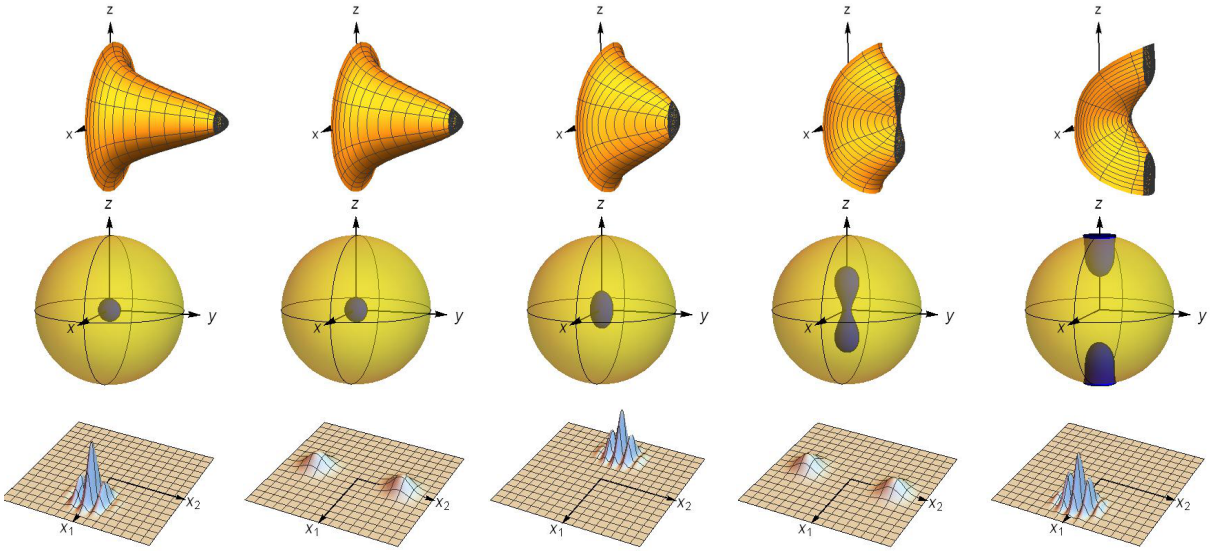

Figure 2.6: Evolution of the sum of the two coherent states $(\alpha_+^1, \alpha_-^1) = (3, 0)$ and $(\alpha_+^2, \alpha_-^2) = (0, 3)$. Visual conventions are as in Fig. 2.5, with $\lambda = 0.18$. The reduced shape probability in the bottom row consists of two gaussians rotating in opposite senses. This particular cyclic deformation initially elongates and eventually splits the little dark spot into two, one climbing up the z-axis and the other going down (top and middle rows). This is a purely quantum scenario that can give rise to a Schroedinger cat.

experimentally verifiable. Thus, *e.g.*, a triatomic molecule, like H_3^+, set to vibrate in a state with non-zero s and vanishing angular momentum expectation value, ought to "rotate" w.r.t. the lab. More accurately, its quantum state after one period of the vibration should be related to the initial one by a rotation, intermediate states being, in general, quite distinct. Our analytical results are only valid for nonlinear molecules but, other than this limitation, do not require any particular symmetry. In fact, the presence of asymmetry may provide the means to detect the rotation. For example, if the molecule possesses permanent electric dipole moment, and a large enough population is polarized so that a macroscopic dipole moment can be measured in the lab, the excitation of suitable vibrational modes, without imparting angular momentum, should cause the dipole moment to rotate.

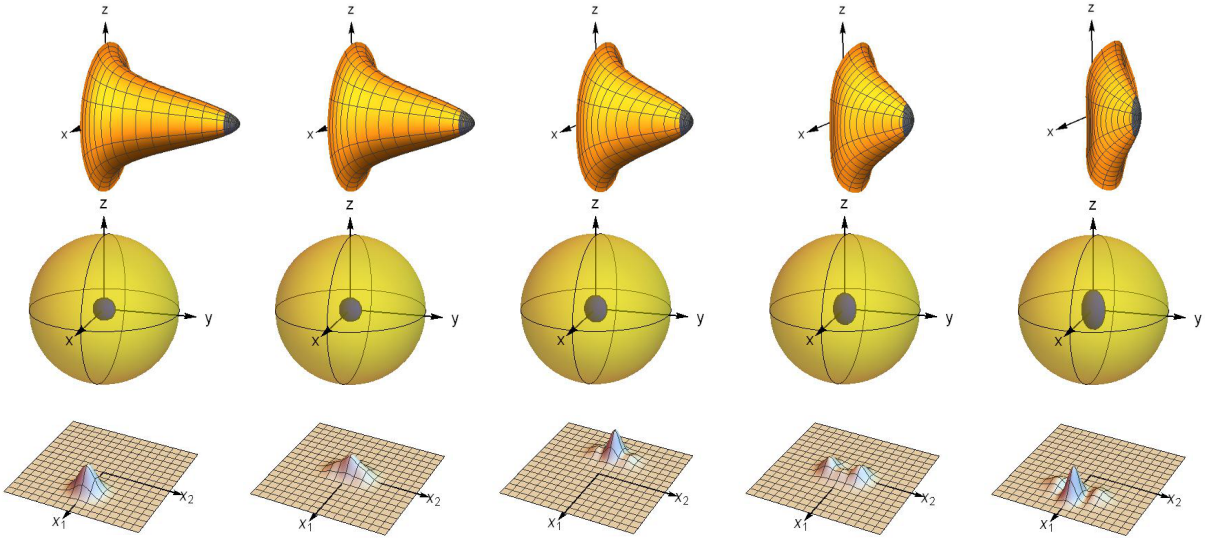

Figure 2.7: Conventions as in Fig. 2.5, with $\lambda = 0.35$ and $(\alpha_+, \alpha_-) = (\sqrt{2}, \sqrt{2})$, which implies $(\alpha_1, \alpha_2) = (2, 0)$. The gaussian wavefunction in this case simply oscillates along the x_1-axis, with its expectation value tracing a curve that encloses zero area. The central peak of the orientation wavefunction (dark spot at the origin of $SO(3)$) stays initially still, but gets gradually elongated along the z-axis.

2.4 Four body model

We've seen that in the three body model, we can model the falling cat problem in a simplified but quantum version. Even more, we could study other examples with purely quantum characteristics. One part which is missing in the quasi rigid three body problem, is that the shape deformations can only induce rotations along one axis, and then we cannot observe quantum effects given by non-commuting relations of the components of $\mathbf{L}$. This part can be analyzed in the four body problem. The shape space in the four-point case, is six dimensional, with a very complicated topological structure [62, 61] — but still, a quasi-rigid model, with its wavefunction concentrated around some equilibrium shape, should be manageable.

It is sufficient to consider a simple system consisting of four point-like particles of equal masses m interacting with each other through a harmonic potential in the quasi-rigid approximation, such that it mildly oscillates around its equilibrium configuration assumed to be a tetrahedron of length a (see Fig. 2.8).

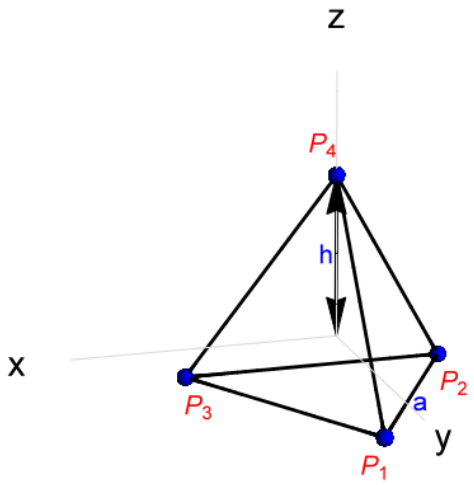

Figure 2.8: The equilibrium configuration of the four-body system.

As in the three body system, we consider the free traslational dynamics of the system, with 3 coordinates defining its orientation and 6 rotation-invariant coordinates defining its shape. As usual, the body's orientation is defined by a rotation, $\mathsf{R}_{\hat{\mathbf{n}}}(\phi)$ in the angle-axis representation $(\phi, \hat{\mathbf{n}})$, and the shape coordinates will be the normal modes x_μ ($\mu = 1, \ldots, 6$), see Appendix A. In Fig. 2.9 the normal modes are shown: the set (x_1, x_2, x_3) forms a triplet, while (x_4, x_5) is a doublet and x_6 is the breathing mode, with frequencies $\omega = \sqrt{2}, 1, 2$, respectively. In the 4-body case, any possible rotation can be induced by a change of its shape involving only the triplet modes, so for the sake of simplicity we set $x_4(t) = x_5(t) = x_6(t) = 0$ for the rest of the chapter. It can be shown then that the dynamics of the (simplified) 4-body is governed by the quasi-rigid Hamiltonian which is equivalent to a 3D-isotropic harmonic oscillator coupled to a spherical rigid rotor (see Appendix A),

$$H = \frac{1}{2}(p_1^2 + p_2^2 + p_3^2) + \frac{1}{2}(x_1^2 + x_2^2 + x_3^2) + \frac{\lambda^2}{2}(\mathbf{L} - \mathbf{S})^2 \,, \tag{2.36}$$

where λ is a dimensionless parameter, $\mathbf{L}$ is the angular momentum expressed in the body frame, p_i is the momentum conjugate to the shape coordinate x_i, and the internal angular momentum $\mathbf{S}$ given by

$$S_x = -\frac{1}{2}\mathrm{S}^{23} \,, \quad S_y = -\frac{1}{2}\mathrm{S}^{31} \,, \quad S_z = -\frac{1}{2}\mathrm{S}^{12} \,, \tag{2.37}$$

with $\mathrm{S}^{ij} = x_i p_j - x_j p_i$. Notice that $\mathbf{S}$ is a vector in the physical space, while S^{ij} is the angular momentum in the $x_i - x_j$ plane of shape space $(i, j = 1, 2, 3)$.

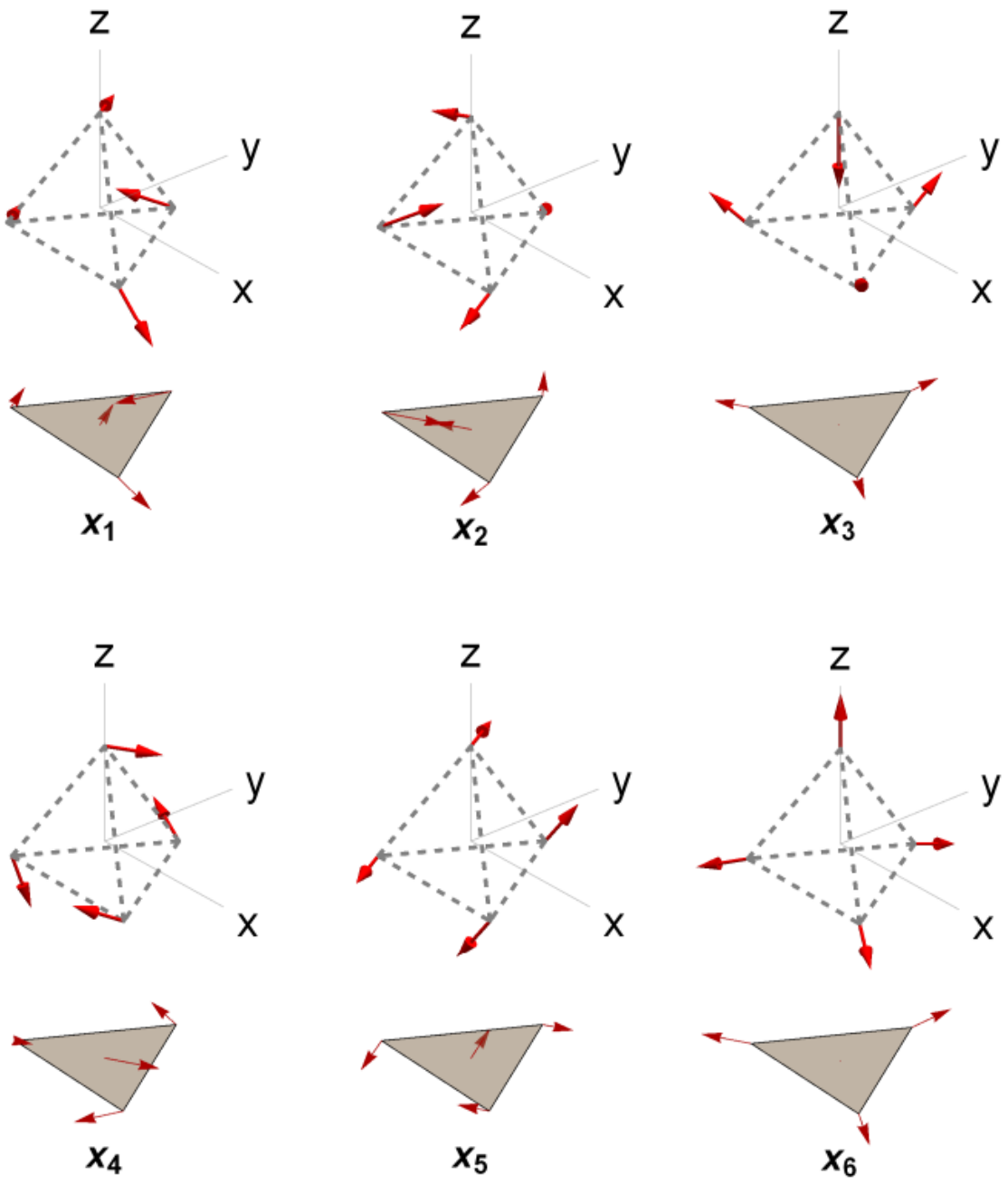

Figure 2.9: Normal modes of the four body system. The dashed tetrahedron corresponds to the equilibrium shape. The gray triangle represents the projection of the normal mode in the $x-y$ plane.

As in the three body problem, the vanishing angular momentum condition gives us the connection $\hat{\mathbf{n}}\,\dot{\phi} = -\lambda^2 \mathbf{S}(t)$ and the shape evolution up to leading order in λ $x_i(t) = x_{0i}\cos\omega_i t + p_{0i}/\omega_i \sin\omega_i t$. Consequently the evolution of the orientation is already fixed by the connection. By the symmetry of the equilibrium configuration, any path in shape space involving only the doublet modes cannot produce a rotation in the 4-body problem. To prove the latter statement, let us suppose that a solution of the equations of motion $\mathbf{s}(t)$ given by the doublet (x_4, x_5) induces a rotation about the axis $\hat{\mathbf{n}}$ with angular velocity $\dot{\eta}$. The tetrahedron configuration has a point non-axial symmetry group[2], and then there exists an element of this group such that its action on the solution $\mathbf{s}'(t)$ induces a rotation about an axis $\hat{\mathbf{n}}'$, but this action does not change the frequency. Therefore, $\mathbf{s}'(t)$ must correspond to a linear combination of the same doublet modes and then $\hat{\mathbf{n}}' \propto \hat{\mathbf{n}}$, concluding $\hat{\mathbf{n}}$=0. We can generalize this result to the following statement: *A system with a point non-axial symmetry group in its equilibrium configuration, cannot change its orientation by a cyclic change of shapes created by a doublet normal modes.*

2.5 The quantum case

Let us start with the quantum version of the Hamiltonian (2.36). The internal angular momentum in the shape space (2.37) is analog to the orbital angular momentum in the physical space, except for a "-2" factor which can be absorbed in by a redefinition $\mathbf{S} \to -2\mathbf{S}$, so that its components satisfy the usual angular momentum relations

$$[S_i, S_j] = i\epsilon_{ijk} S_k \,. \tag{2.38}$$

We perform this redefinition in (2.36) without actually relabeling the operator $\mathbf{S}$, then the Hamiltonian takes the form:

$$H = \sqrt{2}\left(N + \frac{3}{2}\right) + \frac{\lambda^2}{2}\left(\mathbf{L}^2 + \mathbf{L}\cdot\mathbf{S} + \frac{1}{4}\mathbf{S}^2\right) , \tag{2.39}$$

where $N = N_1 + N_2 + N_3$ and N_i is the number operator associated with the shape coordinate x_i. We shall omit the constant term in (2.39) all along the text. The previous Hamiltonian is split into four commuting terms,

$$H_1(x) = \sqrt{2}N\,, \quad H_2(x) = \frac{\lambda^2}{8}\mathbf{S}^2\,, \quad H_I(\mathsf{R}, x) = \frac{\lambda^2}{2}\mathbf{L}\cdot\mathbf{S}\,, \quad H_O(\mathsf{R}) = \frac{\lambda^2}{2}\mathbf{L}^2\,, \tag{2.40}$$

[2] A point non-axial group G is a group consisting of space transformations such that there is not an invariant line under all the elements of G.

so that the evolution operator $U(t) = e^{-iHt} = U_1(t)U_2(t)U_I(t)U_O(t)$ can be calculated separately for each of them.

We remind the reader that the total angular momentum in the body frame $\mathbf{L}$ is a left invariant vector field [63], and thus its components satisfy the commutation relations $[L_i, L_j] = -i\epsilon_{ijk}L_k$. Therefore all the expressions defined in terms of $\mathbf{L}$ differ from those defined in terms of the usual angular momentum operator. In Appendix D we show how to translate expressions written in terms of the left invariant vector $\mathbf{L}$ from those written in terms of the usual angular momentum operator, see also [14].

2.5.1 Coherent states

Let us reproduce the "most classical" state as in the three body problem: a coherent state. We consider that, at $t = 0$, the state of the system is $\Psi(\mathsf{R}, x) = \psi(x)\Phi(\mathsf{R})$, with $\psi(x) = \psi_{\vec{\alpha}}(x_1, x_2, x_3)$ a coherent state in shape space associated to the normal modes. For the orientational wavefunction we use the same that in the three body problem $\Phi(\mathsf{R}) = N_\Phi e^{\cos\eta}$. The result of applying $U_1(t)$ and $U_O(t)$ on $\Psi(\mathsf{R}, x)$ is

$$U_1(t)U_O(t)\Psi(\mathsf{R}, x) = \psi_{\vec{\alpha}_t}(x)\sum_{lkm} c^l_{km}(t)D^l_{km}(\alpha,\, \beta,\, \gamma)\,, \tag{2.41}$$

where $\vec{\alpha}_t = \vec{\alpha}e^{-i\omega t}$, $c^l_{km}(t) = c^l_{km}e^{-i\frac{l(l+1)}{2}\lambda^2 t}$ and $\omega = \sqrt{2}$. However, the applications of $U_2(t)$ and $U_I(t)$ are not trivial when the shape wavefunction corresponds to a coherent state, so we calculate them perturbatively. The evolution is explored with the reduced probability densities (2.35). As it is expected, the time-evolution of the coherent state in shape space induces a displacement of the orientation reduced density in $SO(3)$ in any direction, a feature which makes this system fundamentally different w.r.t.the three body problem. The effects of the shape wavefunction evolution on the orientation of the system, to order $O(\lambda^2)$, are encoded in $\langle S_i\rangle$, and to $O(\lambda^4)$ in $\langle S_iS_j\rangle$. In particular, for the shape coherent state $\psi_{\vec{\alpha}(\mathbf{r})}(x)$ with $\vec{\alpha}(\mathbf{r}) = r/\sqrt{2}\left(\hat{\theta} + i\hat{\varphi}\right) = r/\sqrt{2}\,(\cos\theta\cos\varphi - i\sin\varphi, \cos\theta\sin\varphi + i\cos\varphi, -\sin\theta)$, $\langle\mathbf{S}\rangle = r^2\hat{\mathbf{r}}$, and then the time-evolution of $\psi_{\vec{\alpha}(\mathbf{r})}(x)$ induces a rotation of the state along $\hat{\mathbf{r}} = (\cos\varphi\sin\theta, \sin\varphi\sin\theta, \cos\theta)$. In Fig. 2.10 we plot the evolution of the state initially given by a product of a shape coherent state $\psi_{\vec{\alpha}(\mathbf{r})}(x)$ and the orientation state $\Phi(\eta)$, with $r = 2$, $\theta = \pi/4, \varphi = \pi/4$, $\lambda = 0.3$, for $t = 2\pi n/4\omega$, $n = 0, 1, \ldots, 4$. It can be observed that the locus of points in $SO(3)$ where the system is most probably oriented (dark spot) is moving in the direction $\langle\mathbf{S}\rangle$, resembling a classical-like behavior

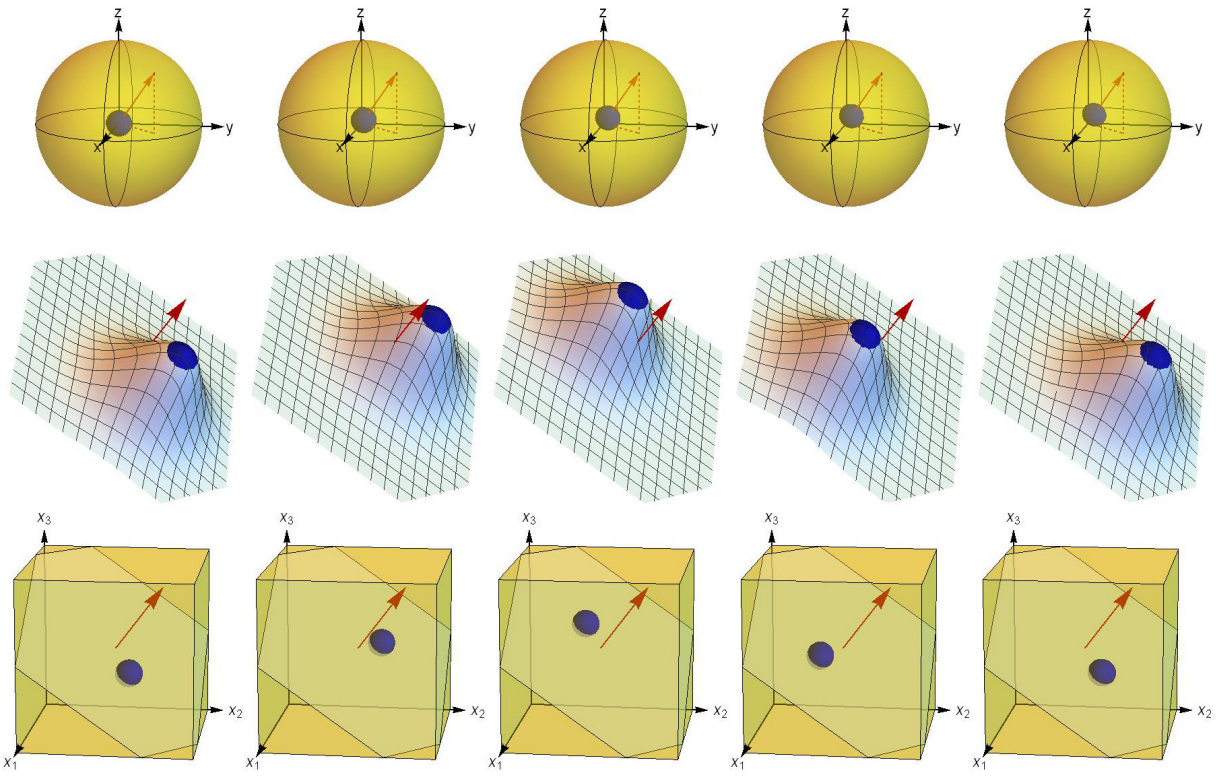

Figure 2.10: Sequence of the orientation change along the direction $\hat{\mathbf{r}}$ (red arrow) with $\theta = \varphi = \pi/4$ and $r = 2$, produced by a coherent state $\psi_{\vec{\alpha}(\mathbf{r})}(x)$. The top row depicts the reduced orientation probability density $P_t^O(\mathsf{R})$ in $SO(3)$, where the little dark spot corresponds to the region $P_t^O(\mathsf{R}) \geq 0.90\text{max}\,(P_t^O)$, for $t = \frac{2\pi n}{4\omega}$, $n = 0, 1, \ldots, 4$. The bottom row is analogous to the top one but with $P_t^S(x)$ in the shape space. The middle row depicts $P_t^S(x)$ in the shape space, restricted to the plane of rotation.

and as expected for the "most classical" quantum state. The dispersion of the orientation-reduced probability $P_t^O(\mathsf{R})$ will take place for a time scale much larger than the one when the change of its orientation occurs since, as discussed, the former is of order λ^4 while the latter is of order λ^2.

2.5.2 Anticoherent states

We will next consider the evolution of the opposite case, the "less localized" state in shape space: an anticoherent one. The initial state describing the orientation degrees of freedom will, as in

the other examples, be the localized state $\Phi(\mathsf{R}) = N_\Phi e^{\cos\eta}$. Thus, the initial total state in this case will be given by the tensor product of $\Phi(\mathsf{R})$ and an anticoherent state in the shape space sector.

We can apply exactly all the evolution operators $U_i(t)$ to the initial state except for the one generated by the interacting Hamiltonian H_I. To compute the action of U_I let us write $U_I(t) = e^{i\Lambda\mathbf{B}\cdot\mathbf{S}} = \sum_\mu (i\Lambda)^\mu (\mathbf{B}\cdot\mathbf{S})^\mu/\mu!$ where $\Lambda = \lambda^2 t/2$ and we have introduced the auxiliary operator $\mathbf{B} = -\mathbf{L}$ (see Appendix D). The operator $(\mathbf{B}\cdot\mathbf{S})^k$ for each k can be further expressed in terms of tensor operators (subsection 1.4) as

$$(\mathbf{B}\cdot\mathbf{S})^k = \sum_{\sigma=0}^{j} \alpha_\sigma^{(k)}(l,s) \sum_{\mu=-\sigma}^{\sigma} T^{(l)\dagger}_{\sigma\mu} \otimes T^{(s)}_{\sigma\mu}\,, \tag{2.42}$$

where $j = \min(2l, 2s, k)$, and k and σ must have the same parity (see Appendix C). The evolution of the state of the system, described by the density matrix $\rho(t) = |\Psi(t)\rangle\langle\Psi(t)|$, is thus given by

$$\rho(t) = U_I(t)\rho U_I(t)^\dagger = \sum_{N=0}^{\infty} \frac{(i\Lambda)^N}{N!} [\mathbf{B}\cdot\mathbf{S}, \ldots, [\mathbf{B}\cdot\mathbf{S}, \rho]]\ldots]\,, \tag{2.43}$$

where ρ can be written as a linear combination of operators of the form $\rho^l \otimes \rho^s = |m_1, l_1^{k_1}\rangle\langle m_2, l_2^{k_2}| \otimes |n_1, s_1^{m_{1s}}\rangle\langle n_2, s_2^{m_{2s}}|$, where the states $|m_1, l_1^{k_1}\rangle$ and $|n_1, s_1^{m_{1s}}\rangle$ are eigenstates of $(\mathbf{L}^2, L_z, L_{sz})$ and $(N, \mathbf{S}^2, S_3)$ with eigenvalues $(l(l+1), k, m)$ and $(n, s(s+1), m_s)$, respectively (see Appendix D). Since equation (2.43) is linear, the time evolution of the system for any state ρ can be computed as the sum of its constituent blocks $\rho^l \otimes \rho^s$.

The orientation-reduced probability density can therefore be written as

$$P_t^O(\mathsf{R}) = \langle \mathsf{R}|\mathrm{Tr}_s(\rho(t))|\mathsf{R}\rangle =: \sum_{N=0}^{\infty} \frac{(i\Lambda)^N}{N!} P_t^{(N)}(\mathsf{R})\,, \tag{2.44}$$

where $\langle \mathsf{R}|m, l^k\rangle = \langle \alpha, \beta, \gamma|m, l^k\rangle = D^{l*}_{mk}(\alpha, \beta, \gamma)$ and Tr_s stands for the partial trace over the shape degrees of freedom. As it can be observed, the computation of $P_t^O(\mathsf{R})$ reduces to calculate terms of the form $\mathrm{Tr}_s((\mathbf{B}\cdot\mathbf{S})^h \rho (\mathbf{B}\cdot\mathbf{S})^{h'})$, with $h, h' \in \mathbb{N}$, which can be written in terms of tensor operators as

$$\mathrm{Tr}_s((\mathbf{B}\cdot\mathbf{S})^h \rho (\mathbf{B}\cdot\mathbf{S})^{h'}) = \sum_{\sigma,\sigma'} \alpha_\sigma^{(h)}(l_1, s_1)\alpha_{\sigma'}^{(h')}(l_2, s_2) \sum_{\mu,\mu'} \left(T^{(l_1)\dagger}_{\sigma\mu} \rho^l T^{(l_2)\dagger}_{\sigma'\mu'}\right) \otimes \mathrm{Tr}_s\left(T^{(s_1)}_{\sigma\mu} \rho^s T^{(s_2)}_{\sigma'\mu'}\right). \tag{2.45}$$

The above expression is nonzero only if $s_1 = s_2 = s$ and $n_1 = n_2 = n$, in which case the density matrix associated with the shape state can be expressed as $\rho^s = \sum_{KQ} \rho^s_{KQ} T^\dagger_{KQ}$ with $\rho^s_{KQ} = \mathrm{Tr}(\rho^s T_{KQ})$, and therefore

$$\mathrm{Tr}_s\big((\mathbf{B}\cdot\mathbf{S})^h \rho (\mathbf{B}\cdot\mathbf{S})^{h'}\big) = \sum_{\sigma,\sigma'} \alpha^{(h)}_\sigma(l_1,s)\alpha^{(h')}_{\sigma'}(l_2,s) \sum_{\mu,\mu'} \left(\sum_{KQ} \rho_{KQ} \mathrm{Tr}_s(T_{\sigma\mu} T^\dagger_{KQ} T_{\sigma'\mu'}) \right) \big(T^{(l_1)\dagger}_{\sigma\mu} \rho^l T^{(l_2)\dagger}_{\sigma'\mu'}\big) \,. \tag{2.46}$$

In particular, when $h' = 0$, the following relation holds

$$\begin{aligned} \mathrm{Tr}_s\big((\mathbf{B}\cdot\mathbf{S})^h \rho\big) &= \sum_\sigma \alpha^{(h)}_\sigma(l_1,s) \sum_\mu \left(\sum_{KQ} \rho_{KQ} \mathrm{Tr}_s(T_{\sigma\mu} T^\dagger_{KQ}) \right) \big(T^{(l_1)\dagger}_{\sigma\mu} \rho^l\big) \\ &= \sum_\sigma \alpha^{(h)}_\sigma(l_1,s) \sum_\mu \rho_{\sigma\mu} \big(T^{(l_1)\dagger}_{\sigma\mu} \rho^l\big) \,, \end{aligned} \tag{2.47}$$

and a similar one is satisfied for $h = 0$. When $h, h' \neq 0$, the general expression of the trace of three tensor operators (C.8) must be used. The term $P^{(N)}_t(\mathsf{R})$ contains only contributions of the form $\mathrm{Tr}_s\Big((\mathbf{B}\cdot\mathbf{S})^h \rho (\mathbf{B}\cdot\mathbf{S})^{h'}\Big)$ with $h + h' = N$ or, in tensor operators, of the form $\mathrm{Tr}_s\Big(T_{\sigma\mu}\rho^s T_{\sigma'\mu'}\Big)$, with $\sigma' \leq h'$, $\sigma \leq h$. Then, due to Eq. (C.8) and the triangle condition on the 3j-symbols, $P^{(N)}_t(\mathsf{R})$ involves only coefficients $\rho^s_{\alpha\beta}$ with $\alpha \leq \sigma + \sigma'$. Based on the previous discussion, we conclude that for the density matrix $\rho = \rho^l \otimes \rho^s = \rho^b \otimes \rho_{a(x)}$, where $\rho_{a(x)}$ is the density matrix corresponding to a q-anticoherent state,

$$\begin{aligned} \mathrm{Tr}_s\Big((\mathbf{B}\cdot\mathbf{S})^h \rho (\mathbf{B}\cdot\mathbf{S})^{h'}\Big) &= \tfrac{1}{2s+1} \mathrm{Tr}_s\Big((\mathbf{B}\cdot\mathbf{S})^h (\rho^b \otimes \mathbb{1})(\mathbf{B}\cdot\mathbf{S})^{h'}\Big) \\ &= \tfrac{1}{2s+1} \sum_{\sigma=0}^{2s} \alpha^{(h)}_\sigma(l_1,s)\alpha^{(h')}_\sigma(l_2,s) \sum_\mu T^{(l_1)\dagger}_{\sigma\mu} \rho^b T^{(l_2)}_{\sigma\mu} \,, \end{aligned} \tag{2.48}$$

for all h, h' such that $h + h' \leq q$. From the properties of $\alpha^h_\sigma(l,s)$ (see Appendix C) it follows that $\mathrm{Tr}_s\Big((\mathbf{B}\cdot\mathbf{S})^h \rho (\mathbf{B}\cdot\mathbf{S})^{h'}\Big) = 0$ when h and h' have different parity, and therefore $P^N_t(\mathsf{R}) = 0$ for $N \leq q$ and N odd.

With the help of the above results, it can be finally proved that the orientation reduced probability density for anticoherent states of order $q \geq 3$ to order $O(\Lambda^3)$ is

$$\begin{aligned} P^O_t(\mathsf{R}) &= \langle \mathsf{R}|\rho^b|\mathsf{R}\rangle - \tfrac{\Lambda^2}{2(2s+1)} \Big(\big(\alpha^{(0)}_0(l_1,s)\alpha^{(2)}_0(l_2,s) + \alpha^{(0)}_0(l_2,s)\alpha^{(2)}_0(l_1,s)\big) \langle \mathsf{R}|T^{(l_1)\dagger}_{00} \rho^b T^{(l_2)}_{00}|\mathsf{R}\rangle \\ &\qquad -2\alpha^{(1)}_1(l_1,s)\alpha^{(1)}_1(l_2,s) \sum_\mu \langle \mathsf{R}|T^{(l_1)\dagger}_{1\mu} \rho^b T^{(l_2)}_{1\mu})|\mathsf{R}\rangle \Big) \\ &= \langle \mathsf{R}|\rho^b|\mathsf{R}\rangle - \tfrac{\Lambda^2 s(s+1)}{6} \Big(\big(l_1(l_1+1) + l_2(l_2+1)\big) \langle \mathsf{R}|\rho^b|\mathsf{R}\rangle \\ &\qquad - \tfrac{2\sqrt{l_1(l_1+1)(2l_1+1)l_2(l_2+1)(2l_2+1)}}{3} \sum_\mu \langle \mathsf{R}|T^{(l_1)\dagger}_{1\mu} \rho^b T^{(l_2)}_{1\mu}|\mathsf{R}\rangle \Big) \,, \end{aligned} \tag{2.49}$$

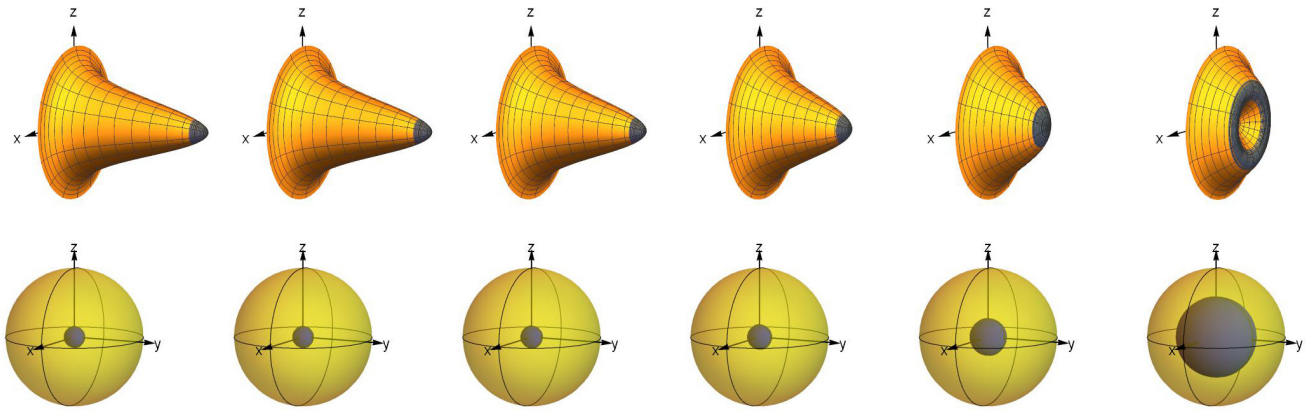

Figure 2.11: Evolution of $P_t(\mathsf{R})$ in $SO(3)$ and in the cutoff plane xy of $SO(3)$ for $\Lambda = 0.08n$ with $n = 0, 1, \ldots, 5$, when the shape state is 3-anticoherent and has $s = 3$.

which, by virtue of the expressions of $T^{(l)}_{1\mu}$ in terms of the components of $\mathbf{L}$ (see Appendix C), takes the form

$$P^O_t(\mathsf{R}) = \left(1 - \Lambda^2 \frac{s(s+1)}{6}\mathbf{L}^2\right) P^O_0(\mathsf{R}) + \mathscr{O}(\Lambda^4)\,. \tag{2.50}$$

The latter result is also valid for any density matrix $\rho = \sum c_{\mathbf{l}_i,\mathbf{s}_i} |\mathbf{l}_1\rangle\langle\mathbf{l}_2| \otimes |\mathbf{s}_1\rangle\langle\mathbf{s}_2|$, where the sum is over $\mathbf{l}_i$ and $\mathbf{s}_i$ for $i = 1, 2$ with $\mathbf{l}_i = (m_i, l_i^{k_i})$ and $\mathbf{s}_i = (n_i, s_i^{m_{si}})$. The time evolution does not distinguish a preferred direction, and then gives rise to an isotropic evolution, in the sense that $P^O_t(\mathsf{R})$ evolves at the same rate in each direction of $SO(3)$ as seen in the angle-axis representation. We plot in Fig. 2.11 $P^O_t(\mathsf{R})$ when the shape state corresponds is the octahedron state $|\psi_{\text{oct}}\rangle$ (see subsection 1.6.3), a 3-anticoherent spin-3 state. We see that the evolution is isotropic, as the dark region in figure 2.11 is expanding uniformly in all directions. Meanwhile, in fig. 2.12 we present the plot of $P^O_t(\mathsf{R})$ when the shape state is the triangular prism $|\psi_{\text{TP}}\rangle$, which is a 2-anticoherent spin-3 state. Comparing both evolutions, we can appreciate a similar evolution up to the last two frames, where the Λ^3 term becomes significant and then the evolution turns into anisotropic.

We can calculate explicitly the anisotropic evolution of $P^O_t(\mathsf{R}) = P^O_t(\mathsf{R}(\eta, \hat{\mathbf{n}}(\theta, \varphi))$ with its expansion in spherical harmonics for each Λ and η

$$P^O_t(\mathsf{R}) = \sum_{lm} f_{lm}(\eta, \Lambda) Y_{lm}(\theta\,, \varphi)\,, \tag{2.51}$$

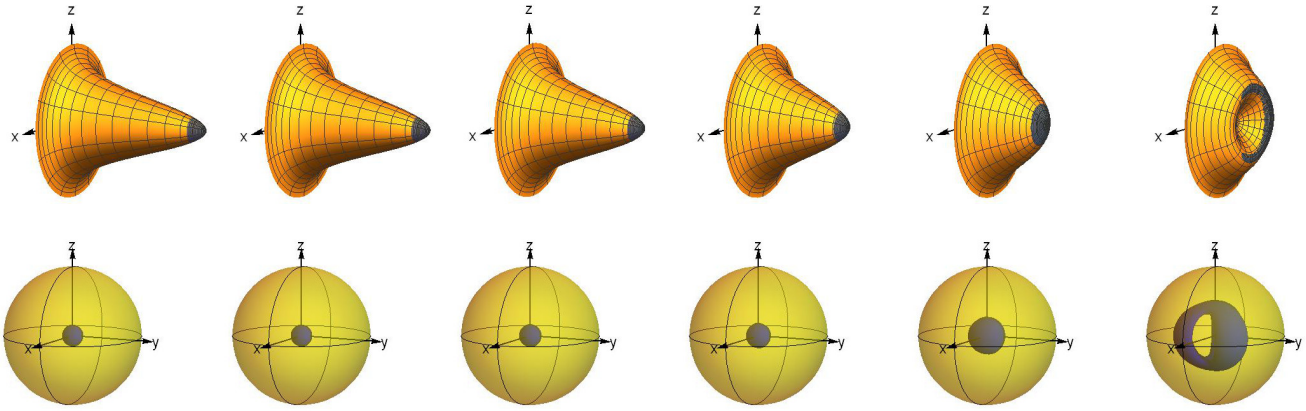

Figure 2.12: Evolution of $P_t(\mathsf{R})$ in $SO(3)$ and in the cutoff plane xy of $SO(3)$ for $\Lambda = 0.08n$ with $n = 0, 1, \ldots, 5$, when the shape state is the triangular prism, which is 2-anticoherent and has $s = 3$.

with the rotational invariant quantities $c_l(\eta\,, \Lambda)$

$$c_l(\eta\,, \Lambda) := \left(\sum_{m=-l}^{l} |f_{lm}(\eta, \Lambda)|^2 \right)^{1/2} . \tag{2.52}$$

An isotropic evolution occurs when $c_l(\eta, \Lambda) = 0$ for $l > 0$ for all Λ, which is the case for the octahedral state up to third order of Λ. While, for the triangular prism case, c_3 is different to zero. In Fig. 2.13 we present the plots of $c_0(\eta, \Lambda)$ and $c_3(\eta, \Lambda)$. Due to the spread of $c_0(\eta, \Lambda)$, the values of $c_3(\eta, \Lambda)$ become comparable and for that reason we can see the anisotropy evolution in the figure 2.12. $c_0(\eta, \Lambda)$ is the same for the octahedral and the triangular prism case.

To finish with this section, we calculate perturbatively the shape reduced density $P_t^S(q)$ for states with orientational part as given in the last examples. Considering only the interaction term of the Hamiltonian $U_I = \frac{\lambda^2}{2}\mathbf{L}\cdot\mathbf{S}$, it's obtained that

$$P_t^S(q) = \left(1 - \frac{c_1^2\Lambda^2}{2}\mathbf{S}^2\right) P_0^S(q) + \mathscr{O}(\Lambda^4)\,. \tag{2.53}$$

The evolution is similar than the case of the orientational reduced density $P_t^O(\mathsf{R})$ when the shape state is at least 3-anticoherent. When the shape state is eigenvector of the N and $\mathbf{S}^2$ operators, the shape wavefunction ψ and also its probability density $P_t^S(q)$ is factorizable in two normalized functions $P_t^S(q) = R(r,t)\chi(\theta,\phi,t)$, where (r,θ,ϕ) are the spherical coordinates in the shape space. The octahedron and triangular prism states satisfy this property and they have

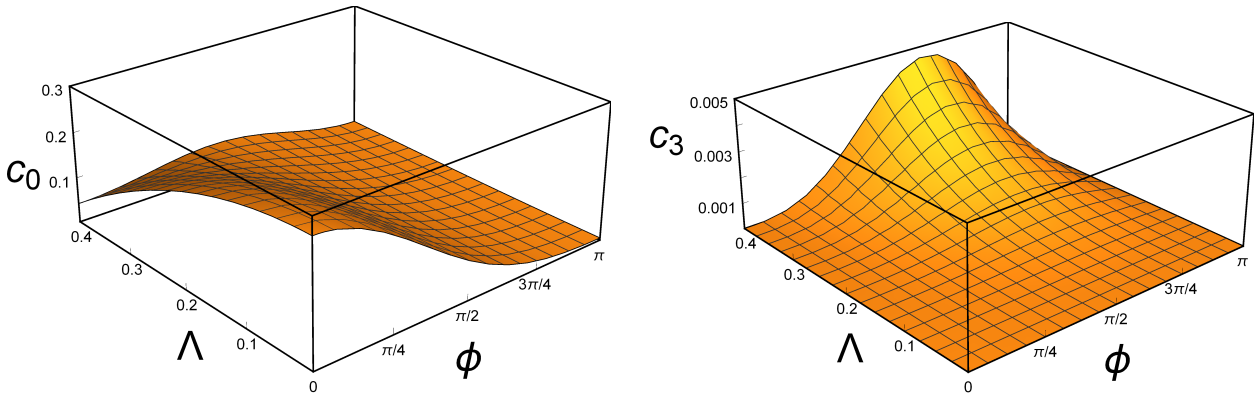

Figure 2.13: Coeffcients c_0 y c_3 to measure the anisotropy of $P_t^O(\mathsf{R})$ when the internal state is the triangular prism. To the octahedral case, we have the same function of c_0 but $c_3(\eta, \Lambda) = 0$.

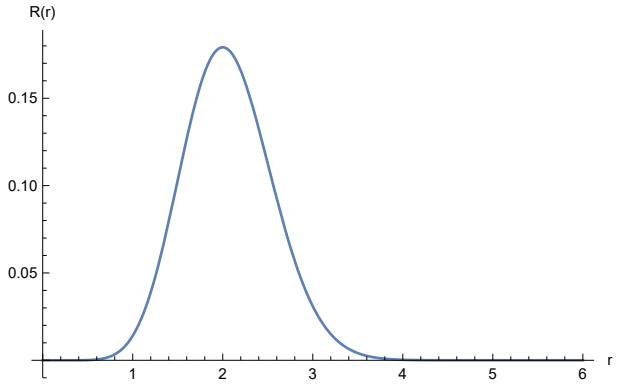

Figure 2.14: Radial function $R(r)$ of the shape reduced density $P_t^S(q)$ when the orientational wavefunction is $\Phi(\eta) = N_\Phi e^{\cos(\eta)}$ and the shape state satisfy $N|\psi\rangle = 3|\psi\rangle$, $\mathbf{S}^2|\psi\rangle = 3(3+1)|\psi\rangle$, like the octahedron and the triangular prism states.

the same radial function $R(r)$ which is constant over time (see Fig. 2.14). On the other side, the angular function written in the spherical harmonics basis, we turn out all the coefficients decreasing as Λ^2, except the coefficient associated of $Y_0^0(\theta, \phi)$. It means the evolution will decreased the inhomogeneous part of the state, as we can see in the Figs. 2.15 and 2.16 for octahedron and triangular prism cases, respectively. The radius in the direction $\hat{\mathbf{n}}(\theta, \phi)$ is equal to the value of $\chi(\theta, \phi)$. We can observe the symmetries of the constellations in the shape reduced probabilities densities, and how the graphs are only reescaled with respect to the time. In the last screen of the graphics ($\Lambda = 0.4$), we obtain a scaling of 5/6 and the shape of the functions doesn't change.

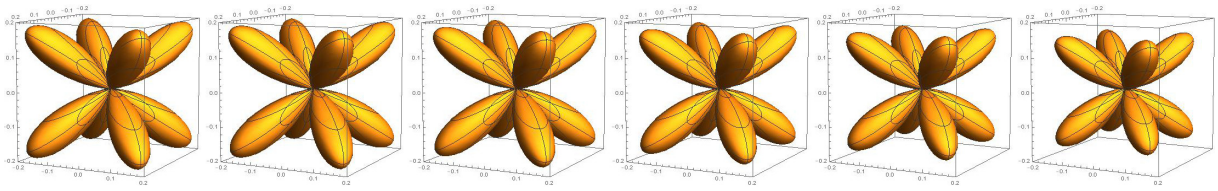

Figure 2.15: Evolution of the angular function of $P_t^S(q)$, $\chi(\theta,\phi)$ of the octahedron state for $\Lambda = 0.08n$, with $n = 0, 1, \ldots, 5$. The radius in the direction $\hat{\mathbf{n}}(\theta,\phi)$ is equal to the value of $\chi(\theta,\phi)$. The function is only rescaled by 5/6 in the last snapshot.

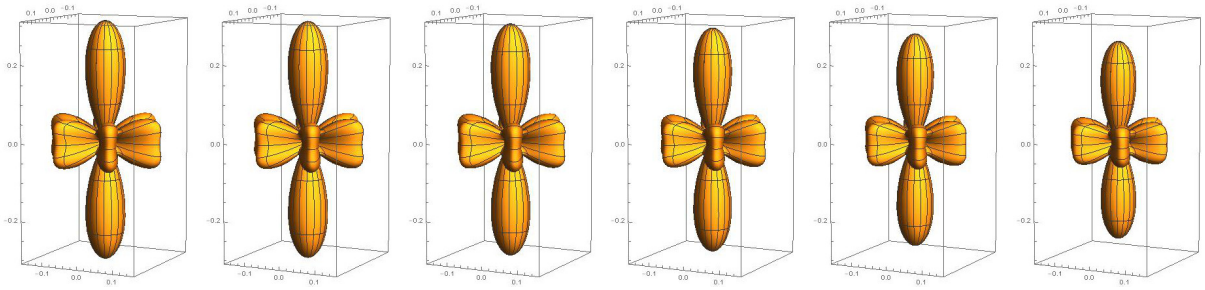

Figure 2.16: Evolution of the angular function of $P_t^S(q)$, $\chi(\theta,\phi)$ of the triangular prism state for $\Lambda = 0.08n$, with $n = 0, 1, \ldots, 5$. The radius in the direction $\hat{\mathbf{n}}(\theta,\phi)$ is equal to the value of $\chi(\theta,\phi)$. The function is only rescaled by 5/6 in the last snapshot.

The evolved state with the octahedron internal state is a superposition of states with a rotation in every axis, which is the opposite evolution that in the coherent case. Suppose we have a cluster of particles which fits with our model and we are monitoring the evolution of its dipole moment, which has an initial expectation value $\langle \mathbf{P} \rangle_0 = \mathbf{r}$. If the internal state is coherent in each period of cyclic shape evolution, we observe that the expectation value of $\mathbf{P}$ has rotated, $\langle \mathbf{P} \rangle_t = \mathsf{R}\,\mathbf{r}$. However, if the internal state is an anticoherent one, $\langle \mathbf{P} \rangle$ would decrease by the isotropic evolution. With these two extreme cases we explained how an experimentalist can predict properties of the internal states via monitoring the orientations evolution. The internal state of the system is not always admissible to the experimenter, however, it's encoded in the orientations evolution, and indeed, it doesn't depend to the initial orientations state. In fact, if it's possible to observe the evolution with different orientations states, one is able to obtain more information of the internal state.

2.5.3 Shape states with axial symmetry

To conclude this chapter, we give an idea of the engineering in the shape state to do an specific orientational evolution. In the last two subsections, we obtain that the coherent and anticoherent states in the shape space sector induce a directional or isotropic evolution in the orientational wavefunction, respectively. Now, we will build shape states with axial symmetry and observe that the induced evolution is also axial. In all the examples that we will exposed later we have observed that the S^2 term of the hamiltonian only increases the dispersion of $P_t^S(x)$ over time. To focus in the effects of the interaction term of the Hamiltonian, we don't consider the S^2 term. Let us remember that a coherent state with $\vec{\alpha} \in \mathbb{C}^3$ and such that

$$\begin{array}{rclcl} \mathrm{Re}(\vec{\alpha}(\theta,\phi)) & = & \frac{r}{\sqrt{2}}\hat{\theta} & = & \frac{r}{\sqrt{2}}(\cos\theta\cos\phi, \cos\theta\sin\phi, -\sin\theta)\,, \\ \mathrm{Im}(\vec{\alpha}(\theta,\phi)) & = & \frac{r}{\sqrt{2}}\hat{\phi} & = & \frac{r}{\sqrt{2}}(-\sin\phi, \cos\phi, 0)\,, \end{array} \tag{2.54}$$

has an expectation value of the angular momentum, and then induces a rotation along the axis $\mathrm{Re}(\vec{\alpha}) \times \mathrm{Im}(\vec{\alpha})$. Now, we consider a superposition of the coherent states $\psi_{\vec{\alpha}(\theta,\phi)}(x_1, x_2, x_3)$ for every $\phi \in (0, 2\pi)$, with

$$\begin{array}{rcl} \psi(x_1,x_2,x_3;r,\theta) & = & N\int \psi_{\vec{\alpha}}(x_1,x_2,x_3)\,d\phi\,, \\ & = & Ne^{-\frac{1}{2}\left(x_1^2+x_2^2+(x_3+r\sin\theta)^2\right)}\int \exp\left[(x_2\cos\theta - ix_1)r\sin\phi + (x_1\cos\theta + ix_2)r\cos\phi)\right]d\phi \\ & = & Ne^{-\frac{1}{2}\left(x_1^2+x_2^2+(x_3+r\sin\theta)^2\right)}J_0\left(r\sin\theta\sqrt{x_1^2+x_2^2}\right)\,, \end{array} \tag{2.55}$$

where N is the normalization factor

$$N^{-1} = \pi^{3/4}e^{-\frac{(r\sin\theta)^2}{4}}\sqrt{I_0\left(\frac{(r\sin\theta)^2}{2}\right)}\,, \tag{2.56}$$

and $J_n(z)$ is the Bessel function of the first kind, and $I_n(z)$ the modified Bessel function of the first kind.

We show in the figure 2.17 the locus expectation values of the position (blue arrow and cone), the momentum (red arrow and cone) in the shape space (x_1, x_2, x_3), and the expectation value of the angular momentum in the physical space (purple arrow and cone), of the constituent coherent states of (2.55) for $\theta = \pi/2$ and $\pi/3$.

We can also obtain its decomposition over the eigenstates of the 3D-isotropic harmonic oscillator (see Appendix E), with a uniform distribution of N states around the ring, and taking

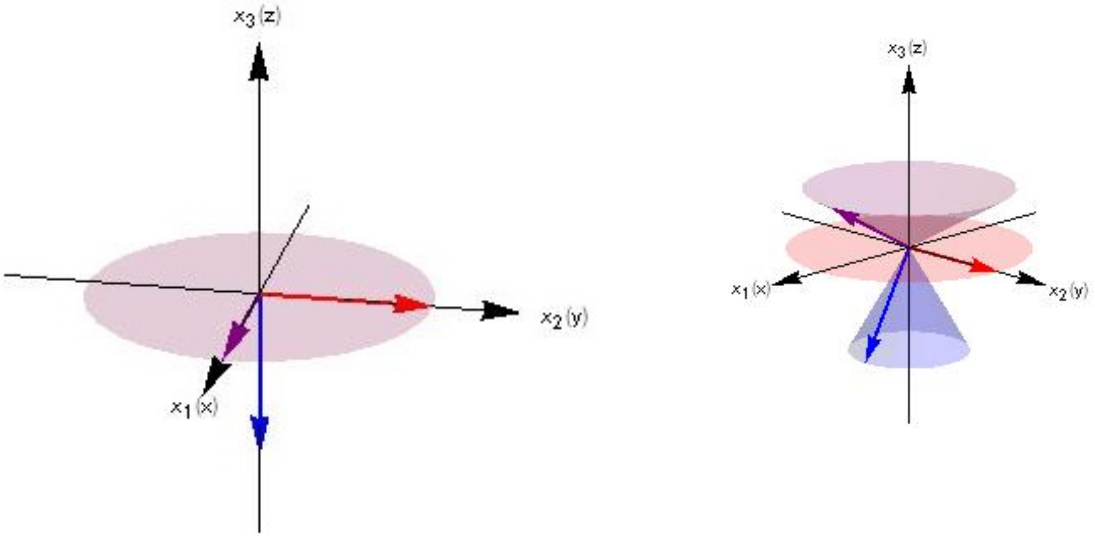

Figure 2.17: The blue (red) cone shows the direction of the expectation value of the position (momentum) of each constituent coherent state of (2.55) in the shape space (x_1, x_2, x_3), and the purple cone are the respective rotation axes of each coherent state in the physical space (x, y, z), for $\theta = \pi/2$ (left) and $\theta = \pi/3$ (right).

the $N \to \infty$ limit for $\theta = \pi/2$,

$$\begin{aligned}
|\psi\rangle &= N_0 \sum_{k=0}^{N-1} \left| \tfrac{r}{\sqrt{2}}(-i \sin \tfrac{2\pi k}{N}, i \cos \tfrac{2\pi k}{N}, -1) \right\rangle \\
&= N_0 \left| -\tfrac{r}{\sqrt{2}} \right\rangle_3 \sum_{n_1,n_2=0}^{\infty} \left(i \tfrac{r}{\sqrt{2}} \right)^{n_1+n_2} \tfrac{(-1)^{n_1}}{\sqrt{n_1!}\sqrt{n_2!}} \sum_{k=0}^{N-1} \tfrac{1}{N} \left(\sin \tfrac{2\pi k}{N} \right)^{n_1} \left(\cos \tfrac{2\pi k}{N} \right)^{n_2} |n_1, n_2\rangle \\
\lim_{N\to\infty} &= N_0 \left| -\tfrac{r}{\sqrt{2}} \right\rangle_3 \sum_{n_1,n_2=0}^{\infty} \left(i \tfrac{r}{\sqrt{2}} \right)^{n_1+n_2} \tfrac{(-1)^{n_1}}{\sqrt{n_1!}\sqrt{n_2!}} \int_0^{2\pi} (\sin x)^{n_1} (\cos x)^{n_2} \, dx |n_1, n_2\rangle \\
&= N_0 \left| -\tfrac{r}{\sqrt{2}} \right\rangle_3 \sum_{n_1,n_2} \left(-\tfrac{r^2}{2} \right)^{n_1+n_2} \tfrac{\sqrt{(2n_1)!(2n_2)!}}{4^{n1+n2} n_1! n_2! (n_1+n_2)!} |2n_1, 2n_2\rangle \,,
\end{aligned} \tag{2.57}$$

with $N_0^{-1} = 2\pi \sqrt{I_0\left(\frac{r^2}{2}\right)}$.

The equation (2.55) tells us that a non-trivial time evolution of $P_t^O(\mathsf{R})$ is seen up to second order of λ^2. Now, we calculate the time evolution of this state. The evolution operator $U_1(t)$ changes $r \to re^{-i\sqrt{2}t}$ (except in the normalization constant). The figure 2.18 shows us the time evolution of (2.55) for $\lambda = 0.3$, $r = 2.3$ and $\theta = \pi/2$ (top row). We can see $P_t^O(\mathsf{R})$ spreads uniformly along the x-y plane.

In the fig. 2.19, we use $\theta = \pi/3$, $r = 2.3$ and $\lambda = 0.3$. We were expecting that the state rotates around the purple cone of figure 2.17. However, our state doesn't lift in the z direction,

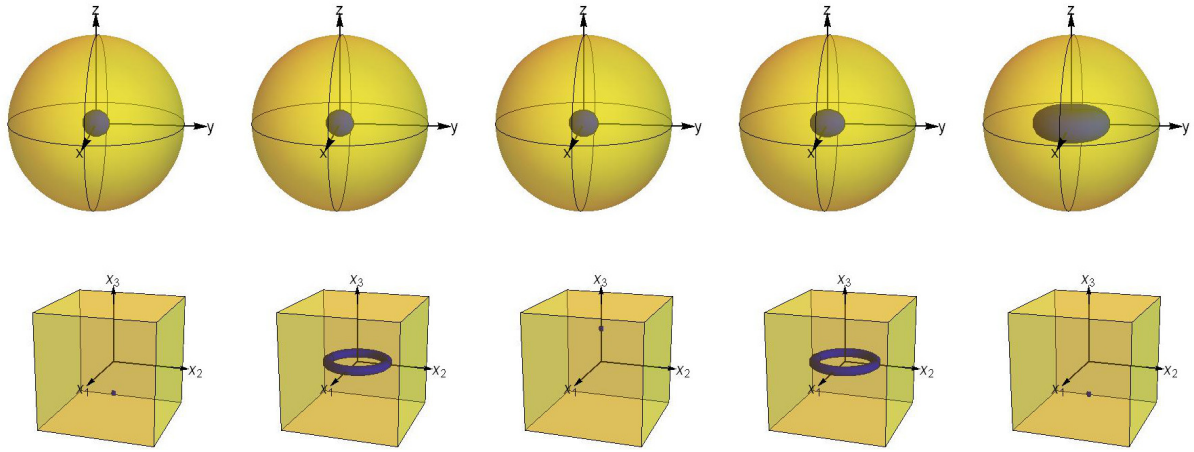

Figure 2.18: The top (bottom) row is $P_t^O(\mathsf{R})$ ($P_t^S(x_i)$) of the wavefunction (2.55) with $t = 2\pi k/n$, $n = 0, 1, \ldots, 4$, $\theta = \pi/2$, $r = 2.3$ and $\lambda = 0.3$ $P_t^S(x_i)$ initially is concentrated in the x_3 axis, then it spreads uniformly around the $x_1 - x_2$ plane, getting its maximum where $t = \pi/2$. After that, the wavefunction concentrates again in the positive x_3 axis and reversed the evolution. Meanwhile, $P_t^O(\mathsf{R})$ spreads uniformly in the x-y plane.

and is because the superposition has a destructive interference along this component. We need to add a relative phase in the superposition,

$$\psi(x_1, x_2, x_3; r, \theta) = N \int e^{if(\phi)} \psi_{\vec{\alpha}}(x_1, x_2, x_3)\, d\phi\,, \tag{2.58}$$

where $f(\phi + 2\pi) = f(\phi)$. In particular, we use $f(\phi) = n\phi$. Then

$$\psi(x_1, x_2, x_3; r, \theta) = N J_n(r \sin\theta \rho_s) e^{-\frac{1}{2}\left(\rho_s^2 + (x_3 + r\sin\theta)^2\right) + in\phi_s}\,, \tag{2.59}$$

with

$$N^{-1} = \pi^{3/4} e^{-\frac{(r\sin\theta)^2}{4}} \sqrt{I_n\left(\frac{(r\sin\theta)^2}{2}\right)}\,, \tag{2.60}$$

where $x_1 = \rho_s \cos\phi_s$, $x_2 = \rho_s \sin\phi_s$. We plot the state for $n = 2, 4$, in figures 2.20 and 2.21, with $\lambda = 0.3$, $r = 2.3$, $\theta = \pi/2$, like the state shown in fig. (2.18) (which is the case with $n = 0$). The probability density of orientation raises up in the z axis and spread uniformly in the $x - y$ plane. This can be understand in this way: the $n = 0$ case is, by construction, an infinite superposition of coherent states, all with initial position ($t = 0$) concentrated in $x_3 = r$. Every coherent state has a momentum on a different direction in the $x_1 - x_2$ plane, and then, to $t > 0$, each one moves

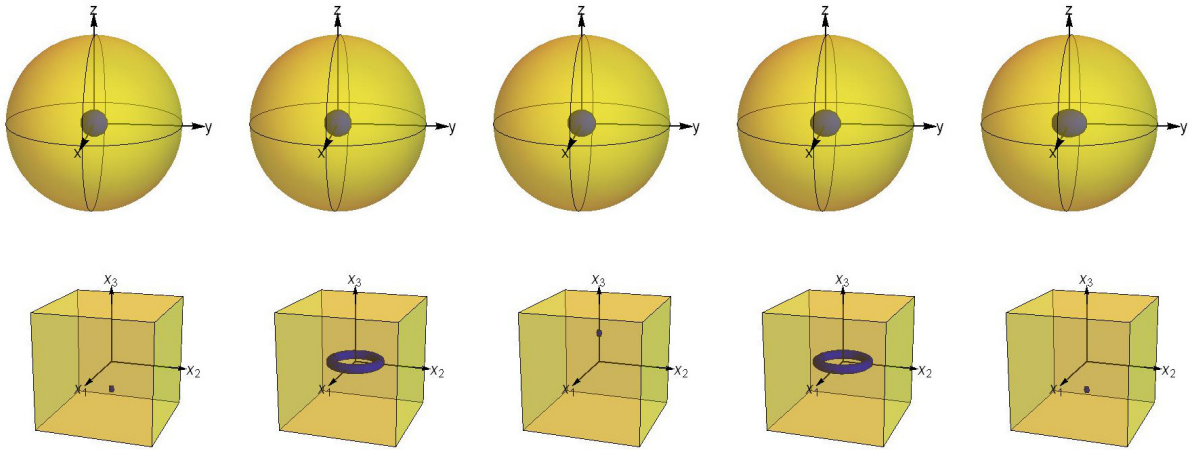

Figure 2.19: The top (bottom) row is $P_t^O(\mathsf{R})$ ($P_t^S(x_i)$) of the wavefunction (2.55) with $t = 2\pi k/n$, $n = 0, 1, \ldots, 4$, $\theta = \pi/3$, $r = 2.3$ and $\lambda = 0.3$. Spite of the initial coherent states, which lift $P_t^O(\mathsf{R})$ in the z direction, the final state doesn't, only spreads uniformly in the $\mathbf{x} - \mathbf{y}$ plane. $P_t^S(x_i)$ initially is concentrated in the x_3 axis, and then it spreads uniformly around the $x_1 - x_2$ plane, getting its maximum when $t = \pi/2$.

to its respective direction, turning the localized state to one with same probability in a ring of the $x_1 - x_2$ plane. After that, the state concentrates again in the x_3 axis but now in $x_3 = -r$. Now, if we put the relative phase $e^{in\phi}$ of each coherent state, we add an additional momentum with direction $\hat{\phi}$, magnitude proportional to n, and sense sgn (n). Each coherent state raises up and twists in the shape space, given n cycles in a period. In conclusion, $n = 0$ case only spreads and comprises around the $x_1 - x_2$ plane in its evolution, and with $n \neq 0$, the state spreads and comprises while twists in all its evolution. P_t^S with $n \neq 0$ is never concentrated in the x_3 axis, because there are destructive interference in this axis, the contrary situation that in $n = 0$.

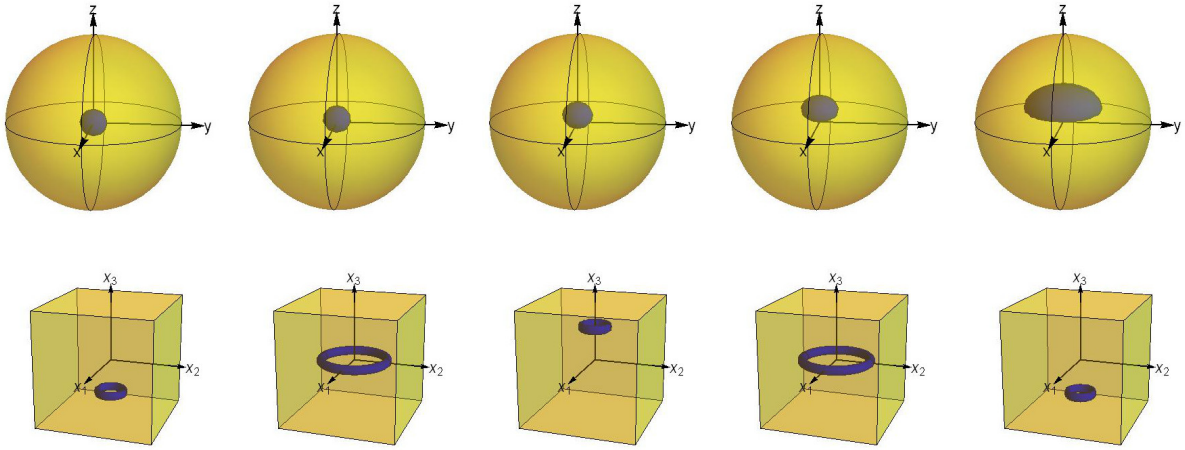

Figure 2.20: The evolution of the system (2.59) with $n = 2$ and the same values of the state shown in fig. 2.18. P_t^O spreads uniformly in the xy plane while raises up in the z axes.

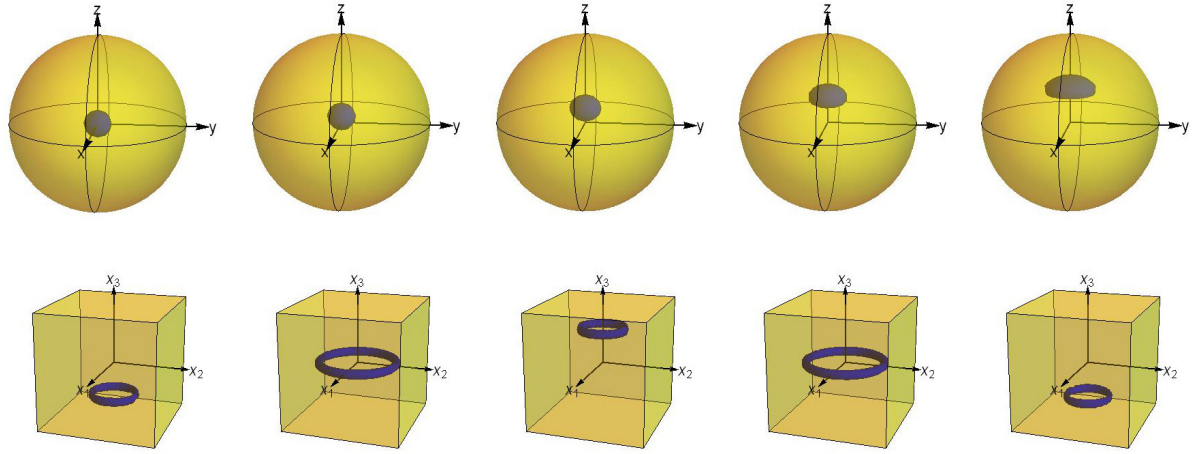

Figure 2.21: The evolution of the system (2.59) with $n = 4$ and the same values of the state shown in fig. 2.18. We see that the ring in P_t^S has a bigger radius and P_t^O raises up in the z axes more quickly than the $n = 2$ case.

Part II

Shapes in the Hilbert Space of Spin States

Chapter 3

Geometry of the spin coherent states

Geometry is knowledge of the eternally existent.

Pythagoras

In this chapter, we study algebraic and geometric properties of the Hilbert space of spin-s states, in particular those related to the set of the most classical states, which is the set of the spin coherent states. One of our key tools is the Majorana representation, which is extensively reviewed section 3.1 . In section 3.2 we discuss the Hilbert space as a principal fiber bundle with the group $SO(3)$ (or $SU(2)$). In the last two sections, we concentrate in the algebraic and geometric properties of the set of spin coherent states.

We make some conventions of our notation, different to the first part of the text. General directions in physical $\mathbb{R}^3$ will be denoted by c, n, m, *etc.*, while x, y, z will be reserved for the cartesian axes. We denote by $|n\rangle$ the spin coherente (SC) state in the direction n in a general spin-s, and reserve the symbol $|\hat{n}\rangle$ for the spin-1/2 states, so that we can write without problems the formula $|n\rangle = |\hat{n}\rangle \otimes \ldots \otimes |\hat{n}\rangle$. Our discussion takes place either in the Hilbert space $\mathscr{H}^{N+1}$ of the system, or in the projective Hilbert space $\mathbb{P}(\mathscr{H}^{N+1}) \equiv \mathbb{P}^N$, where points are equivalence classes of normalized states differing by a phase factor, and can be identified with the corresponding density matrix. We often omit the superindex when the dimension of the spin state space is clear from the context. Accordingly, we denote the projection of the state $|\Psi\rangle \in \mathscr{H}$ by $[\Psi]$ or $\rho_\Psi \in \mathbb{P}$. Finally, the Majorana constellation of a state $|\Psi\rangle$ (or $[\Psi]$), consisting of the stars $\{n_k\}_{k=1}^N$ is denoted by $|n_1, n_2, \ldots, n_N\rangle$, note that the ordering of the stars is irrelevant. We also sometimes refer the Majorana stars of a state with their corresponding

(via stereographic projection) complex numbers, say, $\{\gamma_1, \ldots, \gamma_N\}$.

3.1 Majorana representation revisited

In section 1.5, we give the most abstract definition of the Majorana representation, which indeed is the first definition given by Majorana [66]. Now, to extract all the information that this representation can give us, we expose three more intuitive constructions.

3.1.1 Spin-s state from spin-1/2 constituents

It is well known that the spin-s state space is mathematically equivalent to the totally symmetric sector of the $2s$-fold tensor power of the spin-1/2 state space. In other words, even though a particular spin-s system might owe its angular momentum to, say, a pair of particles orbiting each other, the properties, in a certain state of the system, under rotations, are indistinguishable from those of a system of $2s$ spin-1/2 particles, in a particular, totally symmetric (under exchange of any pair of particles) state. The latter can always be obtained by considering first a separable state $|\hat{n}_1\rangle \otimes \ldots \otimes |\hat{n}_N\rangle$, where $|\hat{n}\rangle$ is a spin-1/2 state, and subsequently symmetrizing it by summing over all permutations of the particles in the available tensor factors, to obtain the totally symmetric state $|\Psi\rangle$,

$$|\Psi\rangle = |n_1, \ldots, n_N\rangle = \frac{A_\Psi}{N!} \sum_{\sigma \in S_N} |\hat{n}_{\sigma_1}\rangle \otimes \ldots \otimes |\hat{n}_{\sigma_N}\rangle \,, \tag{3.1}$$

where A_Ψ is a normalization factor,

$$A_\Psi^2 = \frac{N!}{\sum_{\sigma \in S_N} \langle \hat{n}_1 | \hat{n}_{\sigma_1}\rangle \ldots \langle \hat{n}_N | \hat{n}_{\sigma_N}\rangle} \,, \tag{3.2}$$

and S_N is the permutation group of N objects. Thus, any spin-s state is equivalent to a state $|\Psi\rangle$ as in (3.1), and the Majorana constellation of the former is the set of unit vectors $\{n_i\}$, $i = 1, \ldots, N$, that appears in (3.1).

3.1.2 A laboratory definition

The above considerations lead us to an operational definition of the N (possibly coinciding) directions n_i associated to an arbitrary spin-s state $|\Psi\rangle$ (see, *e.g.*, [3]). Independent that if the system in question is made up of spin-1/2 particles, we may use the representation of $|\Psi\rangle$

in (3.1) to conclude that there are, in general, N directions in space such that, if a Stern-Gerlach apparatus is pointed along them, the probability of measuring the minimal spin projection $-s$ is zero. Indeed, if the apparatus is pointed to an arbitrary direction m, and the total spin projection in that direction is measured to be $-s$, this means that, in the constituent spin-1/2 picture, each spin-1/2 was measured to have projection $-1/2$. If now the direction m coincides with one of the stars n_i, the probability that that particular spin, which "points along" n_i, will project to $-1/2$ is zero (since $|\hat{n}_i\rangle$ and $|-\hat{n}_i\rangle$ are orthogonal states), and hence the probability that the total projection of the system is measured to be $-s$ is also zero. In fact, that same reasoning reveals that if n_i has multiplicity k (*i.e.*, there are k stars coinciding there), then a measurement of the spin projection along that direction has zero probability of producing any of the values $-s$, $-s+1$, ..., $-s+k-1$.

3.1.3 Majorana polynomial as a transition amplitude

In view of the above, it should not come as a surprise that the inner product $\langle -n|\Psi\rangle$ is actually proportional to the Majorana polynomial $p_{|\Psi\rangle}(\zeta)$, where $\zeta = \tan\frac{\theta}{2}e^{i\phi}$ is the stereographic image of $n = (\sin\theta\cos\phi, \sin\theta\sin\phi, \cos\theta)$.

We begin by clarifying the relation, alluded to above, between $p_{|\Psi\rangle}(\zeta)$ and $\langle -n|\Psi\rangle$. For a spin-1/2 state we have

$$|\hat{n}\rangle = \cos\frac{\theta}{2}|\hat{z}\rangle + e^{i\phi}\sin\frac{\theta}{2}|-\hat{z}\rangle\,, \quad |-\hat{n}\rangle = \sin\frac{\theta}{2}|\hat{z}\rangle - e^{i\phi}\cos\frac{\theta}{2}|-\hat{z}\rangle\,, \tag{3.3}$$

so that

$$\langle -\hat{n}|\hat{n}_i\rangle = \cos\frac{\theta}{2}\cos\frac{\theta_i}{2}e^{-i\phi}(\zeta-\zeta_i) = \cos\frac{\theta}{2}e^{-i\phi}\frac{\zeta-\zeta_i}{\sqrt{1+|\zeta_i|^2}}\,. \tag{3.4}$$

Using (3.1) for $|\Psi\rangle$ we then find

$$\langle -n|\Psi\rangle = A_\Psi\left(\cos\frac{\theta}{2}e^{-i\phi}\right)^N\prod_{i=1}^N\frac{\zeta-\zeta_i}{\sqrt{1+|\zeta_i|^2}}\,. \tag{3.5}$$

On the other hand, the coefficient c_s of the maximal power of ζ in $p_{|\Psi\rangle}(\zeta)$ is equal to $\langle z|\Psi\rangle$, so that

$$p_{|\Psi\rangle}(\zeta) = \langle z|\Psi\rangle\prod_{i=1}^N(\zeta-\zeta_i) = A_\Psi\prod_{i=1}^N\frac{(\zeta-\zeta_i)}{\sqrt{1+|\zeta_i|^2}}\,, \tag{3.6}$$

since $\langle\hat{z}|\hat{n}_i\rangle = \cos\theta_i/2 = (1+|\zeta_i|^2)^{-1/2}$. Comparing the last two equations we arrive at

$$\langle -n|\Psi\rangle = \left(\cos\frac{\theta}{2}e^{-i\phi}\right)^N p_{|\Psi\rangle}(\zeta)\,. \tag{3.7}$$

3.2 Spin states space as a principal fiber bundle

The Hilbert space of spin-s states $\mathbb{P}^N$ ($N = 2s$), has a natural action of $SO(3)$, where for a state

$$|\Psi\rangle = \sum_m c_m |s, m\rangle \,, \tag{3.8}$$

the action of a rotation R is $\mathsf{R}|\Psi\rangle = \sum_{m,m'} c_m D^{(s)}_{mm'}(\mathsf{R})|s, m'\rangle$, with $D^{(s)}_{mm'}$ the Wigner D-matrices in the s representation. We can define a equivalence relation such that two states $|\Psi_1\rangle$, $|\Psi_2\rangle$ are equivalent iff $|\Psi_1\rangle = \mathsf{R}|\Psi_2\rangle$ for some $\mathsf{R} \in SO(3)$. Then, as in the n-body problem studied in the first part of the text, a principal fiber bundle is defined, where the total space is $\mathbb{P}^N$, the fibers are diffeomorphic to $SO(3)$, and the base space is the quotient $\mathbb{P}^N/SO(3) \equiv \mathscr{S}$. Each point of $\mathscr{S}$ represents the orbit of a state $|\Psi\rangle$ under the action of $SO(3)$. With the help of the Majorana representation, we can *visualize* the points of $\mathscr{S}$. Each equivalence class consists of all the states with same *constellation shape*, differ only by their orientation in the Bloch sphere; for that reason we also call $\mathscr{S}$ the *shape space*. Generically all the states have a fiber diffeomorphic to $SO(3)$, except for those with axial symmetry, which are the classes of the states $|s, m\rangle$. For these classes, the fiber is reduced to a 2-dimensional subset of $SO(3)$. In terms of quantum information, our equivalence relation are the local unitary (LU) transformations, which for the symmetric states of qubits are collective $SU(2)$ rotations, and the base space is labelled by the invariant quantities under LU transformations. One important application to this is that the entanglement (independent to which definition you take) is a function in the base space, *i.e.*, only depends by LU invariants [32].

The coordinates of $\mathscr{S}$ in terms of the coefficients c_m in (3.8) are scalar quantities invariant under the Wigner functions of the respective s representation which, in general, are not trivial to find [37]. Using the expansion of the density matrix in terms of the tensor operators $T_{\mu\nu}$ or the tensor representation defined in [38], one can find shape coordinates in a methodical way. Another way is via Majorana representation, where the coordinates of the total space are the roots $\{\zeta_k\}_{k=1}^N$ of $P_\Psi(\zeta)$. Shape coordinates can be given by scalar quantities of the stars' direction, *i.e.*, scalar quantities of the unitary vectors $\{n_k\}_{k=1}^N$ obtained via stereographic projection of $\{\zeta_k\}_{k=1}^N$.

Let us give some examples. For $s = 1/2$, the shape space is only one point, because all the constellations of one star are equivalent via a rotation. For $s = 1$, the total space is $\mathbb{P}^2$ which is

of (real) dimension $4s = 4$, and the dimension of the shape space $\mathscr{S}$ is 1. An immediate shape coordinate is the arclength between the stars $\theta \in [0, \pi]$. The orbit of the spin coherent states, which its constellation is one star with degeneracy N (see Fig. 1.2) has shape coordinate $\theta = 0$ and we will see below that the fiber is a 2-sphere. On the other hand, the orbit of the state $|1, 0\rangle$, which constellation is a pair of antipodal stars, has shape coordinate $\theta = \pi$ and the fiber is diffeomorphic to $\mathbb{R}P^2$. The other points in $\mathscr{S}$ have a fiber diffeomorphic to $SO(3)/Z^2$ [11]. This decomposition of $\mathbb{P}^2$ into subsets (in this case, the fibers) topologically different is called a *stratification* of $\mathbb{P}^2$. For more discussion to the constellation shapes of orbits with $s > 1$, see [8].

The Hilbert space $\mathbb{P}^N = \mathbb{C}P^N$ is, by definition, the space of rays in $\mathbb{C}^{N+1}$, *i.e.*, the space of equivalent classes of $\mathbb{C}^{N+1}/\{0\}$ where $p_1, p_2 \in \mathbb{C}^{N+1}/\{0\}$ are equivalent if $p_1 = \lambda p_2$, with $\lambda \in \mathbb{C}$. For the subset of points in $\mathbb{C}^{N+1}$, $p = (Z^0, \ldots, Z^N)$ with $Z^k \neq 0$, we define the *affine coordinates* $(z^0, \ldots, z^{k-1}, z^{k+1}, \ldots z^N)$ with $z^j = Z^j/Z^k$. The affine coordinates are also coordinates in a subset (chart) of $\mathbb{P}^N$ in a subset (chart). For the spin-s states, we choose as the coordinates (also called the *homogeneus coordinates*) $(Z^0, \ldots, Z^N)$, the coefficients c_m in equation (3.8) and then the affine coordinates in terms of their ratios. The metric induced in $\mathbb{P}^N$ by $\mathbb{C}^{N+1}$ is the Fubini-Study metric [11]

$$g \equiv 2g_{a\bar{b}} dz^a d\bar{z}^{\bar{b}} = \frac{1}{1+|z|^2} \left(dz^a d\bar{z}_a - \frac{\bar{z}_a dz^a dz_b \bar{z}^b}{1+|z|^2} \right) , \tag{3.9}$$

with $z = (z^1, \ldots, z^n)$. The coefficients of the metric $g_{a\bar{b}}$ can be written in terms of the derivatives of a function $K = \ln \sqrt{1+|z|^2}$. These properties proved that $\mathbb{P}^N$ is a *Kähler manifold.* and K is called the *Kähler potential* [10].

Returning to our principal fiber bundle, we can calculate the metric induced in an orbit of a state (in a fiber). This reduced metric has been calculated for some families which appear in every spin value s (see [57, 56]). We will only calculate the case of interest for us, which is the orbit of the spin coherent states. Using the expansion of a general SC state (1.51), we obtain that $1+|z|^2 = (1+\zeta\bar{\zeta})^{2s}$ with $\zeta = \tan(\theta/2)e^{i\phi}$ is the stereographic projection of the direction of the SC state $|n\rangle$. Also, the transformation between the affine coordinates and the coordinates $(\zeta, \bar{\zeta})$ is holomorphic, and therefore the metric in the new coordinates is just

$$g = g_{\zeta\bar{\zeta}} d\zeta d\bar{\zeta} , \quad g_{\zeta\bar{\zeta}} = \partial_\zeta \partial_{\bar{\zeta}} \ln(1+\zeta\bar{\zeta})^{2s} . \tag{3.10}$$

With some algebra we obtain

$$g_{\zeta\bar{\zeta}} = \frac{2s}{\left(1+\zeta\bar{\zeta}\right)^2}\,, \tag{3.11}$$

which is the metric of a 2-sphere induced by $\mathbb{R}^3$ with radius $r = \sqrt{s/2}$, in the complex coordinates given via stereographic projection. With this result, we obtain that the orbit of the spin coherent states for each value of s is indeed "round", *i.e.*, is isometric to a 2-sphere. The spin coherent sphere will be denoted as S^2_{SC}. On the other hand, there is an induced metric in the shape space, however, for $s \geq 3/2$ is a hard task to find it. For $s = 1$, because is one dimensional, the induced metric doesn't have a fundamental meaning.

3.2.1 An obvious application: the quantum GPS

Let us take an ensemble of pure generic spin s states $|\psi_i\rangle = |\psi\rangle$, with an specific shape and orientation. We assume that they were affected in a period of time by some magnetic field, or interaction, such that our initial states obtain an unknown rotation $|\psi_f\rangle = \mathsf{R}|\psi\rangle$. Now, we take samples of our final state and measure the overlap with SC states, which is equivalent to knowing the value of the Husimi function $H_{\psi_f}(n)$ [11] of $|\psi_f\rangle$ in the direction n,

$$H_{\psi_f}(n) \equiv |\langle n||\psi_f\rangle|^2 = |\langle n|\mathsf{R}|\psi\rangle|^2\,. \tag{3.12}$$

The question is the following: how many measurements like (3.12) we need to do to figure out the unknown rotation? The question can be rephrased in terms of the principal fiber bundle. We are interested to find the point $\mathsf{R}|\psi\rangle$ in the fiber associated to the state $|\psi\rangle$[1]. Now, imposing the equation $|\langle n_1\rangle\psi_f|^2 = M_1^2$ for known $|n_1\rangle$ and $M_1 \in \mathbb{R}$, is equal to requiring that $|\psi_f\rangle$ must live in the sphere centered in $|n_1\rangle$ with radius M_1 (Fubini-Study distance). The question is now the following, how many spheres centered in a point of the SC states' orbit we need to obtain a unique intersection with the orbit of $|\psi\rangle$ in $|\psi_f\rangle$?

The level surfaces of the Husimi function of a general state are: empty, a finite set of points, or a finite set of closed curves which are topologically circles (see Fig. 3.1, and also Fig. 3.3). Let $\mathscr{C}_1$ be one closed curve in the 2-sphere such that $H_{|\psi\rangle}(v) = M_1$ for each $v \in \mathscr{C}_1$. Now, let us remark that $H_{\mathsf{R}\psi}(v) = H_\psi(\mathsf{R}^T v)$, and then we can think that we rotate the SC state instead of $|\psi\rangle$. For each direction $v \in \mathscr{C}_1$, the locus of rotations such that $\mathsf{R}^T v_0 = v$ is 1-dimensional

[1]The initial orientation of the state $|\psi\rangle$ is our *zero*, and the other points in the fiber are labeled with $\mathsf{R}|\psi\rangle$

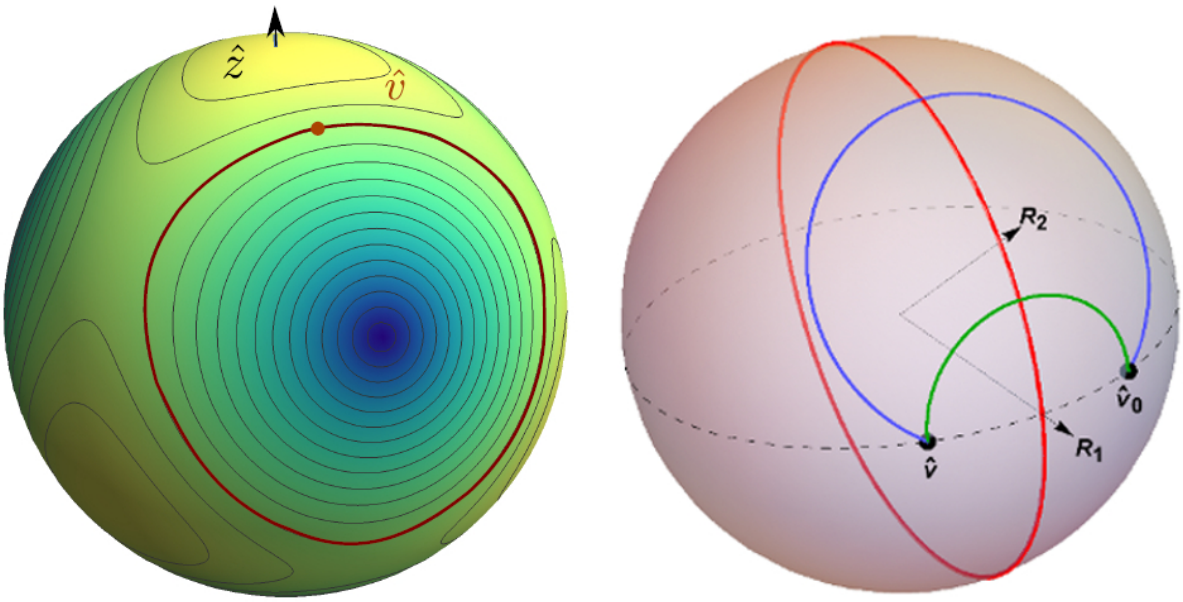

Figure 3.1: (Left) Husimi function for a particular state $H_{|\psi\rangle}(n)$ over the 2-sphere, where warmer colors correspond to bigger values of H. We draw some level surfaces, and mark one of them in brown. (Right) Choosing one point $\vec{v}$ in the brown curve of the left image, now we ask about the locus of rotations R such that for an initial point $\hat{v}_0$, satisfy that $\hat{v} = \mathsf{R}\hat{v}_0$, for instance the rotations R_1 and R_2 shown in the figure. The rotations have its rotation axis in the red curve and, for each rotation axis there is a unique rotation angle modulo 2π satisfying the required condition. Then, each point of the red curve specifies one rotation, and only the rotations of antipodal directions are the same. Even with this antipodal equivalence, the set of rotations that sends $\hat{\mathbf{v}}_0$ to $\hat{\mathbf{v}}$ is topologically a circle.

and is topologically a circle (The explanation is given in Fig. 3.1). With this we conclude that the intersection of a sphere centered in the SC states' orbit with the orbit of $|\psi\rangle$ is topologically a finite set of tori (see Fig. 3.2). The intersection is two-dimensional, so we will need two additional equations like (3.12) to obtain a 0-dimensional solution. In general, the intersection of three spheres with the orbit of a state is a finite set of points, and, to distinguish between them it is used another sphere. Therefore, the answer of our question is 4. When the state has some symmetry, the rotation is obtained modulo the rotations which leaves the state invariant. In Fig. 3.2 we draw an intersection of two spheres with the orbit of $|\psi\rangle$ in the axis-angle representation.

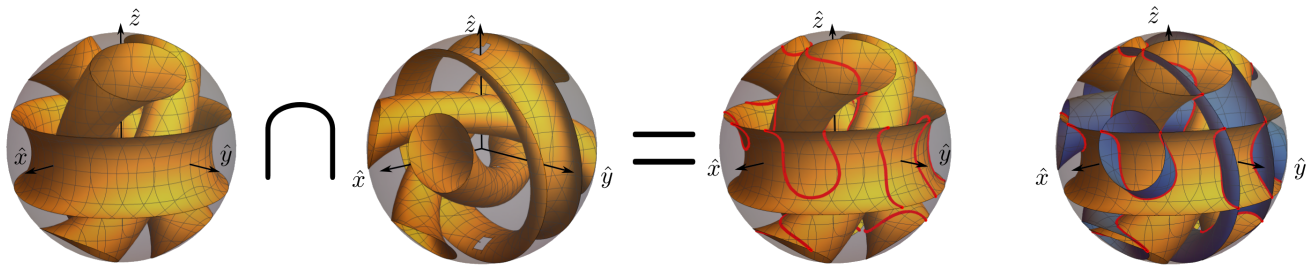

Figure 3.2: Locus of points (rotations) of $SO(3)$ in the angle-axis representation which satisfies the equation $H_\psi(n_k) = M_k$ for a particular state $|\psi\rangle$ and two values of n_k and M_k, respectively. We can observe that both locus are topologically a set of tori, where we remember that the antipodal points in the shell of the $SO(3)$ sphere are identified. The intersection of both sets is a one dimensional set which is marked in red color.

Each sphere intersects the orbit of $|\psi\rangle$ in a finite set of tori, and the intersection between them is 1-dimensional. We called this procedure the *quantum GPS* by the similarity (and indeed, the inspiration) of a GPS system. Below we give the equivalent terms. The obtention of a rotation with quantum systems is a search field in many areas, in special in quantum metrology [18, 24], where there are experiments in process. Of course, our situation doesn't considered deviations and experimental error, and to do a more realistic protocol we need to take them into account.

	GPS	Quantum GPS
Total space	$\mathbb{R}^3$	$\mathbb{P}^N$
The point of interest lives in a	2-sphere	fiber diff. to $SO(3)$
The intersection are	circles	set of tori

3.3 Algebraic properties of $S^2_{\mathbf{SC}}$

3.3.1 Spin Coherent bases

The constellation shape associated to S^2_{SC} consists of a star with degeneracy N. As we mention before, the unit operator may be resolved in SC states, $\mathbb{1} = (2s+1)\int |n\rangle\langle n| d\Omega/4\pi$, implying that any state can be written as an infinite linear combination of SC states. The following theorem shows that, in fact, *any* $N+1$ SC states will do [81, 87]:

Theorem 1. *Any set of $N+1$ distinct SC states $\{|c_k\rangle\}_{k=0}^N$ forms a basis in the Hilbert space $\mathscr{H}^{N+1}$.*

Proof. Let γ_k be the complex number associated, via stereographic projection, to the direction c_k and let $|\Psi\rangle$ be an arbitrary state with N associated complex numbers $\{\zeta_k\}_{k=1}^N$ (*i.e.*, the ζ_k's are the roots corresponding to the stars of $|\Psi\rangle$). The expansion

$$|\Psi\rangle = \sum_{k=0}^{N} \alpha'^k |c_k\rangle \tag{3.13}$$

implies the following relation for the corresponding Majorana polynomials

$$\prod_{j=1}^{N} \frac{(\zeta-\zeta_j)}{(1+|\zeta_j|^2)^{1/2}} = \sum_{k=0}^{N} \frac{\alpha^k}{(1+|\gamma_k|^2)^{N/2}} (\zeta-\gamma_k)^N \,, \tag{3.14}$$

with $\alpha^k = \alpha'^k A_{n_k}/A_\Psi = \alpha'^k/A_\Psi$, and where the A's are the normalization factors introduced in (3.1), (3.2) (note that for an SC state $|n\rangle$, $A_n = 1$). Expanding each side we obtain

$$\sum_{j=0}^{N} (-1)^{N-j} \zeta^j b_{N-j} = \sum_{j=0}^{N} (-1)^{N-j} \zeta^j \binom{N}{j} \sum_{k=0}^{N} \tilde{\alpha}^k \gamma_k^{N-j} \,, \tag{3.15}$$

where

$$\tilde{\alpha}^k = \frac{\alpha^k}{(1+|\gamma_k|^2)^{N/2}} \left(\prod_{m=1}^{N} \left(1+|\zeta_m|^2\right)^{1/2} \right) , \tag{3.16}$$

and b_j are the symmetric polynomials of the numbers $\{\zeta_k\}_{k=1}^N$, with $b_N = \prod_{i=1}^N \zeta_i$ and $b_0 = 1$. Comparing the powers of ζ on both sides in (3.16), we obtain the following system of equations

$$\begin{pmatrix} 1 & 1 & \dots & 1 \\ \gamma_0 & \gamma_1 & \ddots & \gamma_N \\ \vdots & \ddots & \ddots & \vdots \\ \gamma_0^N & \gamma_1^N & \dots & \gamma_N^N \end{pmatrix} \begin{pmatrix} \tilde{\alpha}^0 \\ \tilde{\alpha}^1 \\ \vdots \\ \tilde{\alpha}^N \end{pmatrix} = \begin{pmatrix} \tilde{b}_0 \\ \tilde{b}_1 \\ \vdots \\ \tilde{b}_N \end{pmatrix} , \tag{3.17}$$

with $\tilde{b}_j = \binom{N}{j}^{-1} b_j$. The matrix in the left hand side of the above equation, which we will denote by V, is of the Vandermonde form, and is invertible if and only if all the numbers γ_i are distinct. □

Using the known formula for the inverse of a Vandermonde matrix [93] we find that $(\mathsf{V}^{-1})_{ij}$ is the coefficient of the term ζ^j in the polynomial $P_i(\zeta)/P_i(\gamma_i)$, where $P_i(\zeta) = \prod_{k=0,k\neq i}^N (\zeta-\gamma_k)$

(the indices in these formulas run from 0 to N). We remark that the last theorem says that *any* set of $N+1$ SC states $\mathscr{B} = \{|c_k\rangle\}_{k=0}^{N}$ forms a basis without any restriction whatsoever on their relative positions, proximity, *etc.* For every non-orthogonal basis, as $\mathscr{B}$, the dual basis $\mathscr{B}^* = \{|c^k\rangle\}_{k=0}^{N}$ is defined as the set of states $|c^k\rangle$ such that

$$\langle c^j|c_i\rangle = \delta^j{}_i\,, \quad i,j = 0,\ldots,N\,. \tag{3.18}$$

The definition of the dual basis implies a resolution of the unity,

$$\sum_{i=0}^{N} |c^i\rangle\langle c_i| = \mathbb{1}\,. \tag{3.19}$$

For a generic basis, the only way to obtain the dual basis is solving system of equations (3.18). However, to a SC basis $\mathscr{B}$ it is easy to obtain $\mathscr{B}^*$. It is easy to see that a spin state $|\Psi\rangle = |n_1,\ldots,n_N\rangle$ is orthogonal to any SC state whose direction is antipodal to one of the stars associated to $|\Psi\rangle$, $\langle -n_i|\Psi\rangle = 0$. In particular, if $|\Psi\rangle$ has no degeneracy (*i.e.*, coincident stars), it is orthogonal to N SC states, which shows that the dual basis element $|c^i\rangle$ is given by

$$|c^i\rangle = \frac{|-c_0,-c_1,\ldots,\widehat{-c_i},\ldots,-c_N\rangle}{\langle c_i|-c_0,-c_1,\ldots,\widehat{-c_i},\ldots,-c_N\rangle}\,, \tag{3.20}$$

where the wide hat denotes omission. Note that the denominator in (3.20) is nonzero, since $|\hat{c}_i\rangle$ is only orthogonal to $|-\hat{c}_i\rangle$ and no other spin-1/2 state. We remark also that (3.19) implies that

$$|\Psi\rangle = \langle c^i|\Psi\rangle|c_i\rangle\,, \tag{3.21}$$

which is an alternative to solving (3.17). Note that $\langle c^i|c^i\rangle \neq 1$.

3.3.2 Adapted SC bases

We now wish to associate (*i.e.*, one with N distinct stars), an *adapted SC basis* $\{|c_i\rangle\}_{i=0}^{N}$, the elements of which, as the name suggests, are all SC states. For $|\Psi\rangle = |n_1\,,\ldots\,,n_N\rangle$, the elements $\{c_i\}_{i=1}^{N}$ are just given by the stars of $|\Psi\rangle$, $c_i = n_i$, $i = 1,\ldots,N$. The remaining element $|c_0\rangle$ is defined as follows: there is a unique 1D linear subspace that is orthogonal to all $|n_i\rangle$, $i = 1,\ldots,N$. In fact, it consists of the complex multiples of the state $|\tilde{\Psi}\rangle$ *antipodal* to $|\Psi\rangle$, *i.e.*, the state whose stars are antipodal to those of $|\Psi\rangle$, $|\tilde{\Psi}\rangle = |-n_1,\ldots,-n_N\rangle$. This state is not itself SC, but has, generically, a single closest SC state, in the FS metric of $\mathbb{P}$ — this latter state is chosen as

$|c_0\rangle$. Central inversion of a constellation is an isometry for the FS metric, such that, if $|c_0\rangle$ is the closest SC state to $|\tilde{\Psi}\rangle$, the SC state $|-c_0\rangle$ is the one closest to $|\Psi\rangle$. The above may be summarized neatly as follows: *the $N+1$ elements of the SC basis adapted to a generic state $|\Psi\rangle$ are defined by the antipodes of the extremal points (one maximum and N minima) of its Husimi function $H_\Psi(n) = |\langle n|\Psi\rangle|^2$.*

We give some examples of the adapted spin basis. Denote by n_i, $i = 1, \ldots, N$, the stars of the state $|\Psi\rangle$ and by ζ_i their projections in the complex plane. Similarly, denote by c_k, $k = 0, \ldots, N$, the stars of an arbitrary SC basis, and by γ_k their complex projections. Finally, denote by α_k, $k = 0, \ldots, N$ the expansion coefficients in (3.14).

Adapted SC basis for spin 1/2

Any two distinct SC states form a basis in the Hilbert space $\mathscr{H}^2$. For $|\Psi\rangle = |\hat{n}\rangle$ the adapted SC basis is $(|\hat{c}_0\rangle, |\hat{c}_1\rangle) = (|-\hat{n}\rangle,\ |\hat{n}\rangle)$ and the corresponding expansion coefficients are trivially $(\alpha_0, \alpha_1) = (0, 1)$.

Adapted SC basis for spin 1

For $s = 1$, any set of 3 SC states forms a basis in $\mathscr{H}^3$. Relations (3.17) become

$$\left(1+\zeta_1\bar{\zeta_1}\right)^{1/2}\left(1+\zeta_2\bar{\zeta_2}\right)^{1/2}\begin{pmatrix} \frac{\alpha^0}{1+\gamma_0\bar{\gamma}_0} \\ \frac{\alpha^1}{1+\gamma_1\bar{\gamma}_1} \\ \frac{\alpha^2}{1+\gamma_2\bar{\gamma}_2} \end{pmatrix} \equiv \begin{pmatrix} \tilde{\alpha}^0 \\ \tilde{\alpha}^1 \\ \tilde{\alpha}^2 \end{pmatrix} = \begin{pmatrix} \frac{s_{11}s_{22}+s_{12}s_{21}}{2\gamma_{01}\gamma_{02}} \\ \frac{s_{10}s_{22}+s_{12}s_{20}}{2\gamma_{10}\gamma_{12}} \\ \frac{s_{10}s_{21}+s_{11}s_{20}}{2\gamma_{20}\gamma_{21}} \end{pmatrix}, \tag{3.22}$$

where $s_{ij} \equiv \zeta_i - \gamma_j$, and $\gamma_{ij} \equiv \gamma_i - \gamma_j$. We orient the constellation of $|\Psi\rangle$ so that the two stars are in the x-y plane, bisected by the x axis. Then, $\zeta_1 = \gamma_1 = e^{i\phi}$ and $\zeta_2 = \gamma_2 = e^{-i\phi}$, with $0 < \phi < \pi/2$. The SC state closest to $|\Psi\rangle$ has its star at x, so $\gamma_0 = -1$. Relations (3.22) give

$$\begin{pmatrix} \alpha^0 \\ \alpha^1 \\ \alpha^2 \end{pmatrix} = \begin{pmatrix} 1-\cos\phi \\ e^{-i\phi}/2 \\ e^{i\phi}/2 \end{pmatrix}. \tag{3.23}$$

Adapted SC basis for spin 3/2

Our last example is a state with $s = 3/2$. For the general case, the (tilded) expansion coefficients are

$$\begin{pmatrix} \tilde{\alpha}^0 \\ \tilde{\alpha}^1 \\ \tilde{\alpha}^2 \\ \tilde{\alpha}^3 \end{pmatrix} = \begin{pmatrix} \frac{s_{11}s_{22}s_{33}+s_{12}s_{23}s_{31}+s_{13}s_{21}s_{32}}{3\gamma_{01}\gamma_{02}\gamma_{03}} \\ \frac{s_{10}s_{22}s_{33}+s_{12}s_{23}s_{30}+s_{13}s_{20}s_{32}}{3\gamma_{10}\gamma_{12}\gamma_{13}} \\ \frac{s_{10}s_{21}s_{33}+s_{11}s_{23}s_{30}+s_{13}s_{20}s_{31}}{3\gamma_{20}\gamma_{21}\gamma_{23}} \\ \frac{s_{10}s_{21}s_{32}+s_{11}s_{22}s_{30}+s_{12}s_{20}s_{31}}{3\gamma_{30}\gamma_{31}\gamma_{32}} \end{pmatrix}, \tag{3.24}$$

where

$$\begin{pmatrix} \tilde{\alpha}^0 \\ \tilde{\alpha}^1 \\ \tilde{\alpha}^2 \\ \tilde{\alpha}^3 \end{pmatrix} \equiv \left(\prod_{i=1}^{3} \left(1 + \zeta_i \bar{\zeta}_i\right)^{1/2} \right) \begin{pmatrix} \frac{\alpha^0}{(1+\gamma_0\bar{\gamma}_0)^{3/2}} \\ \frac{\alpha^1}{(1+\gamma_1\bar{\gamma}_1)^{3/2}} \\ \frac{\alpha^2}{(1+\gamma_2\bar{\gamma}_2)^{3/2}} \\ \frac{\alpha^3}{(1+\gamma_3\bar{\gamma}_3)^{3/2}} \end{pmatrix}, \tag{3.25}$$

and with the associated SC basis, $\{\gamma_0, \gamma_i = \zeta_i\}_{i=1}^{N}$, they reduce to

$$\begin{pmatrix} \tilde{\alpha}^0 \\ \tilde{\alpha}^1 \\ \tilde{\alpha}^2 \\ \tilde{\alpha}^3 \end{pmatrix} = \begin{pmatrix} 0 \\ \frac{-(\gamma_2-\gamma_3)^2}{3(\gamma_1-\gamma_2)(\gamma_1-\gamma_3)} \\ \frac{-(\gamma_3-\gamma_1)^2}{3(\gamma_2-\gamma_1)(\gamma_2-\gamma_3)} \\ \frac{-(\gamma_1-\gamma_2)^2}{3(\gamma_3-\gamma_1)(\gamma_3-\gamma_2)} \end{pmatrix}, \tag{3.26}$$

independent of the choice of γ_0. Note that $\alpha^0 = 0$, and $\alpha^1, \alpha^2, \alpha^3$ do not depend of γ_0. This result can be generalized to any half-integer spin state, as the following proposition asserts, and originates in the fact that, for such states, $\langle\Psi|T|\Psi\rangle = 0$, where T is the time-reversal operator, that acts like the antipode map on constellations.

Proposition 2. *The expectation value of the time-reversal operator T in a half-integer spin state vanishes.*

Proof. For $s = 1/2$, $T = -i\sigma_y K$, where K is the complex conjugate operator — for higher spins, T is just the tensorial power of this expression. It is easily seen that $T^2|n_1, \ldots, n_N\rangle = (-1)^N|n_1, \ldots, n_N\rangle$, and T is antiunitary, $(T|\Psi_1\rangle, T|\Psi_2\rangle) = (|\Psi_2\rangle, |\Psi_1\rangle)$, where we denote the inner product between two states as $(\cdot, \cdot)$. With these properties of T in mind, we compute $(-1)^N(|\Psi\rangle, T|\Psi\rangle) = (T^2|\Psi\rangle, T|\Psi\rangle) = (|\Psi\rangle, T|\Psi\rangle)$, and therefore, for $N = 2s$ odd, $(|\Psi\rangle, T|\Psi\rangle) = 0$. □

In our case, for $|\Psi\rangle = |n_1, \ldots, n_N\rangle$, we have $|c^0\rangle \propto |-n_1, \ldots, -n_N\rangle$, so that $\alpha^0 \propto \langle c^0|\Psi\rangle = 0$ for s half-integer (N odd).

3.3.3 Extrema of the Husimi function

We derive a necessary and sufficient condition for an SC state $|n_0\rangle$ to be closest to a generic state $|\Psi\rangle$. SC states $|n\rangle$, nearby $|n_0\rangle$, can be obtained by a rotation,

$$|n\rangle = R|n_0\rangle = e^{-ibS_-}e^{-iaS_z}e^{-icS_+}|n_0\rangle\,, \tag{3.27}$$

where the reference frame has been rotated so as to make n_0 coincide with z, and a, b, $c \in \mathbb{C}$ are functions of the rotation parameters (see, *e.g.*, the supplementary material in [38]). With $S_+|n_0\rangle = 0$ and $S_z|n_0\rangle = s|n_0\rangle$, we get

$$H_\Psi(n) = e^{2s\Im(a)}\langle\Psi|e^{-ibS_-}|n_0\rangle\langle n_0|e^{i\bar{b}S_+}|\Psi\rangle\,, \tag{3.28}$$

where $\Im$ denotes imaginary part. Taking the derivative with respect to b, and setting it equal to zero, at $b = 0$, gives

$$\langle\Psi|S_-|n_0\rangle\langle n_0|\Psi\rangle = 0\,. \tag{3.29}$$

When the second factor in the left hand side above vanishes, $|n_0\rangle$ is orthogonal to $|\Psi\rangle$, and we get an SC state at maximal distance (equal to $\pi/2$) from $|\Psi\rangle$ — this only happens for n_0 antipodal to any of the stars of $|\Psi\rangle$. For $|n_0\rangle$ to be closest to $|\Psi\rangle$ the first factor must vanish, implying that

$$\langle n_0, s-1|\Psi\rangle = 0\,, \quad |n_0, s-1\rangle \equiv |-n_0, n_0, \ldots, n_0\rangle\,, \tag{3.30}$$

where $(n_0 \cdot S)|n_0, k\rangle = k|n_0, k\rangle$. We turn now to a characterization of the nature of the critical points of the Husimi function H_Ψ.

Theorem 3. *Consider a critical point n_0 of the Husimi function H_Ψ and expand $|\Psi\rangle$ in the $n_0 \cdot S$ eigenbasis, $|\Psi\rangle = \sum_{m=-s}^{s}\rho_m e^{i\alpha_m}|n_0, m\rangle$. Then*

1. *If $\rho_s = 0$ then n_0 is a global minimum of H_Ψ ($[n_0]$ is at a maximal distance from $[\Psi]$).*
2. *If $\rho_{s-1} = 0$, and $\sqrt{s}\rho_s > \sqrt{2s-1}\rho_{s-2}$, then n_0 is a local maximum of H_Ψ ($[n_0]$ is at a minimal distance from $[\Psi]$).*

3. *If* $\rho_{s-1} = 0$, *and* $\sqrt{s}\rho_s < \sqrt{2s-1}\rho_{s-2}$, *then* n_0 *is a saddle point of* H_Ψ*: moving along the* $\phi = (\alpha_{s-2} - \alpha_s)/2 \mod \pi$ *direction on the sphere* n_0 *is a local minimum, while in the orthogonal direction it is a local maximum.*

Proof. If $\rho_s = |\langle n_0|\Psi\rangle| = 0$ then H_Ψ attains a global minimum at n_0 since it is either positive or zero. For the other critical points, the condition for criticality is $\rho_{s-1} = |\langle n_0, s-1|\Psi\rangle| = 0$, as we have already proved. To further characterize the critical points, we will expand the Husimi function around them, up to second order in the angular distance. Assume, as before, that n_0 is along the z axis and consider an SC state close to $|z\rangle$ characterized by the angles θ and ϕ. Then we have, up to second order in θ,

$$\begin{aligned} H_\Psi &= \left|\langle\Psi|e^{-iS_z\phi}e^{-i\theta S_y}|z\rangle\right|^2 \\ &= \left|\langle\Psi|\left((1-\frac{s\theta^2}{4})|z\rangle \quad + \frac{\theta^2}{4}e^{2i\phi}\sqrt{s(2s-1)}|z,s-2\rangle\right)\right|^2 \\ &= (1-\frac{s\theta^2}{2})\rho_s^2 + \frac{\theta^2}{2}\sqrt{s(2s-1)}\rho_{s-2}\rho_s\cos(2\phi-\alpha_{s-2}+\alpha_s) \\ &= H(z) - \frac{\theta^2}{2}\Delta + \mathscr{O}(\theta^3)\,, \end{aligned}$$

where

$$\Delta \equiv s\rho_s^2 - \sqrt{s(2s-1)}\rho_{s-2}\rho_s\cos(2\phi - \alpha_{s-2} + \alpha_s)\,,$$

and $\rho_{s-1} = 0$ was used. In order for H_Ψ to have a local maximum, it is necessary for Δ to be positive for all ϕ. On the other hand, the minimum value of Δ is obtained when $2\phi - \alpha_{s-2} + \alpha_s = 2k\pi$, $k \in \mathbb{Z}$, and for that minimum to be positive it must hold

$$\sqrt{s}\rho_s > \sqrt{2s-1}\rho_{s-2}\,,$$

which proves the second case of the theorem. If the previous inequality is reversed the minimum value of Δ will be negative. Given that its maximal value is evidently positive, we have a saddle point, and the stated principal directions follow easily. This concludes the last case of the proof. □

It has been shown in [67] that a spin-s state $|\Psi\rangle$, with maximal star degeneracy less than $\lfloor (N+1)/2 \rfloor$, can be written as a linear combination of at most $\lfloor (N+1)/2 \rfloor$ SC states, which depend on $|\Psi\rangle$ ($\lfloor\cdot\rfloor$ denotes integer part). Note that the moduli of the expansion coefficients

$\langle c^i|\Psi\rangle$ in that equation are invariant under rotations of $|\Psi\rangle$ — whether they provide coordinates in the quotient (shape) space $\mathscr{S}$ is an open question.

For the maxima of the Husimi function of a state $|\Psi\rangle$, it turns out that the level curves around them have a universal circular behavior. Consider a state $|\Psi\rangle = |c_1, \ldots, c_N\rangle$ and the corresponding Husimi function defined over $S^2_{\rm SC}$. Note that $H_\Psi(-c_i) = 0$, $i = 1, \ldots, N$. We assume, without loss of generality, that a particular $-c_i$ points toward the north pole. This implies that in the expansion of $|\Psi\rangle$ in S_z-eigenstates, the maximal projection eigenstate is absent, $|\Psi\rangle = \sum_{k=-N}^{N-1}\langle z, k|\Psi\rangle|z, k\rangle$. Given any nearby SC state $|n\rangle$, characterized by the angles (θ, ϕ), with $\theta \ll 1$, we compute

$$\begin{aligned} H_\Psi(n) &= |\langle z|e^{i\theta S_y}e^{i\phi S_z}|\Psi\rangle|^2 \\ &= |\langle z|(\mathbb{1} + i\theta S_y)e^{i\phi S_z}|\Psi\rangle|^2 + O(\theta)^3 \\ &= \frac{1}{16}|2\sqrt{2s}\theta e^{i\phi(s-1)}\langle z, s-1|\Psi\rangle|^2 + O(\theta^3) \\ &= \frac{s}{2}|\langle z, s-1|\Psi\rangle|^2\theta^2 + O(\theta^3)\,, \end{aligned}$$

where we used the expression of $|\Psi\rangle$ in terms of the eigenstates of S_z to obtain the last line. Since there is no ϕ dependence, to this order in θ, we conclude that the level curves are circles. In Fig. 3.3 we plot the Husimi function of a particular state in the complex plane (via stereographic projections) and it is observed that the maxima are circular peaks.

3.3.4 Closest SC states

In the last subsections, we give a criteria to the closest SC state to a general state $|\Psi\rangle$, and with this we define an adapted basis. To obtain a well defined and unique adapted basis, we should have only one closest SC state, otherwise we should pick one of them. However, most of the states have only a unique closest SC state.

Remark. *The set of states such that the closest SC state is not unique is of measure zero. In fact, this set is at most of dimension* $4s - 1$.

Proof. Consider two distinct SC states $[c_1]$ and $[c_2]$ and let $[\Psi]$ be any state such that $[c_1]$ and $[c_2]$ are both the closest SC states of $[\Psi]$. As shown in (3.30) this implies that $\langle c_1, s-1|\Psi\rangle = \langle c_2, s-1|\Psi\rangle = 0$. These are two complex equations so that the locus of states that satisfy them

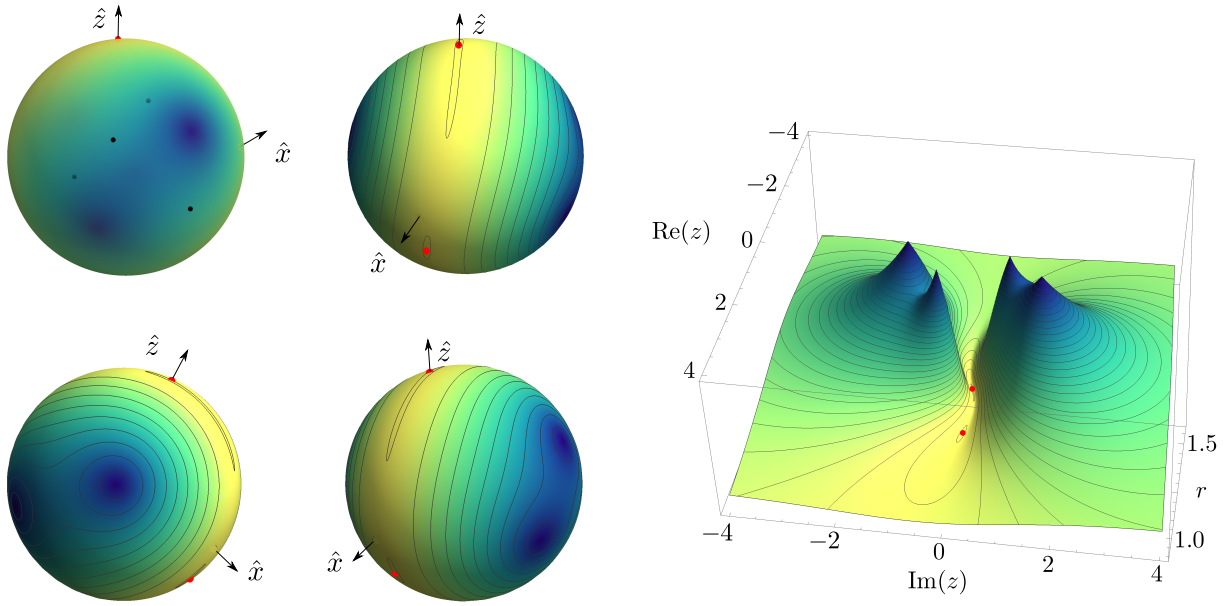

Figure 3.3: **Top left sphere**: constellation of the spin-2 state $[\Psi] \approx (0.634, 0, 0.417 + 0.292i, 0.053 + 0.048i, 0.553 + 0.167i)$, which has two closest SC states. **Top right and bottom two spheres:** Plots of S^2_{SC}, from different viewpoints, with level curves of the Fubini-Study distance to $[\Psi]$. Warmer colors correspond to shorter distances. The two red points denote the two closest SC states to $[\Psi]$. **Right plot:** The above distance function, plotted over the stereographic projection of S^2_{SC} on the complex plane. The conical maxima correspond to the directions antipodal to the stars of $[\Psi]$.

has real dimension $4s-4$. Since they must also satisfy the condition $|\langle c_1|\Psi\rangle| = |\langle c_2|\Psi\rangle|$ for them to be equidistant, the dimension of all the states whose closest SC state are $[c_1]$ and $[c_2]$ is at most $4s-5$. Finally note that the space of the pair of SC states $[c_1]$ and $[c_2]$ is of dimension 4. Because of these observations, the space of states where the closest SC state is not unique is of dimension at most $4s-1$, as claimed. □

For $s = 1$, there are no states with more than one closest SC state, except for those whose stars are antipodal — in this latter case the closest SC states form a great circle in the plane that bisects perpendicularly the diameter connecting the antipodal points. For $s = 3/2$ all states with two closest SC states possess a symmetry plane, as is shown below. For $s = 2$ there are states with more than one closest SC states that have no particular symmetry — an example is

shown in figure 3.3.

Theorem 4. *Let $[\Psi]$ be a spin-3/2 state with two closest SC states. Then the constellation associated to $|\Psi\rangle$ is symmetric with respect to the plane that bisects perpendicularly the segment connecting the stars of the closest SC states.*

Proof. Suppose, without loss of generality, that the closest equidistant coherent states point in the directions $n_1 = (\theta, \phi = \pi/2)$ and $n_2 = (\theta, \phi = 3\pi/2)$ — the bisecting plane is then the x-z plane. This implies that

$$\langle n_1, 1/2|\Psi\rangle = 0\,, \quad \langle n_2, 1/2|\Psi\rangle = 0\,, \quad \langle n_2|\Psi\rangle = e^{i\gamma}\langle n_1|\Psi\rangle\,, \tag{3.31}$$

with γ a real number. Writing $|\Psi\rangle = (A, B, C, D)$ and imposing the above conditions leads to

$$\begin{aligned} A &= \lambda(1 + 3\cos\theta)\cos(\gamma/2)\,,\\ B &= 2\lambda\sqrt{3}\sin(\gamma/2)\cos^2(\theta/2)\cot(\theta/2)\,,\\ C &= -\sqrt{3}\lambda\cos(\gamma/2)(1 + \cos\theta)\,,\\ D &= -\lambda(1 - 3\cos\theta)\sin(\gamma/2)\cot^3(\theta/2)\,, \end{aligned}$$

where λ, which can be taken as real, and it is fixed by the normalization condition on $|\Psi\rangle$. The important point here is that all components of $|\Psi\rangle$ are real, implying that the coefficients of the corresponding Majorana polynomial are also real. Therefore, all the roots of the latter are either real or come in conjugate pairs, so that, when projected stereographically onto the sphere, they give rise to a constellation symmetric with respect to the x-z plane, as claimed. □

3.4 Geometrical properties of $S^2_{\rm SC}$

3.4.1 Intersectology with complex lines

A complex line is defined as a two (complex) dimensional subspace of $\mathbb{C}^{N+1}$ projected in $\mathbb{P}^N$. This definition can be generalized for k-planes, which will be studied in the next chapter. Given two orthogonal states $|\psi_1\rangle$, $|\psi_2\rangle$, each point (state) in its complex line $\mathscr{L}$ can be parametrized as $|\psi\rangle = |\psi_1\rangle + \zeta|\psi_2\rangle \in \mathscr{L}$, with $\zeta \in \mathbb{C} \cup \infty$. Taking as homogeneous coordinates $(Z_0, Z_1) = (1, \zeta)$, we calculate the induced metric (3.9) in the complex line

$$g_{\mathscr{L}} = \frac{d\zeta d\bar{\zeta}}{\left(1 + \zeta\bar{\zeta}\right)^2}\,. \tag{3.32}$$

Therefore, any complex line is isometric to a 2-sphere. In this subsection we will explore how these 2-spheres intersect S^2_{SC}. Theorem 1 places severe restrictions in this regard.

Corollary 5. *For $s \geq 1$, any complex line in $\mathbb{P}$ intersects S^2_{SC} at most twice.*

Proof. Suppose a complex line ℓ goes through three SC states $\{|n_k\rangle\}_{k=1}^3$, then another (non-SC) state $|\Psi\rangle$ on ℓ can be written in the form $|\Psi\rangle = \alpha_1|n_1\rangle + \alpha_2|n_2\rangle$ and also $|\Psi\rangle = \beta_1|n_1\rangle + \beta_2|n_3\rangle$. Combining the two equations we obtain $(\alpha_1 - \beta_1)|n_1\rangle + \alpha_2|n_2\rangle - \beta_2|n_3\rangle = 0$. However, by theorem 1, any 3 SC states are linearly independent for $s \geq 1$, implying that $|n_1\rangle = |\Psi\rangle$, which is a contradiction. □

Interestingly, Fermat's (last) theorem for polynomials, a classic result in the Diophantine inequalities literature [59], is relevant in this regard, as it states that for $A(\zeta)$, $B(\zeta)$, $C(\zeta)$ relatively prime polynomials, the equation

$$A(\zeta)^n + B(\zeta)^n = C(\zeta)^n\,, \tag{3.33}$$

only has solutions for $n \leq 2$. Taking all three polynomials of the first degree, we deduce that no linear combination of SC states can itself be SC, for $s \geq 3/2$ — our result above is stronger, as it includes the $s = 1$ case.

The following particular case is also of interest:

Proposition 6. *Given two spin-1 states $[Z]$, $[\Xi]$, with constellations $\{\zeta_1, \zeta_2\}$, $\{\xi_1, \xi_2\}$, respectively, the complex line they define intersects S^2_{SC}*

1. *in two points, if the states have no star in common*

2. *in the single point $[\chi]$, if the two states have the star χ in common.*

Proof. We set a linear combination of the two states equal to an SC state, with associated complex root γ, which, in terms of Majorana polynomials, implies

$$\alpha_1(z - \zeta_1)(z - \zeta_2) + \alpha_2(z - \xi_1)(z - \xi_2) = (z - \gamma)^2\,. \tag{3.34}$$

Solving for γ, α_1, α_2, gives

$$\gamma = \frac{\zeta_1\zeta_2 - \xi_1\xi_2 \pm \sqrt{(\zeta_1-\xi_1)(\zeta_1-\xi_2)(\zeta_2-\xi_1)(\zeta_2-\xi_2)}}{\zeta_1+\zeta_2-\xi_1-\xi_2} \tag{3.35}$$

$$\alpha_1 = \frac{2\gamma - \xi_1 - \xi_2}{\zeta_1 + \zeta_2 - \xi_1 - \xi_2} \tag{3.36}$$

$$\alpha_2 = \frac{-2\gamma + \zeta_1 + \zeta_2}{\zeta_1 + \zeta_2 - \xi_1 - \xi_2}\,. \tag{3.37}$$

If the stars of $[Z]$ are different from those of $[\Xi]$, the radical in the right hand side of (3.35) is nonzero, and one obtains two distinct solutions, *i.e.*, the complex line intersects $S^2_{\rm SC}$ in two distinct points. On the other hand, if the two states have one star in common, say, $\zeta_1 = \xi_1 = \chi$, then (3.35) implies $\gamma = \chi$, *i.e.*, the complex line intersects $S^2_{\rm SC}$ in only one point, the SC state $[\chi]$ corresponding to the common star. □

Fixing the state $[Z]$ in the previous proposition, and letting $[\Xi]$ range over $\mathbb{P}$, one arrives at

Corollary 7. *For $s = 1$, every complex line through a non SC state $[Z] = [n_1, n_2]$ intersects $S^2_{\rm SC}$ twice, except for two lines, each of which intersects $S^2_{\rm SC}$ once, at $[n_i]$, $i = 1, 2$.*

Another interesting implication is contained in

Corollary 8. *Given a spin-1 state $|\Xi\rangle$, with constellation $\{\xi_1, \xi_2\}$, and an arbitrary SC state $|n\rangle$, with single (multiple) star ζ, $\zeta \neq \xi_1$, ξ_2, there exists a unique SC state $|n'\rangle$ such that $|\Xi\rangle$ can be written as a linear combination of $|n\rangle$, $|n'\rangle$.*

Proof. Put $\zeta_1 = \zeta_2 = \zeta$ in (3.35) to find

$$\gamma = \frac{(\xi_1 + \xi_2)\zeta - 2\xi_1\xi_2}{2\zeta - (\xi_1 + \xi_2)}\,, \tag{3.38}$$

i.e., the complex number γ corresponding to n' is a Möbius transform of the one corresponding to n, with coefficients that depend on $|\Xi\rangle$. □

The fact that projective lines, defined by pairs of points in $S^2_{\rm SC}$, pass through every point in $\mathbb{P}^2$ can be phrased in terms of secant varieties [97]: the k-secant variety $S_k(A, \mathbb{P})$ of a variety A in a projective space $\mathbb{P}$ is the (Zariski closure of) the union of all secant k-planes to A (*i.e.*, k-planes defined by $k+1$ (non-k-coplanar) points of A).

Corollary 9. *For $s = 1$, the first secant variety of the spin coherent sphere coincides with the ambient projective space, $S_1(S^2_{\rm SC}, \mathbb{P}^2) = \mathbb{P}^2$.*

For higher values of spin, we have the following

Corollary 10. *Through a point* $[\Psi]$ *in* $\mathbb{P}^N$*,* $N \geq 3$*, passes at most one line intersecting* S^2_{SC} *twice.*

Proof. Assume there are two lines through $[\Psi]$ and intersecting S^2_{SC} twice, at $[n_1]$, $[n_2]$, and $[m_1]$, $[m_2]$, respectively. Then the relation $\alpha_1|n_1\rangle + \alpha_2|n_2\rangle = \beta_1|m_1\rangle + \beta_2|m_2\rangle$ may be inferred, and by linear independence of the SC states, $|\Psi\rangle = 0$ follows. □

Note that, as a consequence, for $N \geq 3$, if a state $|\Psi\rangle$ can be written as a linear combination of two SC states, that decomposition is unique. In $\mathbb{P}$, the linear span of two SC states has real dimension at most 6, hence, for $s \geq 2$, there will be states which cannot be expressed as a linear combination of two SC states. For $s = 3/2$ such a decomposition is possible, and unique, for most of the states, as the following proposition asserts

Proposition 11. *For* $s = 3/2$*, any state* $[\Psi]$ *without degenerate constellation lies on a complex line defined by two SC states.*

Proof. Setting $|\Psi\rangle$ equal to a linear combination of the SC states $|n_1\rangle$, $|n_2\rangle$, implies for the corresponding Majorana polynomials

$$(z-\zeta_1)(z-\zeta_2)(z-\zeta_3) = \alpha_1(z-\gamma_1)^3 + \alpha_2(z-\gamma_2)^3\,. \tag{3.39}$$

Solving for γ_1, γ_2, α_1, α_2, we get

$$\begin{aligned}\gamma_{1,2} = A^{-1}\big(&\zeta_1^2(\zeta_2+\zeta_3) + \zeta_2^2(\zeta_3+\zeta_1) + \zeta_3^2(\zeta_1+\zeta_2)\\ &- 6\zeta_1\zeta_2\zeta_3 \pm i\sqrt{3}\zeta_{12}\zeta_{23}\zeta_{31}\big)\end{aligned} \tag{3.40}$$

$$\alpha_1 = \frac{-3\gamma_2 + \zeta_1 + \zeta_2 + \zeta_3}{3(\gamma_1-\gamma_2)} \tag{3.41}$$

$$\alpha_2 = \frac{3\gamma_1 - \zeta_1 - \zeta_2 - \zeta_3}{3(\gamma_1-\gamma_2)}\,, \tag{3.42}$$

with $\zeta_{ik} \equiv \zeta_i - \zeta_k$ and

$$A \equiv 2\left(\zeta_1^2 + \zeta_2^2 + \zeta_3^2 - \zeta_1\zeta_2 - \zeta_2\zeta_3 - \zeta_3\zeta_1\right)\,.$$

□

Consider, as an example, the two representative, $s = 3/2$, non-biseparable states, $|\mathrm{GHZ}\rangle$ and $|\mathrm{W}\rangle$ [27]. The constellation of the first is a maximal equilateral triangle that can, by a suitable rotation, be placed on the equator, with one star on the positive x-axis. For this orientation, the decomposition in two SC states of proposition 11 is $|\mathrm{GHZ}\rangle = \frac{1}{\sqrt{2}}(|z\rangle + |-z\rangle)$. This result is also found in [34].

On the other hand, the constellation of the state $|\mathrm{W}\rangle$ consists of two coincident stars, and a third one, antipodal to the other two. As suggested by proposition 11, such a state cannot be written as a superposition of two SC states, which is also consistent with the results of [67] mentioned earlier. Still, it is of interest to inquire what exactly happens if eqs. (3.40), (3.41), (3.42), are pushed to their limit in this case. It is easily seen that as $\zeta_3 \to \zeta_2$ in (3.39), eq. (3.40) implies that γ_1 and γ_2 tend to ζ_2, while both α_1, α_2 blow up. However, a slight reaccommodation of (3.39),

$$(z-\zeta_1)(z-\zeta_2)(z-\zeta_3) = (\alpha_1+\alpha_2)(z-\gamma_1)^3 + \alpha_2\left((z-\gamma_2)^3 - (z-\gamma_1)^3\right)\,, \tag{3.43}$$

fixes all problems: the coefficient of the first term on the right hand side is constant, $\alpha_1+\alpha_2 = 1$, while the exploding α_2 in the second term is matched with the vanishing difference $(\zeta-\gamma_2)^3 - (\zeta-\gamma_1)^3$, their product having a finite limit,

$$(z-\zeta_1)(z-\zeta_2)^2 = (z-\zeta_2)^3 + \lim_{\zeta_3\to\zeta_2}\alpha_2\big((\zeta-\gamma_2)^3-(\zeta-\gamma_1)^3\big) = (\zeta-\zeta_2)^3 + (\zeta_2-\zeta_1)(\zeta-\zeta_2)^2\,.$$

Clearly, what transpires here is that the spin-3/2 state with a double degeneracy lies on a complex line defined by an SC state and a vector tangent to $S^2_{\rm SC}$ at that same state. Thus, states with degenerate constellations are also in $S_1(S^2_{\rm SC}, \mathbb{P}^3)$ and, combining this with proposition 11 we arrive at a statement analogous to corollary 9, for $s = 3/2$:

Corollary 12. $S_1(S^2_{\rm SC}, \mathbb{P}^3) = \mathbb{P}^3$.

The next result gives us a way to imagine the constellations corresponding to the points (states) of a complex line passing through two SC states.

Theorem 13. *Given two spin-s SC states with roots γ_1, $\gamma_2 \in \mathbb{C}$, respectively. The roots $\zeta_k(t)$, $k = 0, \ldots, N-1$, of a linear combination of their Majorana polynomials*

$$\alpha_1^N(\zeta-\gamma_1)^N - \alpha_2^N(\zeta-\gamma_2)^N$$

where $\alpha_1 = \cos t$, $\alpha_2 = e^{i\Omega}\sin t$, trace out circles that intersect equiangularly at γ_1, γ_2.

Proof. We compute

$$\alpha_1^N(z-\gamma_1)^N-\alpha_2^N(z-\gamma_2)^N=\prod_{k=1}^{N}\Big(\alpha_1(z-\gamma_1)-\xi^k\alpha_2(z-\gamma_2)\Big)=\big(\alpha_1^N-\alpha_2^N\big)\prod_{k=1}^{N}\left(z-\frac{\gamma_1\alpha_1-\gamma_2\xi^k\alpha_2}{\alpha_1-\xi^k\alpha_2}\right), \tag{3.44}$$

with $\xi=e^{i2\pi/N}$ a primitive Nth root of unity, which shows that

$$\zeta_k(t)=\frac{\gamma_1\cos t-\gamma_2 e^{i\Omega}\xi^k\sin t}{\cos t-e^{i\Omega}\xi^k\sin t}\,. \tag{3.45}$$

Consider now the Möbius transformation $M(\zeta)=(\zeta-\gamma_1)/(\zeta-\gamma_2)$ and substitute from (3.45) to find

$$M(\zeta_k(t))=e^{i(\Omega+2\pi k/N)}\tan t\,, \tag{3.46}$$

which is a line through the origin making an angle $\Omega+2\pi k/N$ with the real axis. The proof is completed by noting that Möbius transformations are conformal. □

Some related comments:

1. The theorem could be stated in terms of a linear combination of the states themselves — passing to the corresponding Majorana polynomials involves a rescaling of the coefficients in the linear combination.

2. As usual, "circles" in the complex plane, include the case of straight lines through the origin (see, *e.g.*, left aside of figure 3.4).

3. Given that stereographic projection is also conformal, we may conclude that the trajectories of the stars on the Bloch sphere are also circles intersecting equiangularly. This result has been pointed out before for $s=1$ [34].

4. The theorem provides a proof of the fact that a superposition of two SC states cannot produce a state with degenerate stars, as suggested, for $s=3/2$, in proposition 11.

A particular $s=3/2$ case is depicted in figure 3.4.

We end this subsection with a general statement about the number of distinct stars of a linear combination of *any* two states. To begin with, note that if the states share a star n, with multiplicities, say, r, s, respectively, then a linear combination of them will also have n as a star, with multiplicity equal to $\min(r,s)$. Clearly, an analogous result holds in the case of several

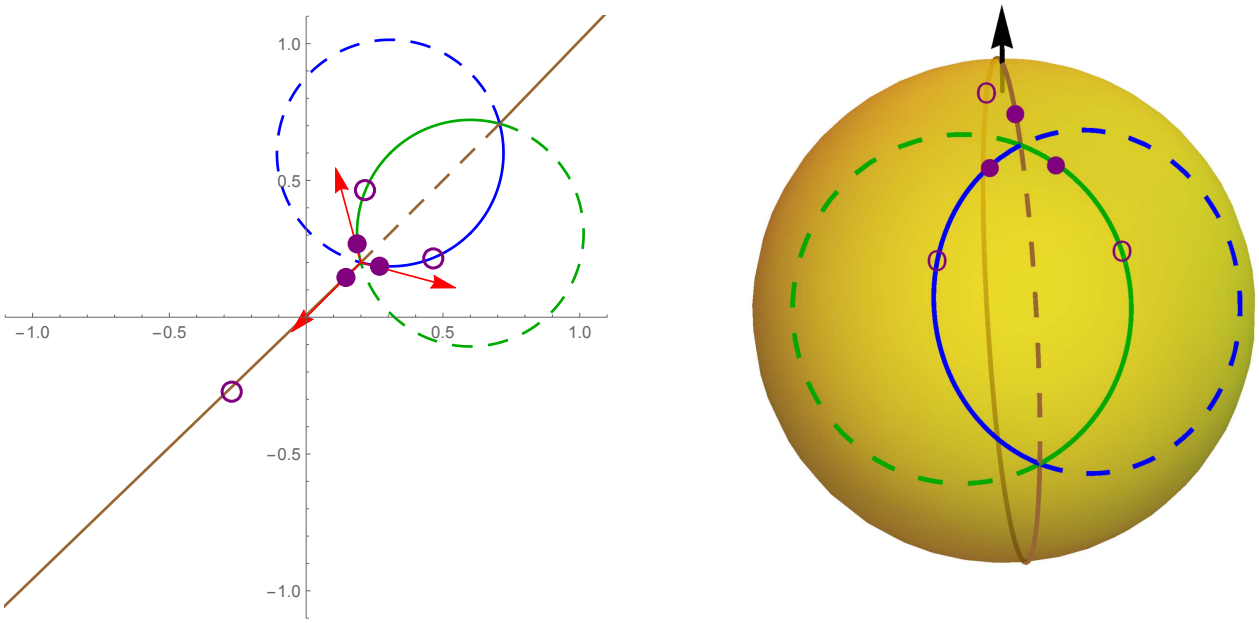

Figure 3.4: Plot of the curves $\zeta_k(t)$ in (3.45) in the complex plane (left) and its stereographic projection (right), for $s = 3/2$, $\gamma_1 = (1+i)/5$, $\gamma_2 = (1+i)/\sqrt{2}$ and $\Omega = 0$. The solid part of each circle takes a root ζ_i from γ_1 to γ_2, for $0 \leq t \leq \pi/2$, while the dashed part returns it from γ_2 to γ_1, for $\pi/2 \leq t \leq \pi$. The red arrows at γ_1, in the top figure, are the vectors tangent to the curves at $t = 0$, with an angle $2\pi/3$ between any two of them. The solid dots and little circles denote the configuration of the constellation at $t = 0.1$ and $t = 0.45$, respectively.

stars $\{n_i\}$ in common, each with different multiplicities $\{r_i\}$, $\{s_i\}$, in the two states. When factoring the linear combination of the two corresponding Majorana polynomials, such common factors may be canceled, and the problem reduces to that of a lower spin, without common stars. Therefore, we may assume, without loss of generality, that the states in question have no stars in common (note that each state may have stars with multiplicity). Then the following result holds

Theorem 14. *Consider two spin-s states, $|\Psi_1\rangle$, $|\Psi_2\rangle$, with n_1, n_2 distinct stars respectively (each with possible multiplicity) of which none are in common between the two states. Then an arbitrary linear combination $|\Phi\rangle = a|\Psi_1\rangle + b|\Psi_2\rangle$ has itself at least $N - n_1 - n_2 + 1$ distinct stars (each with possible multiplicity).*

Proof. The statement is an immediate consequence of Mason's theorem [71, 70, 59]. Let $n_0(F(\zeta))$ denote the number of distinct roots of the complex polynomial $F(\zeta)$. Let A, B, C be relatively prime polynomials such that $A + B = C$. Then Mason's theorem states that

$$\max \deg\{A, B, C\} \leq n_0(ABC) - 1 \,. \tag{3.47}$$

To apply this to our case, put

$$A = ap_{\Psi_1} \,, \quad B = bp_{\Psi_2} \,, \quad C = p_\Phi \,,$$

with the Majorana polynomials, so that $n_0(A) = n_1$, $n_0(B) = n_2$, and, say, $n_0(C) = n_3$. With our assumption about no common roots, if one of the $|\Psi_i\rangle$ has a star at the south pole, and, hence, the degree of its Majorana polynomial is less than N, the other cannot also have a star there, and the left hand side of (3.47) is, in all cases, equal to N. Note also that if C shared a root with, say, A, then it would have to also share it with B, which contradicts our assumptions, so all n_3 distinct roots of C are different from those of A and B. Then the number of distinct roots of the product ABC is $n_0(ABC) = n_1+n_2+n_3$, and the statement follows from (3.47). □

For the case of two SC states, $n_1 = n_2 = 1$, we get $n_3 \geq N - 1$, which is weaker than our result that in fact $n_3 = N$. On the other hand, for two states with star multiplicities, such that $n_1 + n_2 < N$, we get $n_3 \geq 2$, which is a new result: the complex line through such states does not intersect $S^2_{\rm SC}$.

3.4.2 S^2_{SC} immersed in the projective Hilbert space

In this final subsection, we study some properties of the immersion of the S^2_{SC}. As we said before, S^2_{SC} is isometric to the 2-sphere, but, how is this 2-sphere living in the projective Hilbert space? A starting point to imagine this embedding is with the answer of the following question: how many independent directions does $S^2_{\rm SC}$ explore in $\mathbb{P}$? We find that, just like Dali's iconic clocks (topological discs) cannot be contained in any 2-plane, the spin coherent 2-sphere extends in all available directions in $\mathbb{P}$. The precise statement is the following

Theorem 15. *Consider an arbitrary state* $[\Psi]$ *in* $\mathbb{P}$ *and let* $\exp_\Psi$ *be the exponential map defined with the Fubini-Study metric from* $T_{[\Psi]}\mathbb{P}$*, the tangent space at* $[\Psi]$*, to* $\mathbb{P}$*. The inverse image of* $S^2_{\rm SC}$ *under this map,* $\log_\Psi(S^2_{\rm SC})$*, is of maximal dimension in* $T_{[\Psi]}\mathbb{P}$*.*

Proof. We represent $[\Psi] \in \mathbb{P}$ by the density matrix $\rho_\Psi = |\Psi\rangle\langle\Psi|$. Then, a tangent vector in $T_{[\Psi]}\mathbb{P}$ is represented by the matrix $|\Psi\rangle\langle\varphi| + |\varphi\rangle\langle\Psi|$ for some $|\varphi\rangle \in \mathscr{H}$ satisfying $\langle\varphi|\Psi\rangle = 0$. Suppose that $\log(S^2_{\rm SC})$ is contained in an affine subspace of $T_{[\Psi]}\mathbb{P}$ of real dimension lower than $4s$. Then there exists a tangent vector X in $T_{[\Psi]}\mathbb{P}$,

$$X = |\Psi\rangle\langle\chi| + |\chi\rangle\langle\Psi|\,, \quad \text{with } \langle\chi|\Psi\rangle{=}0\,, \tag{3.48}$$

such that the inner product between X and $v_n \equiv \log_\Psi \rho_n$, $\rho_n \equiv |n\rangle\langle n|$, is constant, say, equal to λ, for all SC states $[n]$. Using the explicit expression for v_n in eqs. (3.57) and (3.58) below, we find

$$\lambda = \frac{1}{2}{\rm Tr}(v_n X) = \frac{\omega_{n\Psi}}{2\sin\omega_{n\Psi}}\left(e^{i\eta_{n\Psi}}\langle\chi|n\rangle + e^{-i\eta_{n\Psi}}\langle n|\chi\rangle\right)\,, \tag{3.49}$$

where $\langle n|\Psi\rangle \equiv \cos\omega_{n\Psi} e^{i\eta_{n\Psi}}$, $\omega_{n\Psi} \in [0, \pi/2]$. The condition $\eta_{n\Psi} = 0$ fixes the phase of all $|n\rangle$, except for the isolated points where $\langle n|\Psi\rangle = 0$ — since this latter set is of measure zero, it does not affect our argument below. From (3.49) we find

$$\Re\langle\chi|n\rangle = \frac{\sin\omega_{n\Psi}}{\omega_{n\Psi}}\lambda\,, \tag{3.50}$$

where $\Re$ denotes real part. Now we will consider two cases, $\lambda = 0$ and $\lambda \neq 0$. If $\lambda = 0$ then, by equation (3.50), $\langle n|\chi\rangle$ is imaginary,

$$\langle n|\chi\rangle = \cos\omega_{n\chi} e^{i\eta_{n\chi}} = \pm i\cos\omega_{n\chi}\,. \tag{3.51}$$

The crucial observation at this point is that the real function $f(n) = -i\langle n|\chi\rangle = \pm\cos\omega_{\eta\chi}$, where one of the two possible signs is chosen, cannot change sign on the sphere, since it only has a finite number of isolated zeros. Indeed, assuming that f takes both positive and negative values, one may always choose a curve on the sphere that connects the corresponding points without passing through any of the isolated zeros of f, leading to *absurdum*, as, by the intermediate value theorem, f must have a zero in a certain point of the curve. Having established this fact about f, we use the completeness relation for $|n\rangle$ to arrive at

$$0 = \langle\Psi|\chi\rangle = \frac{2s+1}{4\pi}\int\langle\Psi|n\rangle\langle n|\chi\rangle d\Omega = \pm i\frac{2s+1}{4\pi}\int\cos\omega_{n\Psi}\cos\omega_{n\chi}d\Omega\,, \tag{3.52}$$

which is impossible, since the integrand is non-negative.

If $\lambda \neq 0$, equation (3.50), and the fact that $\langle n|\Psi\rangle$ is real, imply

$$\Re(\langle\chi|n\rangle)\langle n|\Psi\rangle = \frac{\cos\omega_{n\Psi}\sin\omega_{n\Psi}}{\omega_{n\Psi}}\lambda\,,$$

so that

$$\int \Re(\langle\chi|n\rangle)\langle n|\Psi\rangle d\Omega = \lambda \int \frac{\cos\omega_{n\Psi}\sin\omega_{n\Psi}}{\omega_{n\Psi}} d\Omega\,.$$

By the same argument that lead to (3.52), the left hand side is zero, but the integrand in the right hand side is positive almost everywhere, leading again to *absurdum*, which shows that such X does not exist, and the proof is complete. □

The last result implies that if you want to do a "picture" of $S^2_{\rm SC}$ using the exponential map, you will always need a $4s$-dimensional picture to observe the correct image wherever which point (state) $[\Psi]$ you are in $\mathbb{P}$.

The image of S^2_{SC} becomes stranger than before with the following thought. Consider a geodesic $(4s-1)$-sphere of radius r, S_r, centered at $[\Psi]$, *i.e.*, the locus of points in $\mathbb{P}$ that are a fixed geodesic (Fubini-Study) distance r from $[\Psi]$. The intersection points of S_r with $S^2_{\rm SC}$ give those SC states that are at a distance r from $[\Psi]$. For $[\Psi]$ non-SC, and r sufficiently small, the intersection is null. As r increases, it reaches a critical value $r_{\rm c}$ at which $S_{r_{\rm c}}$ just touches $S^2_{\rm SC}$ at, generically, a single point $[n_0]$. The value of $r_{\rm c}$ is the geometrical measure of entanglement of $[\Psi]$ [19], which is defined as the minimum of the distant between $[\Psi]$ and the S^2_{SC}. For $r > r_{\rm c}$, the intersection is one-dimensional, consisting, generically, of the union of topological circles. When r reaches its maximal value $\pi/2$, $S^2_{\rm SC}$ is tangent to $S_{\pi/2}$ "from the inside", touching it at exactly N points, which are the SC states antipodal to the stars (assumed distinct) of $[\Psi]$ — the collection of these states, lifted arbitrarily in $\mathscr{H}$, forms a basis of the orthogonal complement of $|\Psi\rangle$ in $\mathscr{H}$. It is a bit puzzling then that the above two spheres remain tangent at N points, for *any* position of the center $[\Psi]$ of $S_{\pi/2}$ (the N points of tangency, of course, change, as $[\Psi]$ is moved around in $\mathbb{P}$). Looking at figure 3.3, and trying to imagine the surface depicted there wrapped around $S^2_{\rm SC}$, we arrive at the cartoon in figure 3.5, where, for simplicity, we have assumed that $s = 1$, so that there are only two "peaks" on $S^2_{\rm SC}$. But this image is hardly convincing: for example, how are the peaks compatible with the known fact that the restriction of the Fubini-Study metric on $S^2_{\rm SC}$ gives a perfectly "round" sphere, with constant curvature? And how can $S_{\pi/2}$ remain tangent to $S^2_{\rm SC}$ when $[\Psi]$ is moved freely in $\mathbb{P}$? Worse still, how many peaks does $S^2_{\rm SC}$ really have, if any? Now, some of these puzzles are simply byproducts of vague phrasing, naively drawn cartoons, and other easily fixable looseness. For example, $S_{\pi/2}$ in figure 3.5 is actually a codimension-1 object (*e.g.*, 3D for $s = 1$), which

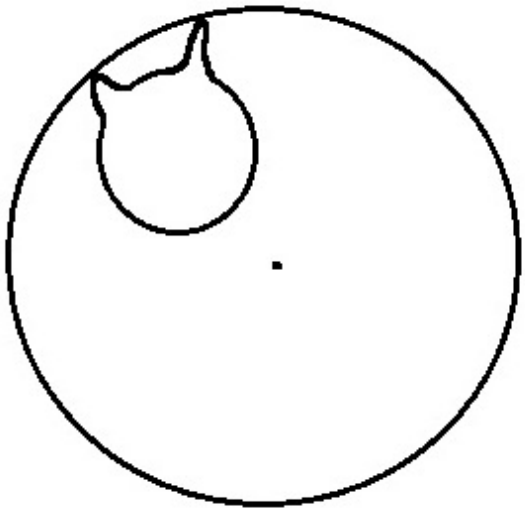

Figure 3.5: Artist's rendition of the geodesic sphere $S_{\pi/2}$ (outlying circle), centered at $[\Psi]$, and of $S^2_{\rm SC}$ (cat shaped curve), tangent to $S_{\pi/2}$ at two points (assuming $s = 1$).

is certainly not what that image conveys. To get a visual idea, we will explicitly do the same calculation as the last theorem for $s = 1$. We assume that the light used to take the picture follows Fubini-Study geodesics, and use the inverse of the exponential map, based at $[\Psi]$, to lift the image of $S^2_{\rm SC}$ into the tangent space at $[\Psi]$ — the result is what we called $\log_\Psi(S^2_{\rm SC})$. The $4(s = 1)$-dimensional object will be projected in a 3-plane. We sketch the calculation, fixing, for simplicity, $s = 1$, and identifying a point $[\Psi]$ with the density matrix $\rho_\Psi = |\Psi\rangle\langle\Psi|$. The two stars n_1, n_2, of $|\Psi\rangle$ are taken in the x-z plane, symmetrically with respect to the z-axis, and making an angle $\alpha \in [0, \pi/2]$ with it, *i.e.*,

$$n_1 = (\sin\alpha, 0, \cos\alpha)\,, \qquad n_2 = (-\sin\alpha, 0, \cos\alpha)\,. \tag{3.53}$$

The corresponding state, in the S_z-basis $(1, 0, -1)$, is

$$|\Psi\rangle = 2b^{-1}\left(\cos^2\frac{\alpha}{2}, 0, -\sin^2\frac{\alpha}{2}\right)\,, \tag{3.54}$$

with $b \equiv \sqrt{3 + \cos 2\alpha}$. The SC states corresponding to the stars are

$$|n_1\rangle = \left(\cos^2\frac{\alpha}{2}, \frac{1}{\sqrt{2}}\sin\alpha, \sin^2\frac{\alpha}{2}\right)\,, \qquad |n_2\rangle = \left(\cos^2\frac{\alpha}{2}, -\frac{1}{\sqrt{2}}\sin\alpha, \sin^2\frac{\alpha}{2}\right)\,. \tag{3.55}$$

The curve

$$|c(t)\rangle = (\cos t - \cot\omega \sin t)|\Psi\rangle + e^{i\eta}\sin t \csc\omega |n\rangle\,, \tag{3.56}$$

in $\mathscr{H}$, where $\langle n|\Psi\rangle \equiv \cos\omega\, e^{i\eta}$, projects to a geodesic $\rho_{c(t)}$ in $\mathbb{P}$, starting, at $t=0$, at ρ_Ψ and reaching, at $t=\omega$, the SC state ρ_n. The tangent vector $\partial_t \rho_{c(t)}|_{t=0} \equiv \dot\rho_c(0)$ is given by

$$\dot\rho_c(0) = -2\cot\omega\rho_\Psi + \csc\omega\left(e^{i\eta}|n\rangle\langle\Psi| + e^{-i\eta}|\Psi\rangle\langle n|\right)\,, \tag{3.57}$$

and is of unit length, as t is arclength along $\rho_c(t)$. Then

$$v_n \equiv \log_\Psi \rho_n = \omega\dot\rho_c(0)\,, \tag{3.58}$$

is the sought image of ρ_n in $T_\Psi\mathbb{P}$, since ω is the geodesic distance between ρ_Ψ and ρ_n. We choose an orthonormal hermitian basis $\{h_1, h_2, h_3, h_4\}$ in $T_\Psi\mathbb{P}$, where

$$H_1 \equiv h_1{+}ih_2 = 2b^{-1}\begin{pmatrix} 0 & 0 & 0 \\ \cos\alpha{+}1 & 0 & \cos\alpha{-}1 \\ 0 & 0 & 0 \end{pmatrix}\,,\quad H_2 \equiv h_3{+}ih_4 = b^{-2}\begin{pmatrix} 1{-}\cos 2\alpha & 0 & -8\sin^4\frac{\alpha}{2} \\ 0 & 0 & 0 \\ 3{+}\cos 2\alpha{+}4\cos\alpha & 0 & \cos 2\alpha{-}1 \end{pmatrix}\,, \tag{3.59}$$

and compute the corresponding components $v_n^i = \frac{1}{2}\mathrm{Tr}(v_n h_i)$,

$$v_n^1 + iv_n^2 = \frac{\sqrt{2}e^{-i\phi}\omega\chi\sin\theta}{b\sin\omega\cos\omega}\,,\quad v_n^3 + iv_n^4 = \frac{4e^{-i2\phi}\omega\chi\xi}{b^2\cos\omega\sin\omega}\,, \tag{3.60}$$

where

$$\chi = \cos^2\frac{\alpha}{2}\cos^2\frac{\theta}{2} - e^{i2\phi}\sin^2\frac{\alpha}{2}\sin^2\frac{\theta}{2}\,,\qquad \xi = \cos^2\frac{\alpha}{2}\sin^2\frac{\theta}{2} + e^{i2\phi}\sin^2\frac{\alpha}{2}\cos^2\frac{\theta}{2}\,, \tag{3.61}$$

and the phase of the SC states was chosen so that $\langle n|\Psi\rangle = \cos\omega \geq 0$. We plot the projection of $\log_\Psi S^2_{\mathrm{SC}}$ in the 123-plane, for $\alpha = \pi/12$, $\pi/3$, and $\pi/2$, in figure 3.6. Since normal coordinates, centered at ρ_Ψ, are being used, ρ_Ψ lies at the origin in the figure and Fubini-Study geodesics through it look like straight lines. A notable, and initially puzzling, feature of the surface shown in that figure, supposedly the image of a topological 2-sphere, is that it seems to have a boundary: one sees a self-intersecting surface that ends on two ellipses (highlighted in blue/violet). The latter are the projections, in the 123-plane, of two circles in the full, 4D tangent space. In their turn, the circles are the inverse images, under the exponential map, of the SC states in the directions antipodal to the stars of ρ_Ψ. What happens here is that $|\Psi\rangle = |n_1, n_2\rangle$ is orthogonal to $|{-}n_i\rangle$, $i = 1, 2$, so that $[\Psi]$ and, say, $[-n_1]$, are antipodal points on the projective line (real 2-sphere) they define. Then $[-n_1]$ is in the cut locus of $\exp_\Psi$ and all vectors tangent to the above 2-sphere at $[\Psi]$, of length $\pi/2$, "point" to $[-n_1]$ — the circles (ellipses) in the figure are

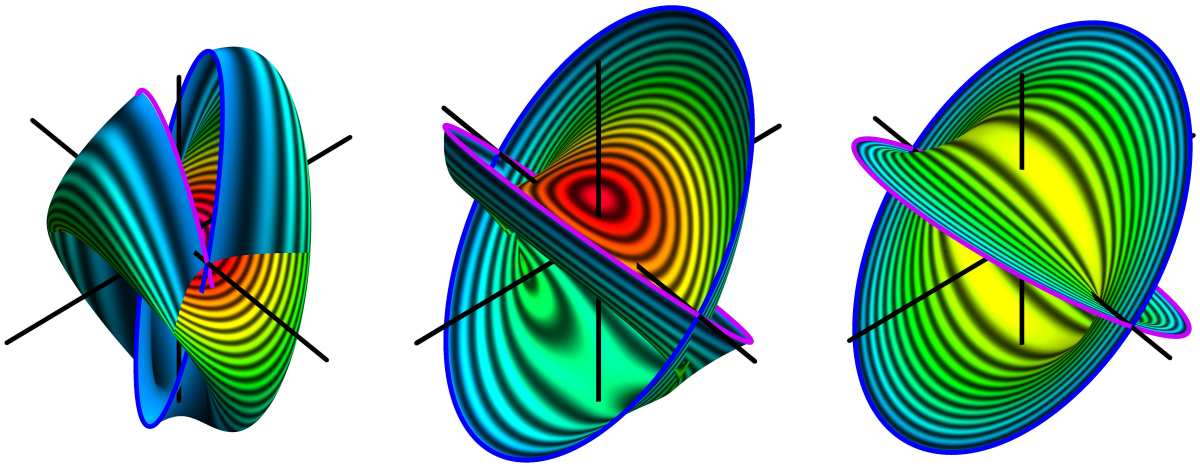

Figure 3.6: Plot of $\log_\Psi(S^2_{\mathrm{SC}})$ with $|\Psi\rangle$ as in (3.54), for $\alpha = \pi/12$ (left), $\pi/3$ (center), $\pi/2$ (right) (projection in the plane 123). The state $[\Psi]$ is at the origin where the axes intersect (not visible). The highlighted ellipses are the inverse images, under $\exp_\Psi$, of the SC states $[-n_1]$, $[-n_2]$ in directions antipodal to the stars of $[\Psi]$ — the singularities of $\log_\Psi$ there blow up individual points to entire circles. The color coding assigns warmer colors to the SC states closest to $[\Psi]$ (red for the north pole of S^2_{SC} in the first two plots, yellow for the 23 meridian in the third plot), and blue to those farthest away (above mentioned ellipses). The rapid brightness modulation marks equidistance from $[\Psi]$ — note how it slows down near the above mentioned extrema.

just the loci of those tangent vectors. Going one dimension up, in the full tangent space, the geodesic sphere $S_{\pi/2}$ would look like a euclidean 3-sphere centered at the origin, where $[\Psi]$ lies, and the above circles are great circles on that sphere. This last statement, of course, needs to be taken with a grain of salt, as $S_{\pi/2}$ is in its entirety in the cut locus of $\exp_\Psi$, but it can be made precise in a limiting sense.

Two further "snapshots" of S^2_{SC} for $\alpha = \pi/3$, from different viewpoints, are shown in figure 3.7 (left and middle plots). In the middle one, the complex line defined by $[n_1]$, $[n_2]$, is also plotted — rather than a topological 2-sphere, it looks like a spherical cap, the reason being that the state $\sqrt{2/3}(|n_1\rangle - |n_2\rangle)$, which belongs to that complex line, is orthogonal to $|\Psi\rangle$, so its logarithm is, as we have seen above, an entire circle (the boundary of the cap). Note that this is the rule rather than the exception: any generic complex line $|\phi_1\rangle + \zeta|\phi_2\rangle$ contains a single state $|\Psi\rangle^\perp$ orthogonal to a given state $|\Psi\rangle$, corresponding to $\zeta = -\langle\Psi|\phi_1\rangle/\langle\Psi|\phi_2\rangle$. That state will blow up

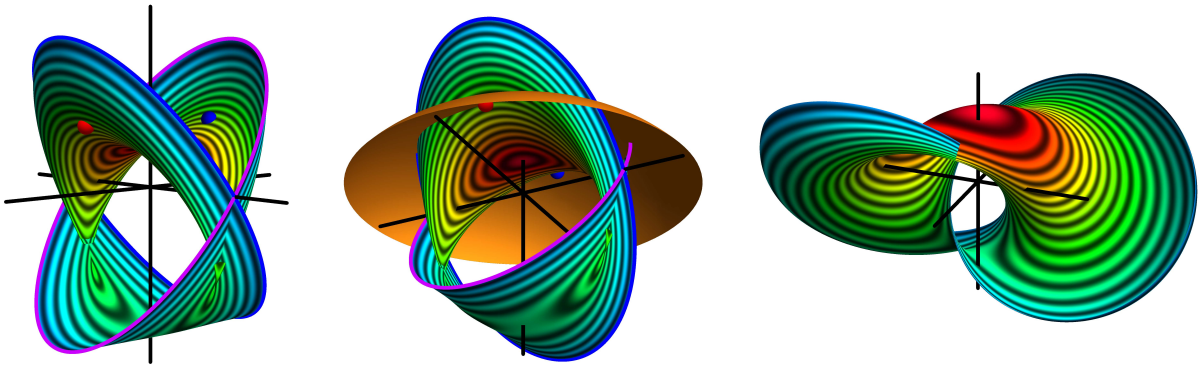

Figure 3.7: **Left and middle:** Shown is the surface in the middle of Fig. 3.6 ($\log_\Psi(S^2_{\rm SC})$ for $\alpha = \pi/3$), from two different viewpoints. The two little spheres on the surface denote the position of the SC states $[n_1]$, $[n_2]$ (see (3.55)), corresponding to the stars of $[\Psi]$ ($[\Psi]$ itself is at the origin). The "spherical cap" superimposed in the figure in the middle is the complex line ℓ passing through $[n_1]$, $[n_2]$ — although topologically a 2-sphere, it appears to have a boundary because the state $|\Psi\rangle^\perp = \sqrt{2/3}(|n_1\rangle - |n_2\rangle)$, which belongs to ℓ and is orthogonal to $|\Psi\rangle$, is blown up into a circle (the boundary of the cap) under $\log_\Psi$. Note that (the projection of) $S^2_{\rm SC}$, rather than a moon-like object in the horizon, appears to "wrap around the sky" when viewed from $[\Psi]$. Note also that, in the full (4D) $T_\Psi\mathbb{P}^2$, ℓ only intersects $S^2_{\rm SC}$ in the two points $[n_1]$, $[n_2]$ — additional intersections appearing in the figure are an artifact of the projection in the 123-hyperplane. **Right:** Stereographic projection from the south 4-pole to the equatorial 123-hyperplane in $T_\Psi\mathbb{P}$ of the image of $S^2_{\rm SC}$ under the map $\dot\rho_c(0)\colon S^2_{\rm SC} \to S^3 \subset T_\Psi\mathbb{P}$ in equation (3.57). The color coding in all three plots is as in figure 3.6.

into a full circle under $\log_\Psi$, and, accordingly, the complex line, rather than a 2-sphere, will look like a cap, with $\log_\Psi([\Psi]^\perp)$ at its boundary.

Another way to visualize $S^2_{\rm SC}$ is to use $\dot\rho_c(0)$, in equation (3.57), to map $S^2_{\rm SC}$ to a surface in the unit tangent sphere S^3 at $[\Psi]$. Thus, the radial information about $S^2_{\rm SC}$ is erased, and the above mentioned surface only records the direction in which each point of $S^2_{\rm SC}$ is viewed from $[\Psi]$. That surface, in turn, may be stereographically projected from the "south" 4-pole to the 123-equatorial plane in $T_\Psi\mathbb{P}$ — the result is plotted in the right in figure 3.7. Note that the two circles that correspond to the SC states $[-n_1]$, $[-n_2]$ are linked.

A further interesting result can be inferred from (3.57). To begin with, that relation is valid

with $|n\rangle$ being replaced by a general (*i.e.*, not necessarily SC) state $|a\rangle$. We use the notation $\langle a|\Psi\rangle = \cos\omega_{a\Psi}e^{i\eta_{a\Psi}}$ for any pair of states. Call v_a the unit vector tangent at $[\Psi]$, pointing towards $[a]$, and similarly for v_b. Then, the angle Θ_{ab} between v_a, v_b, is found to be

$$\cos\Theta_{ab} = \frac{1}{2}\mathrm{Tr}(v_a v_b) = \frac{\cos\omega_{ab}\cos\Omega - \cos\omega_{a\Psi}\cos\omega_{b\Psi}}{\sin\omega_{a\Psi}\sin\omega_{b\Psi}}\,, \tag{3.62}$$

where $\Omega = \eta_{ab} + \eta_{b\Psi} + \eta_{\Psi a}$ is the phase of the Bargmann invariant of the three states involved,

$$\langle a|b\rangle\langle b|\Psi\rangle\langle\Psi|a\rangle = Re^{i\Omega}\,, \tag{3.63}$$

where $R, \Omega \in \mathbb{R}$. Note that, for $\Omega = 0$, (3.62) reduces to the formula for the angle of a spherical geodesic triangle in terms of the lengths (angles) of its sides. This is not an accident, in fact (3.62) *is* the spherical trigonometric formula, only expressed in terms of projective space quantities. To see this, consider the real version of the Hilbert space $\mathscr{H}$, with $\mathscr{H} \ni |\Psi\rangle = (x_0 + iy_0, \ldots, x_N + iy_N) \to (x_0, \ldots, x_N, y_0, \ldots, y_N) = \Psi \in \mathbb{R}^{2N+2}$, so that normalized kets in $\mathscr{H}$ are mapped to the unit sphere S^{2N+1} in $\mathbb{R}^{2N+2}$. The euclidean inner product between two such vectors Ψ, Φ, is easily seen to be given by $\Psi\cdot\Phi = \Re\langle\Psi|\Phi\rangle$, so that the angle s between them satisfies

$$\cos s = \Psi\cdot\Phi = \Re\langle\Psi|\Phi\rangle = \cos\omega_{\Psi\Phi}\cos\eta\,, \tag{3.64}$$

where $\langle\Psi|\Phi\rangle = \cos\omega_{\Psi\Phi}e^{i\eta}$, and $\omega_{\Psi\Phi}$ is the FS distance between $[\Psi]$, $[\Phi]$ in $\mathbb{P}$. When the two states are in phase, *i.e.*, their inner product is positive, their distance on S^{2N+1} is equal to the FS one of their images in $\mathbb{P}$ — (3.62) then follows, keeping in mind that the SC states where assumed in phase with $|\Psi\rangle$.

Chapter 4

k-planes in Hilbert space and applications

If we create a universe, let it not be abstract or vague but rather let it concretely represent recognizable things.

M. C. Escher

4.1 Motivation: A robust non-abelian geometric phase

In 1984, more than 50 years since the birth of the formulation of quantum mechanics, Berry discovered [12] that the phase of an adiabatic cyclic evolution of a state has two contributions: the old known dynamical part $F_d = \int E dt$ and an additional one proportional to the area of the curve in the parametric space of the Hamiltonian. Simon writes this *geometric phase* in terms of an anholonomy in a principal fiber bundle given by a *Berry connection* [91]. It has been generalized, step by step, improving the definition for non-adiabatic, non-unitary, non-cyclic situations [2, 86, 77], and finally it converges in a general definition of the geometric phase for any path in the projective Hilbert space given by Mukunda and Simon [79]. To understand this geometric phase let $\mathbb{P}$ be a finite projective Hilbert space, and consider it as the base space of a principal fiber bundle with fibers diffeomorphic to $U(1)$, where for any two points $|\psi\rangle$, $|\psi'\rangle$ in the same fiber $[\psi]$ there exists $e^{i\alpha} \in U(1)$ such that $|\psi'\rangle = e^{i\alpha}|\psi\rangle$. The total space would be the Hilbert space of unitary vectors. Now, taking a gauge choice in the total space, consider a

one-parameter smooth curve $\mathscr{C} = \{|\psi(s)\rangle | s \in [s_1, s_2]\}$ in the total space, and the next functional $F[\mathscr{C}]$

$$F[\mathscr{C}] = \arg\langle\psi(s_1)|\psi(s_2)\rangle - \Im \int_{s_1}^{s_2} \langle\psi(s)|\dot{\psi}(s)\rangle ds\,, \tag{4.1}$$

where $\Im$ is the imaginary part. The functional is invariant under reparametrizations, because $|\dot{\psi}(s)\rangle ds = d|\psi\rangle(s)$. If we now perform a gauge transformation, it takes $\mathscr{C}$ into a new curve $\mathscr{C}'$, with $|\psi'(s)\rangle = e^{i\alpha(s)}|\psi(s)\rangle$ and

$$F[\mathscr{C}'] = \arg\langle\psi'(s_1)|\psi'(s_2)\rangle - \Im \int_{s_1}^{s_2} \langle\psi'(s)|\dot{\psi}'(s)\rangle ds \tag{4.2}$$

$$= \arg\langle\psi(s_1)|\psi(s_2)\rangle + \alpha(s_2) - \alpha(s_1) - \Im \int_{s_1}^{s_2} \Big(\langle\psi(s)|\dot{\psi}(s)\rangle + i\dot{\alpha}(s)\Big)\, ds = F[\mathscr{C}]\,. \tag{4.3}$$

With the gauge and reparametrization invariance, we prove that $F[\mathscr{C}]$ is a geometric quantity that only depends on the projection of the curve $\mathscr{C}$ in the base space $\pi(\mathscr{C}) \subset \mathbb{P}$. When the curve is given by a Hamiltonian evolution, the second term of (4.1) is the argument of the dynamic phase, and the first term of the total phase, recovering that $e^{iF[\mathscr{C}]}$ is the usual geometric phase.

In some cases the evolution doesn't return to the same state, and we wonder about properties of the unitary transformation between the initial and final states. For instance, if the initial state $|\psi_i\rangle$ is degenerated, it may not end in the same state even in the adiabatic case, but the final state must be in the degenerate subspace of $|\psi_i\rangle$, and we are interested to associate the unitary transformation U restricted in the degenerated subspace such that $|\psi_f\rangle = U|\psi_i\rangle$, where U is the called *non-abelian geometric phase*[1] [96]. As in the "abelian" case, there are generalizations to the adiabatic non-abelian phase, see for instance [4]. Following the ideas of Mukunda and Simon, we define a non-abelian geometric phase. In this case, the base space will be the complex Grassmannian $\mathsf{Gr}_{k,\mathbb{P}}$ manifold, *i.e.*, the space of the (complex) vector subspaces of $\mathbb{P}$, of dimension k. Note that $\mathsf{Gr}(1,\mathbb{P}) = \mathbb{P}$ and $\mathsf{Gr}(N+1,\mathbb{P}) = \{\mathbb{P}\}$, and that $\dim(\mathsf{Gr}(k,\mathbb{P})) = k(N+1-k)$, where $N = 2s$. For each point, we associate a fiber diffeomorphic to $U(k)$. The total space, called *Stiefel manifold* of $\mathbb{P}$ [53], is the set of the k-orthonormal frames of $\mathbb{P}$. The non-Abelian geometric phase of a curve $\mathscr{C}$ in a specific section in the base space is written as

$$U_{geo}[\mathscr{C}] = Q_p[\mathscr{C}] F[\mathscr{C}]\,, \tag{4.4}$$

[1] The name shall not be taken literaly since is a matrix transformation instead to a phase. However, we follow the same notation given in papers and textbooks.

with

$$F[\mathscr{C}] \equiv \mathscr{P} \exp\left[-\int_{s_1}^{s_2} A(s)ds\right], \qquad A_{ij}(s) = \langle \phi_i(s)|\dot{\phi}_j(s)\rangle\,, \tag{4.5}$$

and Q_p is the polar part of the matrix Q (see below), with entries $Q_{ij} = \langle \phi_i(s_1)|\phi_j(s_2)\rangle$. In the next theorem, we prove that U_{geo} is a covariant matrix.

Theorem 16. *U_{geo} is a covariant matrix,* i.e.*, under gauge transformations, $U'_{geo} = U^\dagger(t_1)U_{geo}U(t_1)$.*

Proof. Let us choose a section in the principal fiber bundle, Σ, and define a curve $\mathscr{C}(s)$ in the total space, $\{|\phi_j\rangle(s)\}_{j=1}^k$. A gauge transformation to Σ', defines a new curve $\mathscr{C}'(s)$ given by $|\phi'_j\rangle(s) = |\phi_\mu\rangle(s)U_{\mu j}(s)$ for each $j =, 1, \ldots, k$. The entries of the matrix $A(s)$ as

$$A'_{ij} = \langle \phi'_i|\dot{\phi'}_j\rangle = U^\dagger_{i\nu}\langle \phi_\nu|\dot{\phi}_\mu\rangle U_{\mu j} + U^\dagger_{i\mu}\dot{U}_{\mu j} \tag{4.6}$$

or in a compact way,

$$A' = U^\dagger A U - \dot{U}^\dagger U\,. \tag{4.7}$$

Now, we define the path integral of this matrix along the curve

$$F(s_1, s_2) \equiv \mathscr{P} \exp\left[-\int_{s_1}^{s_2} A(s)ds\right], \tag{4.8}$$

which is indeed the only solution of the following equations [26]

$$F(s_1, s_1) = \mathbb{1}\,, \qquad \partial_{s_1}F(s_1, s_2) = F(s_1, s_2)A(s_1)\,, \qquad \partial_{s_2}F(s_1, s_2) = -A(s_2)F(s_1, s_2)\,. \tag{4.9}$$

To see how $F(s_1, s_2)$ transforms under gauge transformations, let us prove that

$$F'(s_1, s_2) \equiv U^\dagger(s_2)F(s_1, s_2)U(s_1)\,, \tag{4.10}$$

satisfies the equations in (4.9). The first equation is trivial, and the proof of the last one is very similar to the second. Then, let us focus in the proof of the second equation,

$$\partial_{s_2}\left(F'U^\dagger(s_1)\right) = \dot{U}^\dagger(s_2)F + U^\dagger(s_2)\partial_{s_2}F \tag{4.11}$$

$$= \left(\dot{U}^\dagger(s_2)U(s_2) - U^\dagger(s_2)A(s_2)U(s_2)\right)U^\dagger(s_2)F \tag{4.12}$$

$$= -A'(s_2)U^\dagger(s_2)F \tag{4.13}$$

$$= -A'(s_2)F'U^\dagger(s_1)\,. \tag{4.14}$$

The matrix $F(s_1, s_2)$ will be the equivalent of the second term of the abelian case. Now, let us define the matrix Q, with entries

$$Q_{ij} = \langle \phi_i(s_1) | \phi_j(s_2) \rangle \,, \tag{4.15}$$

which transforms to $Q' = U^\dagger(s_1) Q U(s_2)$ under gauge transformations. For Q, we calculate the equivalent of the "phase" of a matrix, which is obtained using the polar decomposition of a matrix [40]. For each matrix Q, the singular value decomposition is $Q = W Q_d V^\dagger$, where W, V are unitary matrices, and Q_d is diagonal. Q_d is unique (up to change of ordering of the diagonal entries), but W and V aren't unique. The *polar* part of Q is defined by $Q_p = W V^\dagger$ which is unique. Now, let us see how Q_p changes under gauge transformations. First we calculate W' and V'

$$Q' = U^\dagger(s_1) Q U(s_2) = \left(U^\dagger(s_1) W \right) Q_d \left(V^\dagger U(s_2) \right) \,, \tag{4.16}$$

and by the uniqueness of Q_d in the singular value decomposition, $Q'_d = Q_d$ and then $W' = U^\dagger(s_1) W$ and $V' = U^\dagger(s_2) V$. Finally,

$$Q'_p = W' V'^\dagger = U^\dagger(s_1) W V^\dagger U(s_2) = U^\dagger(s_1) Q_p U(s_2) \,. \tag{4.17}$$

Q_p is the matricial equivalent of the first term of the abelian case. The non-abelian geometric phase is given by $U_{geo} \equiv Q_p F$ which under gauge transformations, using eqs. (4.17) and (4.10), changes covariantly

$$U'_{geo} = Q'_p F = U'^\dagger(s_1) U_{geo} U(s_1) \,. \tag{4.18}$$

□

In the 1-dimensional case, the last equation is reduced to the exponential of the abelian case (see eq. 4.1). By the covariance and reparametrization invariance of U_{geo}, we conclude that is a geometric quantity associated to the projection in the base space of the curve $\mathscr{C}$, $\pi(\mathscr{C})$.

We are interested in curves produced by rotations, $|\phi_j(s)\rangle = \mathsf{R}(s) |\phi_j(s_1)\rangle = e^{i\vec{\omega}(s)\cdot\mathbf{S}} |\phi_j(s_1)\rangle$. In this case, $A_{ij}(s) = i\vec{\omega}'(s) \cdot \langle \phi_i(s) | \mathbf{S} | \phi_j(s) \rangle$. Now, if the curve passes only for 1-anticoherent states, then $A_{ij}(s) = 0$ and $U_{geo} = Q_p$, which implies that (4.4), more than geometric, is now a topological quantity. This result have been studied in the abelian case for the states $|j, m = 0\rangle$ in [84]. This topological phase means that only depends of the initial and final points in the base space, it doesn't matter the curve, and for practical applications, it doesn't change if the curve

has some noise, for instance, deviations to the magnetic field given in the laboratory producing the rotations, or even the magnetic field by the Earth. A geometric phase with these properties is what we called a robust geometric phase. For $k > 1$ we can generalized the same construction, but now we need 1-anticoherent k-planes, *i.e.*, vectorial subspaces $\mathscr{S}$ of dimension k such that for each pair of states $|\psi_1\rangle$, $|\psi_2\rangle \in \mathscr{S}$, they satisfy that $\langle\psi_1|\mathbf{S}|\psi_2\rangle = 0$. This application inspires us to get a better understanding between the k-planes in $\mathbb{P}$ and its crossover with the action of $SO(3)$. Also, it is important to study the generalization of the anticoherent states, and discover a methodical way to find anticoherent multiplets with a subset of states with the same *shape*.

4.2 The Majorana constellation of a k-plane

As we have said before, the SC states are the spin states that maximize the squared of the spin expectation value $\langle\mathbf{S}\rangle$, which is a set isometric to a 2-sphere, and each state is denoted by a direction $|n\rangle$ such that $n\cdot\mathbf{S}|n\rangle = s|n\rangle$. The notion of SC states is sufficient to built the Majorana polynomial of a state $|\psi\rangle$, defined as the polynomial proportional to the overlap $\langle -n|\psi\rangle \propto p_\psi(\zeta)$, with ζ the stereographic projection of n. One may generalizes this procedure for a k-plane Π in $\mathbb{P}$ considering the trace restricted to Π of the spin vector $\mathbf{S}$,

$$\mathrm{Tr}^{\Pi}\mathbf{S} \equiv \sum_{j=1}^{k}\langle\psi_\mu|\mathbf{S}|\psi^\mu\rangle\,. \tag{4.19}$$

$\mathrm{Tr}^{\Pi}\mathbf{S}$ is basis-independent and, under rotations of the k-plane $D(\mathsf{R})$, it rotates to $\mathsf{R}\mathrm{Tr}^{\Pi}\mathbf{S}$. One may define a *coherent k-plane* as one that maximizes the squared of the (4.19). The coherent k-planes can be identified and, indeed, they are a topological sphere, as in the $k = 1$ case.

Theorem 17. *The set of the coherent k-planes is a topological sphere.*

Proof. As we mentioned before, for a k-plane Π, $\mathrm{Tr}^{\Pi}\mathbf{S}$ rotates as a vector and we can assume that it points along the $\hat{z}$ axis. Let us take an orthonormal basis $\{|\psi_\mu\rangle\}_{\mu=1}^{k}$ for Π. With the previous observation we have

$$\sum_\mu\langle\psi_\mu|S_x|\psi_\mu\rangle = \sum_\mu\langle\psi_\mu|S_y|\psi_\mu\rangle = 0\,, \tag{4.20}$$

so that we only need to look for the subspace (or subspaces) that maximize $\mathrm{Tr}^{\Pi}S_z$. The proof will be by induction and its core is the following mathematical result,

Let A be a Hermitian operator with eigenvalues $\lambda_1 < \cdots < \lambda_N$. Then, for all normalized states $|\psi\rangle$ the inequality $\langle\psi|A|\psi\rangle \leq \lambda_N$ holds. Furthermore, the equality is attained if and only in $|\psi\rangle$ is an eigenvector of A with eigenvalue λ_N.

Let Π be a k-plane such that $\mathrm{Tr}^{\Pi} S_z$ is maximized. We will prove that the set $\{|s, s-j\rangle\}_{j=0}^{k-1} \subset \Pi$ and therefore $\Pi = \mathrm{span}\{|s,s\rangle, \ldots, |s, s-k+1\rangle\}$. First, suppose that $|s\rangle$ is not in Π. Denote as P to the projection operator of the subspace Π and consider $|\psi_1\rangle = QP|s\rangle \in \Pi$ (Q is a normalization constant. If $P|s\rangle = 0$, the following argument will still hold with a few modifications). Consider $|\psi_2\rangle, \ldots, |\psi_k\rangle \in \Pi$ orthonormal to $|\psi_1\rangle$. Then, $\mathrm{Tr}^{\Pi} S_z$ can be computed as follows,

$$\mathrm{Tr}^{\Pi} S_z = \langle\psi_1|S_z|\psi_1\rangle + \sum_{\mu=2}^{k} \langle\psi_\mu|S_z|\psi_\mu\rangle < \langle s|S_z|s\rangle + \sum_{\mu=2}^{k} \langle\psi_\mu|S_z|\psi_\mu\rangle = \mathrm{Tr}^{\Pi'} S_z\,, \tag{4.21}$$

where we used the fact that $|s\rangle$ is an eigenvector with the highest eigenvalue of possible of S_z (and $|\psi_1\rangle$ is not) and $\Pi' = \mathrm{span}\{|s\rangle, |\psi_2\rangle, \ldots, |\psi_k\rangle\}$. The last equality can be checked by noting that the basis $\{|s\rangle, |\psi_2\rangle, \ldots, |\psi_k\rangle\}$ is orthonormal (so we can use it to compute the trace) since, for any $\mu > 1$,

$$\langle\psi_\mu|(|s\rangle - P|s\rangle) = 0 \Rightarrow \langle\psi_\mu|s\rangle = 0\,, \tag{4.22}$$

where the first equality stems from the definition of the projection operator P and the second one can easily deduced by remembering that the basis $\{|\psi_\mu\rangle\}$ is orthogonal by construction with $|\psi_1\rangle \propto P|s\rangle$. Clearly (4.21) is a contradiction since $\mathrm{Tr}^{\Pi} S_z$ was assumed maximal. Therefore, $|s\rangle$ is an element of Π. Now we will prove that $|s-1\rangle$ is also in Π and the reasoning for the remaining states will be completely analogous. Consider the linear subspace orthogonal to $|s\rangle$, $O^{\perp}$. Clearly S_z leaves this space invariant and $\Pi_2 = \mathrm{span}\{|\psi_2\rangle, \ldots, |\psi_k\rangle\} \subset O^{\perp}$, since all of them are orthogonal to $|s\rangle$ as noted in (4.22). Call $S_z^{(2)} : O^{\perp} \to O^{\perp}$ to the restriction of S_z to $O^{\perp}$. Then we have

$$\mathrm{Tr}^{\Pi} S_z = \langle s|S_z|s\rangle + \sum_{\mu=2}^{k} \langle\psi_\mu|S_z|\psi_\mu\rangle = \langle s|S_z|s\rangle + \sum_{\mu=2}^{k} \langle\psi_\mu|S_z^{(2)}|\psi_\mu\rangle = \langle s|S_z|s\rangle + \mathrm{Tr}^{\Pi_2} S_z^{(2)}\,. \tag{4.23}$$

Note that the eigenstate of $S_z^{(2)}$ with the highest eigenvalue is $|s-1\rangle$. Because of this, by using the same argument we used to prove that $|s\rangle \in \Pi$, we can prove that, if $|s-1\rangle$ is not an element of Π_2, we can find a $k-1$ plane $\Pi_2' \subset O^{\perp}$ that contains $|s-1\rangle$ such that

$$\mathrm{Tr}^{\Pi_2} S_z^{(2)} < \mathrm{Tr}^{\Pi_2'} S_z^{(2)}$$

and hence for $\Pi' = \text{span}\{\Pi'_2, |s\rangle\}$, $\text{Tr}^{\Pi'} S_z$ would be higher than $\text{Tr}^{\Pi} S_z$ a contradiction. Using the same argument $k-2$ times more we can prove that $\Pi = \text{span}\{|s\rangle, \ldots, |s-k+1\rangle\}$. Finally, note that this Π satisfy (4.20).

What we just proved was that if Π is such that $\text{Tr}^{\Pi}\mathbf{S}$ points along the $\hat{z}$ axis and its squared norm is maximal, then $\Pi = \text{span}\{|s\rangle, \ldots, |s-k+1\rangle\}$. Because of this and the rotational properties of $\text{Tr}^{\Pi}\mathbf{S}$, the remaining coherent subspaces can be obtained by rotating Π. Since rotations around the $\hat{z}$ axis leave Π invariant, the space of coherent planes is contained in a sphere, each coherent plane associated to a direction in the sphere. What remains to prove is that different directions define different planes. This is trivial, however, (as long as $k \neq N = 2s$) by the following argument. Consider the following planes

$$\Pi_{\hat{n}} = \text{span}\{|\hat{n}, s\rangle, \ldots, |\hat{n}, s-k+1\rangle\}\,, \quad \Pi_{\hat{m}} = \text{span}\{|\hat{m}, s\rangle, \ldots, |\hat{m}, s-k+1\rangle\}\,,$$

with $\hat{n} \neq \hat{m}$. Clearly both spaces are different since $|\hat{n}, -s\rangle$ is orthogonal to all the elements of $\Pi_{\hat{n}}$ but is not orthogonal to $|\hat{m}, s\rangle$ (the only coherent state orthogonal to it is $|\hat{m}, -s\rangle$), an element of $\Pi_{\hat{m}}$. Taking all this in consideration, we can conclude the coherent subspaces is topologically a sphere. □

With the last result we describe the generalization of the spin coherent states. To define the inner product between k-planes, let us review the notion of inner product in states (which would be 1-planes, or lines in $\mathscr{H}^N$). A point $|\psi\rangle$ in the Hilbert space $\mathscr{H}^N$ is a state that for the moment we do not consider normalized and with an associated phase. The inner product in $\mathscr{H}^N$ is given by

$$\langle\psi_1|\psi_2\rangle_{\mathscr{H}} \equiv \langle\psi_1|\psi_2\rangle\,, \tag{4.24}$$

which is just the usual overlap between two states. Now, the inner product in $\mathbb{P}$, can be written in terms of the elements of $\mathscr{H}$, taking into account the normalization of the states, and omitting the phase associated to the $U(1)$ fiber in $\mathscr{H}$,

$$\langle\psi_1|\psi_2\rangle_{\mathbb{P}} \equiv \frac{|\langle\psi_1|\psi_2\rangle_{\mathscr{H}}|}{\sqrt{|\langle\psi_1|\psi_1\rangle_{\mathscr{H}}|}\sqrt{|\langle\psi_2|\psi_2\rangle_{\mathscr{H}}|}}\,, \tag{4.25}$$

As a summary, the last equation is an inner product in $\mathbb{P}$ because, between any representative element of the classes $[\psi_1], [\psi_2] \in \mathbb{P}$, the product (4.25) gives the same value. We generalize the last construction for k frames $\mathscr{H}^k$ and Grassmanians $\text{Gr}_{k,N}$ which will be the analogous to $\mathscr{H}$ and $\mathbb{P}$, respectively.

For two (not necessarily orthonormal) k-frames $|\Psi_1\rangle = \{|\psi_{1\,\mu}\rangle\}$, $|\Psi_2\rangle = \{|\psi_{2\,\nu}\rangle\}$, $1 \leq \mu, \nu \leq k$, we define their inner product as

$$\langle \Psi_1 | \Psi_2 \rangle = \det \langle \Psi_1 \circledast \Psi_2 \rangle \,, \tag{4.26}$$

where $\langle \Psi \circledast \Phi \rangle$ is a matrix of inner products, $\langle \Psi \circledast \Phi \rangle_{\mu\nu} = \langle \psi_\mu | \phi_\nu \rangle$. The standard properties

$$\langle a\Psi | \Phi \rangle = \bar{a} \langle \Psi | \Phi \rangle \,, \quad \langle \Psi | a\Phi \rangle = a \langle \Psi | \Phi \rangle \,, \quad \langle \Phi | \Psi \rangle = \overline{\langle \Psi | \Phi \rangle} \,, \tag{4.27}$$

are satisfied, but non-zero linearly dependent frames have zero norm-squared $|\Psi|^2 = \langle \Psi | \Psi \rangle$, which we will not consider. The group $\mathrm{GL}(k, \mathbb{C})$ acts on $\mathscr{H}_k$ by right matrix multiplication, and the space of orbits is the Grassmannian $\mathrm{Gr}_{k,N}$, since all frames in the same orbit span the same non-degenerate k-plane. Denote by Π_Ψ the k-plane spanned by $|\Psi\rangle$, viewed as an equivalence class of frames, with two frames being equivalent if they span the same plane. Finally, inspired by eq. (4.25), for two k-planes Π_1, Π_2 with (not necessarily orthogonal) bases $\{|\psi_{j\mu}\rangle\}_{\mu=1}^k$, with $j = 1, 2$, we define the inner product

$$\langle \Pi_1 | \Pi_2 \rangle \equiv \frac{\det |\langle \Psi_1 \circledast \Psi_2 \rangle|}{\sqrt{\det |\langle \Psi_1 \circledast \Psi_1 \rangle|} \sqrt{\det |\langle \Psi_2 \circledast \Psi_2 \rangle|}} \,, \tag{4.28}$$

The equation (4.28) is the volume of the projection of Π_1 into Π_2 (and viceversa). In fact, if there is a state $|\psi\rangle \in P_1$ orthogonal to Π_2, then $\langle \Pi_1, \Pi_2 \rangle = 0$.

Lemma 18. *Let Π_1 and Π_2 be two $k-$planes. Then, $\langle \Pi_1, \Pi_2 \rangle = 0$ if and only if there is an element $|\phi\rangle \in \Pi_2$ orthogonal to Π_1.*

Proof. Let $|\psi_\mu\rangle$ and $|\phi_\mu\rangle$ ($\mu = 1, \ldots, k$) be basis for Π_1 and Π_2 respectively. Let P_1 denote the projection operator associated to the subspace Π_1. Suppose the basis $|\psi_\mu\rangle$ for Π_1 is orthonormal. Then,

$$P_1 = \sum_{\mu=1}^{k} |\psi_\mu\rangle\langle\psi_\mu| \,. \tag{4.29}$$

Now, consider the operator P_1 restricted to the space Π_2. With respect to the basis $|\psi_\mu\rangle$, $\mu = 1, \ldots, k$ for Π_1 and $|\phi_\mu\rangle$, $\mu = 1, \ldots, k$ for Π_2, the matricial expression for the restricted operator $P_1|_{\Pi_2}$ can be deduced as follows,

$$P_1|_{\Pi_2} |\phi_\mu\rangle = \sum_{\mu=1}^{k} \langle \psi_\nu | \phi_\mu \rangle |\psi_\nu\rangle \Rightarrow (P_1|_{\Pi_2})_{\nu\mu} = \langle \psi_\nu | \phi_\mu \rangle \,, \tag{4.30}$$

Now, we know that the determinant of this matrix is zero if and only if the kernel of $P_1|_{\Pi_2}$ is non-trivial. Since P_1 is a projection operator, the kernel is not trivial if and only if there is a state $|\phi\rangle$ in Π_2 orthogonal to Π_1. □

Finally, we define the Majorana polynomial of the k-plane Π as

$$p_\Pi(\zeta) \equiv \langle \Pi_{-n}, \Pi \rangle \,, \tag{4.31}$$

with ζ the stereographic projection of n, and the zeros of $p_\Pi(\zeta)$ define the Majorana constellation of the k-plane Π. In the next theorem, we found a familiar to the Majorana polynomial of a k-plane, and its proof is in appendix F.

Theorem 19. *The Majorana polynomial $p_\Pi(z)$ of a k-plane Π with basis $\{|\psi_\mu\rangle\}_{\mu=1}^k$ is, up to a numerical factor, equal to the Wronskian of the Majorana polynomials of the basis $\{p_\psi(z)\}_{\mu=1}^k$*

,

$$p_\Pi(\zeta) = \begin{vmatrix} p_{\psi_0}(\zeta) & p^{(1)}_{\psi_0}(\zeta) & \dots & p^{(k-1)}_{\psi_0}(\zeta) \\ p_{\psi_1}(\zeta) & p^{(1)}_{\psi_1}(\zeta) & \dots & p^{(k-1)}_{\psi_1}(\zeta) \\ \vdots & \vdots & \vdots & \vdots \\ p_{\psi_{k-1}}(\zeta) & p^{(1)}_{\psi_{k-1}}(\zeta) & \dots & p^{(k-1)}_{\psi_{k-1}}(\zeta) \end{vmatrix} . \tag{4.32}$$

For the Majorana representation of a state $|\psi\rangle$, we have the interpretation that n is a star of $p_\psi(\zeta)$ if and only if $\langle -n|\psi\rangle = 0$. In this case, it's different. For convenience, let us denote as $\mathscr{C}_\psi$ and $\mathscr{C}_\Pi$ the constellations of the state $|\psi\rangle$ and the k-plane Π, respectively.

Theorem 20. *Let Π be a k-plane. Then, $\mathscr{C}_\Pi$ has a star in $\hat{n}$ if and only if there is a state $|\phi\rangle \in \Pi$ such that $\mathscr{C}_\phi$ has k (or more) stars in the direction $\hat{n}$.*

Proof. Suppose $\mathscr{C}_\Pi$ has a star in the direction $\hat{n}$. By definition, this happens if and only if $\langle \Pi_{-\hat{n}}, \Pi \rangle = 0$. As noted in lemma 18, this product is zero if and only if there is a state $|\phi\rangle$ orthogonal to all the elements of $\Pi_{-\hat{n}}$. Consider the basis $|-\hat{n}, s\rangle, \dots, |-\hat{n}, s+1-k\rangle$ for this plane. Then, the previous statement is equivalent to the following,

$$\langle -\hat{n}, m|\phi\rangle = \langle \hat{n}, -m|\phi\rangle = 0, \quad m = s, \dots, s-k+1 \,.$$

If we measure the spin for the state $|\phi\rangle$ in the direction $\hat{n}$, this means that the probability of getting the measure $-m$ is zero. By considering the operational definition of the Majorana

representation we see that this happens if and only if $\mathscr{C}_\phi$ has at least k stars in the direction $\hat{n}$. □

For the last result, there is an immediate generalization in one direction

Corollary 21. *Let Π be a k-plane. If there is a state $|\psi\rangle \in \Pi$ with a star n with multiplicity $K \geq k$, then $\mathscr{C}_\Pi$ has a star in n with multiplicity $K - k + 1$.*

However, it is not the unique way to have a star with multiplicity in the constellation of a k-plane.

Corollary 22. *Let Π be a k-plane. If Π has a basis $\{|\psi_\mu\rangle\}_{\mu=0}^{k-1}$ with a common star n (and then, all the states of Π), $\mathscr{C}_\Pi$ has a star in n with multiplicity k.*

Proof. Let us write the Majorana polynomial of each state $|\psi_\mu\rangle$ as $p_\psi(\zeta) = (\zeta - \gamma)\tilde{p}_\psi(\zeta)$, where γ is the complex number associated to n. Then, the Majorana polynomial of Π is

$$p_\Pi(\zeta) = \begin{vmatrix} (\zeta-\gamma)\tilde{p}_{\psi_0}(\zeta) & \tilde{p}_{\psi_0}(\zeta) + (\zeta-\gamma)\tilde{p}^{(1)}_{\psi_0}(\zeta) & \dots & (k-1)\tilde{p}^{k-2}_{\psi_0}(\zeta) + (\zeta-\gamma)\tilde{p}^{(k-1)}_{\psi_0}(\zeta) \\ (\zeta-\gamma)\tilde{p}_{\psi_1}(\zeta) & \tilde{p}_{\psi_1}(\zeta) + (\zeta-\gamma)\tilde{p}^{(1)}_{\psi_1}(\zeta) & \dots & (k-1)\tilde{p}^{k-2}_{\psi_1}(\zeta) + (\zeta-\gamma)\tilde{p}^{(k-1)}_{\psi_1}(\zeta) \\ \vdots & \vdots & \vdots & \vdots \\ (\zeta-\gamma)\tilde{p}_{\psi_{k-1}}(\zeta) & \tilde{p}_{\psi_{k-1}}(\zeta) + (\zeta-\gamma)\tilde{p}^{(1)}_{\psi_{k-1}}(\zeta) & \dots & (k-1)\tilde{p}^{k-2}_{\psi_{k-1}}(\zeta) + (\zeta-\gamma)\tilde{p}^{(k-1)}_{\psi_{k-1}}(\zeta) \end{vmatrix}, \tag{4.33}$$

where in a recursive manner, we can erase the factors of each column without the multiplicand $(\zeta - \gamma)$, reducing the determinant to

$$p_\Pi(\zeta) = \begin{vmatrix} (\zeta-\gamma)\tilde{p}_{\psi_0}(\zeta) & (\zeta-\gamma)\tilde{p}^{(1)}_{\psi_0}(\zeta) & \dots & (\zeta-\gamma)\tilde{p}^{(k-1)}_{\psi_0}(\zeta) \\ (\zeta-\gamma)\tilde{p}_{\psi_1}(\zeta) & (\zeta-\gamma)\tilde{p}^{(1)}_{\psi_1}(\zeta) & \dots & (\zeta-\gamma)\tilde{p}^{(k-1)}_{\psi_1}(\zeta) \\ \vdots & \vdots & \vdots & \vdots \\ (\zeta-\gamma)\tilde{p}_{\psi_{k-1}}(\zeta) & (\zeta-\gamma)\tilde{p}^{(1)}_{\psi_{k-1}}(\zeta) & \dots & (\zeta-\gamma)\tilde{p}^{(k-1)}_{\psi_{k-1}}(\zeta) \end{vmatrix}, \tag{4.34}$$

which clearly has a factor $(\zeta - \gamma)^k$. □

Corollary 23. *Let Π be a k-plane. If Π has a basis $\{|\psi_\mu\rangle\}_{\mu=0}^{k-1}$ with a common star n with multiplicity t, the constellation of Π has a star in n with multiplicity kt.*

Factorizing the common star in the states, we have a new Wronskian associated to states with spin $2s - t$, where the criteria of stars multiplicity must be applied with this new value of spin.

Given two polynomials of one variable $p_1(z)$ and $p_2(z)$ and an arbitrary complex number z_0, it is possible to make a linear combination $ap_1(z) + bp_2(z)$ with a root in z_0. In particular, if both polynomials have a common root, then there is a linear combination with a root of multiplicity two. In the same way, with k polynomials (of degree at least k) and an arbitrary complex number, there is a linear combination with z_0 as a root with multiplicity $k-1$, and the multiplicity increases if the k polynomials have a common root. Then we conclude that the corollary 22 implies 21, but in the opposite sense is not true, a counter example is given in the next section.

Remark. *If* Π *has a basis* $\{|\psi_\mu\rangle\}_{\mu=0}^{k-1}$ *with a common star* n *with multiplicity* t*, then there is a state* $|\phi\rangle \in \Pi$ *with a star in* n *with multiplicity* $t+k-2$*.*

We show some examples in the next section, where they have evidence that the only consequences of degenerated stars in the constellation of a k-plane are the mentioned by the corollaries 21-22.

4.3 Examples

4.3.1 k-planes of spin coherent states

Consider a k-plane Π consisting of the subspace generated by k spin coherent (SC) states $\{|n_k\rangle\}_{j=1}^{k}$. The Majorana polynomial of Π is

$$P_\Pi(z) = \begin{vmatrix} (z-\zeta_1)^N & N(z-\zeta_1)^{N-1} & \dots & \frac{N!}{(N-k+1)!}(z-\zeta_1)^{N-k+1} \\ (z-\zeta_2)^N & N(z-\zeta_2)^{N-1} & \dots & \frac{N!}{(N-k+1)!}(z-\zeta_2)^{N-k+1} \\ \vdots & \vdots & \ddots & \vdots \\ (z-\zeta_k)^N & N(z-\zeta_k)^{N-1} & \dots & \frac{N!}{(N-k+1)!}(z-\zeta_k)^{N-k+1} \end{vmatrix} \tag{4.35}$$

where $N = 2s$ and ζ_j is the complex number associated to n_j via stereographic projection. In each row there is a common factor $(z-\zeta_j)^{N-k+1}$ and in each column a numerical factor. Then

the Wronskian is equal to

$$P_\Pi(z) \propto \left(\prod_{j=1}^{k}(z-\zeta_j)^{N-k+1}\right) \begin{vmatrix} (z-\zeta_1)^{k-1} & (z-\zeta_1)^{k-2} & \dots & 1 \\ (z-\zeta_2)^{k-1} & (z-\zeta_2)^{k-2} & \dots & 1 \\ \vdots & \vdots & \ddots & \vdots \\ (z-\zeta_k)^{k-1} & (z-\zeta_k)^{k-2} & \dots & 1 \end{vmatrix} \tag{4.36}$$

$$= \left(\prod_{j=1}^{k}(z-\zeta_j)^{N-k+1}\right) \prod_{1=\mu<\nu}^{k} (\zeta_\mu - \zeta_\nu)\ . \tag{4.37}$$

Therefore, $\mathscr{C}_\Pi$ consists of k stars in the directions of the constituents SC states, where each star has multiplicity $N-k+1$. This result gives us a criterion to deduce when a subspace has a SC basis (*i.e.*, a basis consisting only by SC states), we just need to observe the constellation of the subspace.

4.3.2 k-planes for s=1

For spin $s=1$, the only non-trivial k-planes are with $k=2$, which are the complex lines[2]. The 2-planes' constellations have $k(2s+1-k)=2$ stars. Let us consider first Π generated by two states, where one has a star doubly degenerated, *i.e.*, a SC state, $\Pi = \text{span}\{|n\rangle, |n_1, n_2\rangle\}$, with associated complex numbers, γ, γ_1 and γ_2, respectively. Using eq. (4.32) we obtain that the roots of $p_\Pi(\zeta)$ are

$$\zeta_1 = \gamma\,, \qquad \zeta_2 = \frac{\gamma\,(\gamma_1+\gamma_2) - 2\gamma_1\gamma_2}{2\gamma - (\gamma_1+\gamma_2)}\,. \tag{4.38}$$

In another case, when $\Pi = \text{span}\{|n, n_1\rangle, |n, n_2\rangle\}$, the new constellation consists of $\zeta_{1,2} = \gamma$. Also, the SC state $|n\rangle$ belongs to the last 2-plane. These results are in agreement with the interpretation of the stars mentioned in the last section. We conclude that when the 2-plane Π is such that all the states $|\psi\rangle \in \Pi$ have a common star n, the constellation of Π is a star in n with multiplicity 2, which indeed is the antipodal constellation to the SC state $|-n\rangle$, the unique orthogonal state to Π. This is not a coincidence, as we prove below.

Corollary 24. *Let Π be a $2s$-plane of spin-s states with a constellation without degenerated stars. The antipodal of $\mathscr{C}_\Pi$ is the constellation of $|\psi\rangle \perp \Pi$.*

[2]It's a bit confusing the terminology, that complex lines are the 2-planes. To avoid confusions, in this chapter we won't use the term "complex lines" anymore.

Proof. The constellation of Π has $N = 2s$ stars $\{n_j\}_{j=1}^N$. By the corollary 21, the SC states $\{|n_j\rangle\}_{j=1}^N \in \Pi$, which, as we discuss in the previous chapter (subsection 3.3.2), are linearly independent. Then, the unique orthogonal state to all of them is $|-n_1,\ldots,-n_N\rangle$. □

As a last observation we remark that these calculations imply also the results for $s = 1$ in section 3.4.1 in an easier way, and therefore, it could be used to generalize these results.

4.3.3 k-planes for s=3/2

Let us first study the 3-planes, which they have a constellation of $k(2s+1-k) = 3$ stars. In this part, let us denote by Π_m the set of the 3-planes such that the star with most multiplicity is with multiplicity m. Π_1 are the 3-planes conformed by the linear combination of three different SC states $\Pi = \text{span}\{|n_j\rangle\}_{j=1}^3$, which has orthogonal complement $\Pi^\perp = |-n_1,-n_2,-n_3\rangle$. On the other hand, Π_3 are the 3-planes Π such that all the states in Π have a common star n, and $\Pi^\perp = |-n\rangle$. We are missing the 3-planes Π whose orthogonal complement is of the type $\Pi^\perp = |-n_1,-n_2,-n_2\rangle$, which must be set Π_2. Doing some calculations, we can obtain that the 3-plane given by $\{|n_1,n_1,n_1\rangle, |n_2,n_2,n_2\rangle, |n_2,n_2,n'\rangle\}$ with $n' \neq n_2$, has the constellation n_1, n_2 and n_2. We summary all this information in the next table, with the convention that $n_i \neq n_j$ for each pair of directions.

$s = 3/2$	Class of 3-planes	$\Pi^\perp$
Π_1	$\{\|n_1\rangle, \|n_2\rangle, \|n_3\rangle\}$	$\|-n_1,-n_2,-n_3\rangle$
Π_2	$\{\|n_1\rangle, \|n_2\rangle, \|n_2,n_2,n_3\rangle\}$	$\|-n_1,-n_2,-n_2\rangle$
Π_3	$\{\|n_1\rangle, \|n_1,n_2,n_2\rangle, \|n_1,n_2,n_3\rangle\}$	$\|-n_1\rangle$

(4.39)

Now, we study the 2-planes, with 4 stars in their constellations. We do a similar table as the above one for this case. To avoid large calculations, the directions p_j depend of the directions n_j. Also, here it could be more than one star with degeneracy. This case is a constellation with two stars doubly degenerated and will be denoted by $\Pi_{2,2}$. For each Π_m, there is only one class except for the cases Π_2 and $\Pi_{2,2}$. Moreover, there are no distinction between the constellations of the two classes of Π_2. For instance, the 2-planes $\Pi_1 = \{|-z, \frac{\sqrt{3}}{2}x + \frac{1}{2}z, -\frac{\sqrt{3}}{2}x + \frac{1}{2}z\rangle, |-z, \frac{-\sqrt{3}}{2}x + \frac{1}{2}z, -\frac{\sqrt{3}}{2}x + \frac{1}{2}z\rangle\}$ and $\Pi_2 = \{|-z\rangle, |z,x,-x\rangle\}$ or in terms of polynomials, $\Pi_1 = \{(z-1/\sqrt{3})^2, (z+1/\sqrt{3})^2\}$ and $\Pi_2 = \{1, z(z-1)(z+1)\}$, have the same constellation.

Therefore, different k-planes may give the same constellation.

$s=3/2$	Class of 2-planes	$\Pi^{\perp}$
Π_1	$\{\|n_1,n_2,n_3\rangle,\|n_4,n_5,n_6\rangle\}$	$\cdots$
Π_2	$\{\|n_1\rangle,\|n_2,n_3,n_4\rangle\}$	$\{\|-n_1,-n_1,p_2\rangle,\|-n_1,p_3,p_4\rangle\}$
Π_2	$\{\|n_1,n_1,n_2\rangle,\|n_1,n_3,n_4\rangle\}$	$\{\|-n_1\rangle,\|p_1,p_2,p_3\rangle\}$
$\Pi_{2,2}$	$\{\|n_1\rangle,\|n_2\rangle\}$	$\{\|-n_1,-n_2,-n_3\rangle,\|-n_1,-n_2,-n_4\rangle\}$
$\Pi_{2,2}$	$\{\|n_1,n_2,n_3\rangle,\|n_1,n_2,n_4\rangle\}$	$\{\|-n_1\rangle,\|-n_2\rangle\}$
Π_3	$\{\|n_1\rangle,\|n_1,n_2,n_3\rangle\}$	$\{\|-n_1\rangle,\|-n_1,p_2,p_3\rangle\}$
Π_4	$\{\|n_1\rangle,\|n_1,n_1,n_2\rangle\}$	$\{\|-n_1\rangle,\|-n_1,-n_1,n_3\rangle\}$

(4.40)

4.4 Anticoherent Multiplets

We define a t-anticoherent multiplet $\{|\Psi_i\rangle\}_{i=1}^{k}$ as a set of l.i. states such that $\langle\Psi_i|T_{\sigma\mu}|\Psi_j\rangle = 0$ with $1 \leq \sigma \leq t$, $-\sigma \leq \mu \leq \sigma$ for $1 \leq i,j \leq k$, with $T_{\sigma\mu}$ the tensorial operators (see section 1.4). By the 3j-symbol of $T_{\sigma,\mu}$, $\langle j,m|T_{\sigma\mu}|j,m'\rangle$ must satisfy that $\mu + m' = m$. For our case, we are interested in 1-anticoherent multiplets, then we look for sets of states such that

$$\langle\Psi_i|T_{1\mu}|\Psi_j\rangle = 0\,, \tag{4.41}$$

for each value of $\mu = 0, \pm 1$. The last condition is satisfied for any couple of states $|s,m_1\rangle$, $|s,m_2\rangle$ such that $|m1 - m2| > 1$. As a first step, we observe that the sets $\{|s,-s+2k\rangle\}_{k=0}^{[s]}$ and $\{|s,-s+2k+1\rangle\}_{k=0}^{[(2s-1)/2]}$ satisfy the last equation, except when the *bra* and *ket* states are the same and with $m=0$, because in this case $\langle s,m|T_{10}|s,m\rangle \neq 0$. This expectation value vanishes when we consider the states $|s,-s+2k\rangle+|s,s-2k\rangle$ and we omit the state $|s,1/2\rangle+|s,-1/2\rangle$ when is necessary (the last one must be omitted because $(\langle s,1/2|+\langle s,-1/2|)T_{10}(|s,1/2\rangle+|s,-1/2\rangle) \neq 0$). The first example is obtained in $s=3$. We give a table of examples (without normalization)

for the first values of s.

$s=3$	
$\circ$	$\|\psi_1\rangle = \|s,3\rangle + \|s,-3\rangle, \quad \|\psi_2\rangle = \|s,1\rangle + \|s,-1\rangle,$
$\circ$	$\|\psi_1\rangle = \|s,2\rangle + \|s,-2\rangle, \qquad \|\psi_2\rangle = \|s,0\rangle,$
$s=7/2$	
$\circ$	$\|\psi_1\rangle = \|s,\frac{7}{2}\rangle + \|s,-\frac{7}{2}\rangle, \quad \|\psi_2\rangle = \|s,\frac{3}{2}\rangle + \|s,-\frac{3}{2}\rangle,$
$s=4$	
$\circ$	$\|\psi_1\rangle = \|s,4\rangle + \|s,-4\rangle, \quad \|\psi_2\rangle = \|s,2\rangle + \|s,-2\rangle, \quad \|\psi_3\rangle = \|s,0\rangle,$
$\circ$	$\|\psi_1\rangle = \|s,3\rangle + \|s,-3\rangle, \quad \|\psi_2\rangle = \|s,1\rangle + \|s,-1\rangle.$

(4.42)

For these examples, the biggest multiplet for each value of spin s has $[s/2]+1$ elements. We plot in the next figures the constellations of some examples mentioned above, and the Majorana constellation associated to its k-plane (k=2 or k=3, respectively).

We consider the 2-plane Π plotted in the figure 4.1, $|\psi_1\rangle = |3,2\rangle + |3,-2\rangle$, and $|\psi_2\rangle = |3,0\rangle$. $\mathscr{C}_\Pi$ has the roots

$$\rho_1 = 0\,, \quad \rho_2 = \infty\,, \quad \rho_{3,4} = \pm i\,, \quad \rho_{5,6} = \pm 1\,, \tag{4.43}$$

with ρ_1 and ρ_2 a 3-degenerate root. A general state of the 2-plane is written as $|\psi_1\rangle + \alpha|\psi_2\rangle$. It is easy to observe that when $\alpha = 2$, the state has double degenerated roots in $\pm i$, and when $\alpha = -2$, there are double degenerated roots in ± 1. Only in these values of α, the polynomial has an equal root as ρ_j with $j = 3,4,5,6$. The whole 2-plane has the root 0 and ∞ once, and only these roots have multiplicity (of order 3) when $\alpha = \infty$, *i.e.*, in the state $|\psi_2\rangle$. All these properties of the 2-plane are in accordance with the previous results (Cor. 21-22).

4.5 Anticoherent multiplets with the same shape

For reasons of convenience, we denote 1-anticoherent multiplets just as anticoherent multiplets. We are interested in an anticoherent cuadriplet $\{|\psi_k\rangle\}_{k=1}^4$ such that each state can be obtained from another making a rotation $|\psi_j\rangle = \mathsf{R}|\psi_k\rangle$. There are several 1-anticoherent states we know and for which the last condition is easy to implement. In this part, we study the orbit of the states of $|s,0\rangle$ under $SO(3)$.

Recall that a set of states $A = \{|\psi_k\rangle\}_{k=1}^N$ is an anticoherent multiplet if $\langle\psi_j|T_{1\mu}|\psi_k\rangle = 0$ for

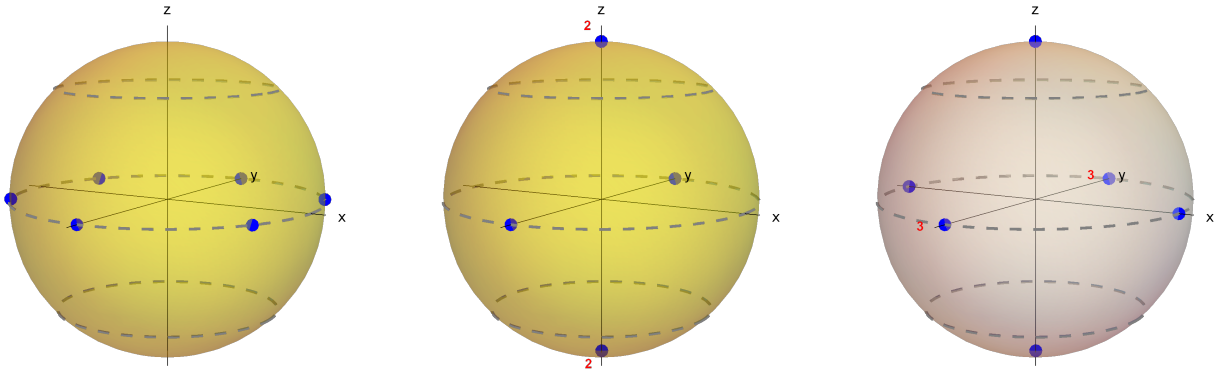

Figure 4.1: Majorana constellations of the states $|3,3\rangle + |3,-3\rangle$ (left), $|3,1\rangle + |3,-1\rangle$ (center), and the associated 2-plane, with 10 stars (right). The red number denotes the multiplicity of the stars. The left constellation is a regular hexagon.

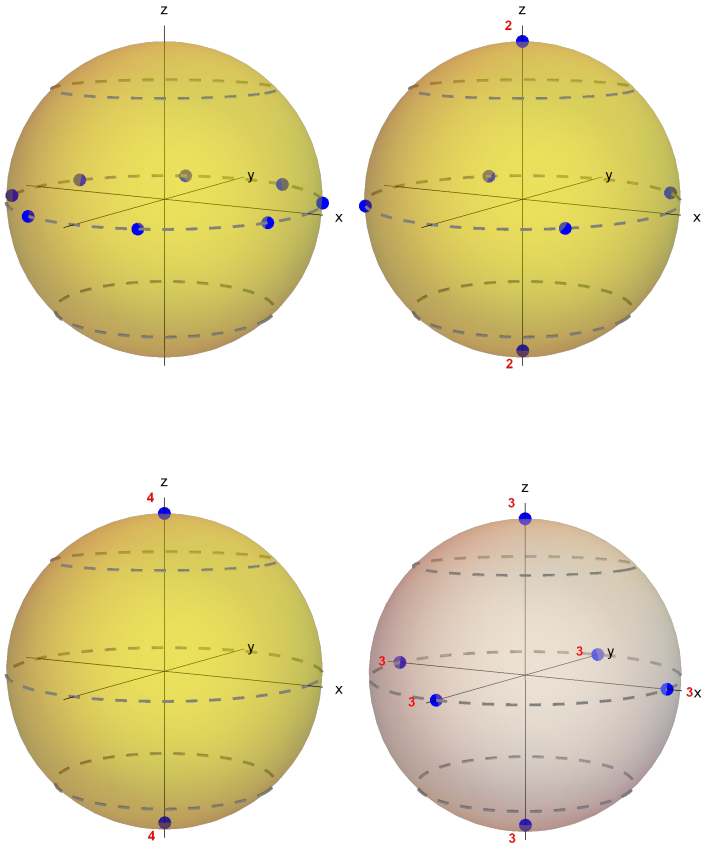

Figure 4.2: Majorana constellations of the states $|4,4\rangle + |4,-4\rangle$ (left up), $|4,2\rangle + |4,-2\rangle$ (right up), $|4,0\rangle$ (left down) and the associated 3-plane, with 18 stars (right down). The left up constellation is an octagon.

each pair of A and $\mu = 0, \pm 1$. Imposing these conditions we obtain [94]

$$\langle s,0|R(\alpha,\beta,\gamma)T_{10}|s,0\rangle = 0\,, \tag{4.44}$$

$$\langle s,0|R(\alpha,\beta,\gamma)T_{1\pm1}|s,0\rangle \propto \pm e^{\mp i\gamma}\frac{\sin\beta}{\sqrt{s(s+1)}}P_s'(\cos\beta)\,, \tag{4.45}$$

with $P_s(x)$ the Legendre polynomials. We obtain that the condition of anticoherence for a pair of states with the shape $|s,0\rangle$ doesn't depend of the angles α and γ. This is easy to understand because the condition must only depend on relative angles between the states (i.e., between the stars of the constellations). Now, our problem to find anticoherent multiplets with the shape of $|s,0\rangle$ is reduced to look for a configuration of stars in the 2-sphere such that their distances (spherical distance) between them is a zero of $P_s'(\cos\beta)$, which are well-known. If there exist an angle β_0 such that $\beta_0 \in (0,\pi)$ and $P_s'(\cos\beta_0) = 0$, then we can always built an anticoherent triplet, consisting in the directions of an equilateral (spherical) triangle with length β_0. It turns out that the angle with these properties exists for any integer value of spin $s > 1$. For an anticoherent cuadriplet with equidistant stars, the only possible configuration is the tetrahedron. Then we search in which value of spin s, $P_s'(\cos\beta_t) = 0$ with $\beta_t = \arccos(-1/3) \approx 1.91063$. In the values of $s \in [1,100]$, we don't obtain an exact zero of the Legendre polynomial for β_t, just an approximate value. There are four zeros with a difference less than 0.001

$$\begin{aligned}
&s = 18\,, \qquad \beta = 1.91082\,, \qquad \Delta\beta = 0.00019\,,\\
&s = 41\,, \qquad \beta = 1.91153\,, \qquad \Delta\beta = 0.00090\,,\\
&s = 69\,, \qquad \beta = 1.90984\,, \qquad \Delta\beta = 0.00079\,,\\
&s = 92\,, \qquad \beta = 1.91044\,, \qquad \Delta\beta = 0.00019\,,
\end{aligned}$$

For $s = 18$, we define the cuadriplet $|\psi_1\rangle = |s,0\rangle$, $|\psi_2\rangle = \mathsf{R}(0,\beta_t,0)|s,0\rangle$, $|\psi_3\rangle = \mathsf{R}(2\pi/3,\beta_t,0)|s,0\rangle$ and $|\psi_4\rangle = \mathsf{R}(4\pi/3,\beta_t,0)|s,0\rangle$. The numerical value of the matrices $\langle\psi_j|T_{1,\mu}|\psi_k\rangle$ are

$$\langle\psi_i|T_{10}|\psi_j\rangle = 10^{-4}\begin{pmatrix} 0 & 0 & 0 & 0\\ 0 & 0 & 1.5i & -1.5i\\ 0 & -1.5i & 0 & 1.5i\\ 0 & 1.5i & -1.5i & 0 \end{pmatrix}, \tag{4.46}$$

$$\langle\psi_i|T_{11}|\psi_j\rangle = 10^{-4}\begin{pmatrix} 0 & 1.3 & -0.65-1.1i & -0.65+1.1i \\ -1.3 & 0 & 0.65+0.37i & 0.65-0.37i \\ 0.65+1.1i & -0.65-0.37i & 0 & -0.75i \\ 0.65-1.1i & -0.65+0.37i & 0.75i & 0 \end{pmatrix}, \tag{4.47}$$

and $\langle\psi_i|T_{1-1}|\psi_j\rangle = \langle\psi_i|T_{1-1}|\psi_j\rangle^*$ This 4-plane, by construction has the tetrahedral symmetry, i.e. $\mathsf{R}\Pi = \Pi$, for each rotation R belonging to the symmetry group of the tetrahedral, and only these ones, as we can conclude seeing its constellation plotted in Fig. 4.3. We can observe a constellation that only has the symmetries of the tetrahedron plus an antipodal symmetry. However, the last one leaves the state invariant, and therefore, is a trivial operator for the basis.

To conclude, we obtain a quasi-anticoherent cuadriplet, where the states lives in the orbit of the state $|s,0\rangle$. In this cuadriplet there are the necessary set of operations to do in quantum computing in the way to model logic gates. With this method we can also look for other configurations of points on the 2-sphere such that, instead to having the same length between each other, they have a (spherical) distance satisfying $P'_s(\cos\beta) = 0$, with this condition we can obtain spherical parallelograms, where they are related to an anticoherent cuadriplet. However, there is less symmetry of the configuration than the tetrahedron configuration (only 1 rotational symmetry), and therefore, they are not useful for quantum computing.

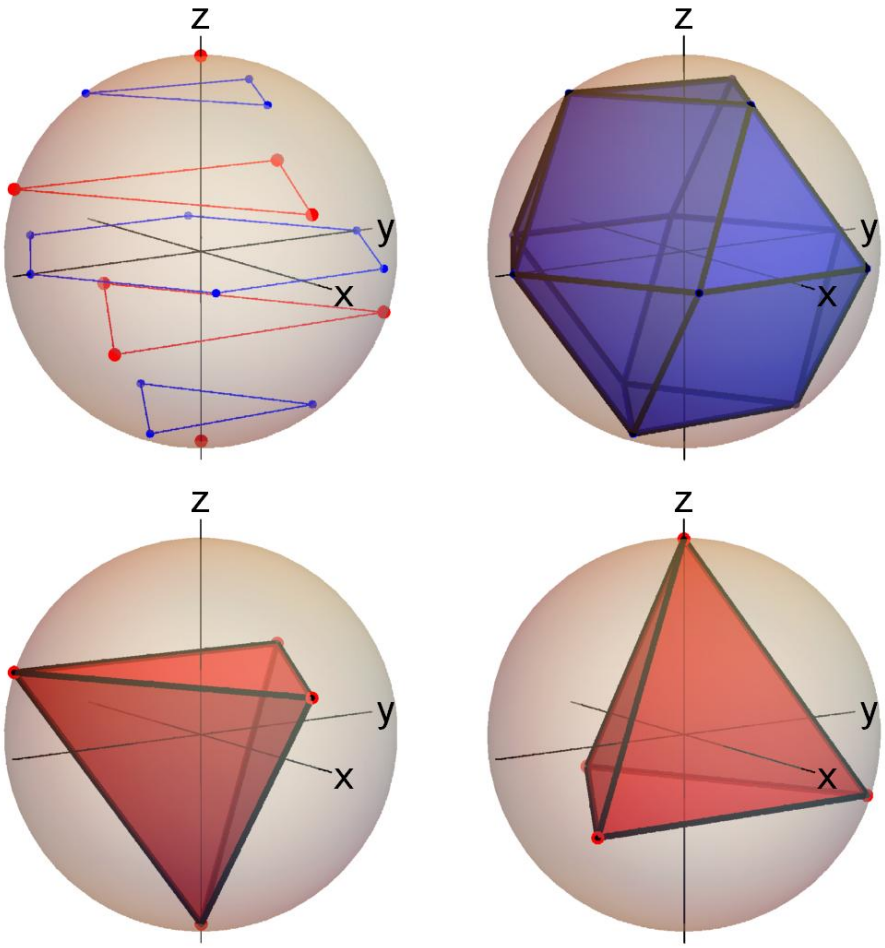

Figure 4.3: Majorana constellations of Π given by the quasi anticoherent cuadriplet. The constellation consists of 132 stars, the red stars have multiplicity 15, and the blue ones are not degenerated. The eight red stars conform two antipodal tetrahedrons (bottom), and the 12 blue stars a cuboctahedron (right top).

Chapter 5

Conclusions

Quantum system of n-point particles

We study the interplay between the dynamics of the shape and orientation degrees of freedom in n-body quantum systems, using the geometric approach to the n-body problem developed in the last decades. In the quasi-rigid approximation, the best shape coordinates are the normal modes, obtaining a covariant Hamiltonian and a physical interpretation of its terms.

We presented a quantum description of the falling, reorienting, zero angular momentum cat, modeled by a system of $n = 3$ and 4 particles. We recovered the classical picture assuming the cat wavefunction in shape space to be a coherent state, and also explored other, more exotic, purely quantum scenarios. Step by step, we assume more complex situations. For $n = 3$, we study the evolution of a state where the shape is a superposition of two coherent states, with internal angular momentum in antipodal directions, which ends in a Schroedinger cat. Also, we present the case when the shape wavefunction doesn't have internal angular momentum, which, opposite to our classical intuition, its orientational wavefunction spreads in a particular direction. For the tetrahedral case for $n = 4$, we exploit the result that we can induce rotations in any direction with shape transformations. To obtain that anticoherent shape states produce an isotropic evolution in the orientational wavefunction with respect to the axis of rotation. We deduced that for a $q-$anticoherent internal state with $q \geq 3$, the evolution is isotropic up to third order in t. We have some perspective that this result is true for each order, and will be studied in the near future. Finally, we design a shape state such that gives an axial evolution in the orientational wavefunction, as an example of engineering shape states for a desired orientational

evolution.

New features will appear considering systems with closed equilibrium configurations. For instance, the appearance of degeneracy between shapes related by mirror reflection, as in the ammonia molecule. In this case, we expect effects by the tunnelling between degenerate minima of the potential. Such developments would also facilitate incursions to molecular and nuclear dynamics.

There is one aspect of our approach that needs to be justified. The falling cat's rotation was visualized by essentially following the maximum of the marginal probability density in $SO(3)$, rather than focusing on the "average orientation". The reason for this choice is that there is no "average orientation" in a configuration space like $SO(3)$ — to see this, consider the simpler case of a particle with uniform probability density around a circle, there is no meaningful assignment of an average position in this case. Thus, simply invoking Ehrenfest's theorem, *i.e.*, that the quantum description of the system will be necessarily recovered, through expectation values, the classical one, is not permissible here, at least not in the above naive form. Recently, there are definitions of the Wigner quasi-probability function for the pair of angle and orbital angular momentum canonical pair given by Kastrup [50, 51, 52], which can be used to define the average orientation more formally.

Shapes in the Hilbert space of spin states

We study questions regarding the intersection of complex lines and Fubini-Study geodesics in quantum projective state space $\mathbb{P}$ with the 2-sphere of spin coherent states $S^2_{\rm SC}$ — a central role in this discussion is played by our result of the linear independence of any $N+1$ SC states. We show that for a generic quantum state $[\Psi]$, there exists an adapted SC basis, defined via the extrema of its Husimi function. We also give a lower bound on the number of distinct stars of a linear combination of two generic spin-s states, and find a simple expression for the constellation of a linear combination of two spin-s SC states. Finally, we compute the image of the SC 2-sphere, for $s = 1$, projected to a 3D subspace of the tangent space to $\mathbb{P}^2$, using (the inverse of) the exponential map. As mentioned before, our motivation in delving into this sort of questions, of a distinctly algebraic geometric flavor, is mainly rooted in our belief that the answers naturally translate into statements that an experimentalist might find not only neat but also useful. Our initial excursion into this territory has left many stones unturned. A basic piece

of information that seems missing is the form of the Majorana constellation obtained by linearly combining two given states. This leads back to the mostly open problem of factorizing a sum of polynomials, but apart from a complete description of the result, which might be presently untenable, one may also envisage partial answers in terms of bounds and inequalities, already unearthed but hidden deeply in the mathematics literature.

For the problem to discover the unknown rotation for a spin state through overlaps with spin coherent states, the visualization of the Hilbert space in a $SO(3)$ principal fiber bundle is the most convenient. We obtain a equivalent interpretation and solving to the latter question with the GPS system. It should be a way to optimize the algorithm when the overlaps have some error, as it could be in the real case. It is planned, in the future, to improve the algorithm for unknown rotations for a realistic case, where the overlap measurements have some noise.

Another promising direction seems to be "intersectology", hopefully streamlined by a more substantial assimilation of algebraic geometric know-how. In particular, we would like to clarify the role higher secant varieties might play in a wide array of problems, and whether direct physical implications may be inferred from it. In the last chapter it is appreciated how our generalization presented here of the Majorana representation to k-planes can become a tool in this subject. The formulation and characterization of the Majorana representation is deeply studied, extending the definition of coherent states and the inner product for k-planes. We obtain the interpretation of the stars of a k-plane, which ends in a crucial difference with the usual stellar representation for states, different k-planes could have the same constellation. We are working to get a better understanding of this new Majorana representation.

Finally, we generalize the geometric phase given by Mukunda and Simon to the non-abelian case. We find that anticoherent multiplets can produce a non-abelian case robust to noise (noise that can produce rotations). We give several examples of the anticoherent multiples, and find a cuasi anticoherent cuadriplet (up to 10^{-4}), which could work for quantum computing. We are still looking for new anticoherent cuadriplets. Also, it could be interesting to study some questions given in the q-anticoherent states, now in q-anticoherent subspaces. For spin states, we know that, at least for the first values of q, the first q-anticoherent state in each order q have a platonic solid as constellation, will it be the same for k-planes?

Appendices

Appendix A

The quasi-rigid Hamiltonian for the four-body system

In this appendix the Hamiltonian for the 4-body system (2.36) is derived in the context of the quasi-rigid approximation (1.3). We consider a system consisting of four point-like particles with mass m_α and position in the space frame $\mathbf{r}_{s\alpha}$ ($\alpha = 1, \ldots, 4$). To define the shape coordinates we use the following Jacobi vectors (see figure A.1)

$$\boldsymbol{\rho}_{s1} = \sqrt{\mu_1}(\mathbf{r}_{s1} - \mathbf{r}_{s3})\,, \qquad \boldsymbol{\rho}_{s2} = \sqrt{\mu_2}(\mathbf{r}_{s2} - \mathbf{R}_{s,13})\,, \qquad \boldsymbol{\rho}_{s3} = \sqrt{\mu_3}(\mathbf{r}_{s4} - \mathbf{R}_{s,123})\,, \tag{A.1}$$

where

$$\mathbf{R}_{s,13} = \frac{m_1\mathbf{r}_{s1} + m_3\mathbf{r}_{s3}}{m_1 + m_3}\,, \quad \mathbf{R}_{s,123} = \frac{m_1\mathbf{r}_{s1} + m_2\mathbf{r}_{s2} + m_3\mathbf{r}_{s3}}{m_1 + m_2 + m_3}\,, \tag{A.2}$$

and μ_i are the reduced masses of the respective clusters,

$$\mu_1 = \frac{m_1 m_3}{m_1 + m_3}\,, \quad \mu_2 = \frac{m_2(m_1 + m_3)}{m_2 + m_1 + m_3}\,, \quad \mu_3 = \frac{(m_1 + m_2 + m_3)m_4}{m_1 + m_2 + m_3 + m_4}\,. \tag{A.3}$$

The shape space is defined as the quotient space $\mathbb{R}^9/SO(3)$ which turns out to be $\mathbb{R}^6$, see [61]. For simplicity we choose the shape coordinates

$$q_1 = \sqrt{\rho_{s1}\cdot\rho_{s1}} \geq 0\,, \quad q_2 = \frac{\rho_{s1}\cdot\rho_{s2}}{q_1}\,, \quad q_3 = \frac{\rho_{s1}\cdot\rho_{s3}}{q_1}\,, \tag{A.4}$$

$$q_4 = \sqrt{\rho_{s2}\cdot\rho_{s2} - x_2^2} \geq 0\,, \quad q_5 = \frac{\rho_{s2}\cdot\rho_{s3} - q_2 q_3}{q_4}\,, \quad q_6 = \sqrt{\rho_{s2}\cdot\rho_{s2} - q_3^2 - q_5^2} \geq 0\,,$$

which clearly are rotation-invariant and can generate all the right-handed configurations of the four body system, with respect to the Jacobi vectors. For the particular system under

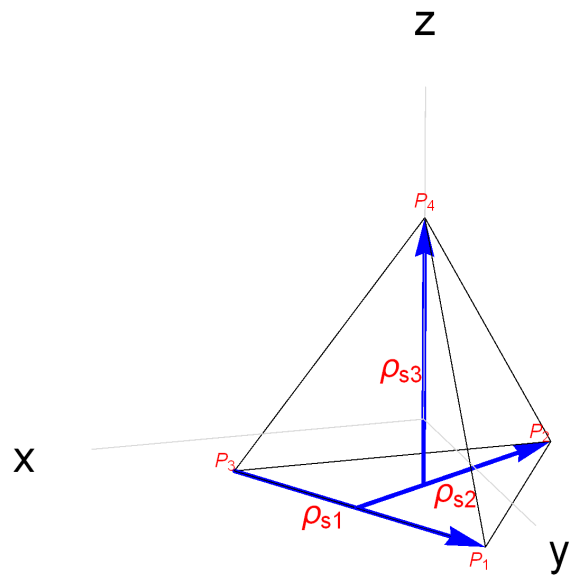

Figure A.1: Jacobi vectors for the four-body system.

consideration, it is convenient to work with a new set of shape coordinates

$$\begin{pmatrix} \tilde{q}_1 \\ \tilde{q}_2 \\ \tilde{q}_3 \\ \tilde{q}_4 \\ \tilde{q}_5 \\ \tilde{q}_6 \end{pmatrix} = \frac{1}{\sqrt{6}} \begin{pmatrix} 0 & \sqrt{2} & 0 & -1 & 0 & 0 \\ \sqrt{2} & 0 & -\sqrt{2} & 0 & 1 & 0 \\ 1 & 0 & 1 & 0 & 0 & -2 \\ 1 & 0 & -1 & 0 & -\sqrt{2} & 0 \\ 0 & -1 & 0 & \sqrt{2} & 0 & 0 \\ \sqrt{2} & 0 & \sqrt{2} & 0 & 0 & \sqrt{2} \end{pmatrix} \begin{pmatrix} q_1 \\ q_2 \\ q_3 \\ q_4 \\ q_5 \\ q_6 \end{pmatrix} . \tag{A.5}$$

To avoid ill-defined scenarios, we restrict our analysis to configurations of the body defined by $\mathbf{r}_{s\alpha} = \mathbf{r}^0_{s\alpha} + \lambda\, \mathbf{x}_{s\alpha}$, where $\mathbf{x}_{s\alpha}$ represents the α-th particle's displacement from its position in the equilibrium configuration $\mathbf{r}^0_{s\alpha}$

$$\begin{aligned} \mathbf{r}^0_{s1} &= \left(0, \tfrac{a}{\sqrt{3}}, -\tfrac{h}{3}\right) , \\ \mathbf{r}^0_{s2} &= \left(-\tfrac{a}{2}, -\tfrac{a}{2\sqrt{3}}, -\tfrac{h}{3}\right) , \\ \mathbf{r}^0_{s3} &= \left(\tfrac{a}{2}, -\tfrac{a}{2\sqrt{3}}, -\tfrac{h}{3}\right) , \\ \mathbf{r}^0_{s4} &= (0, 0, h) , \end{aligned} \tag{A.6}$$

with $h = \sqrt{3}a/\sqrt{8}$, which corresponds to a tetrahedon of length a. Since any deformation of the body can be described as a linear combination of the normal modes, we consider the case where

$\mathbf{x}_{s\alpha}$ corresponds to the μ-th normal mode $\mathbf{x}^{(\mu)} = \{\mathbf{x}_{s1}^{(\mu)}, \ldots, \mathbf{x}_{s4}^{(\mu)}\}$:

$$
\begin{aligned}
\mathbf{x}^{(1)} &= \left\{ (-\tfrac{1}{4\sqrt{2}}, -\tfrac{5}{4\sqrt{6}}, \tfrac{1}{2\sqrt{3}}), (-\tfrac{1}{4\sqrt{2}}, \tfrac{\sqrt{\frac{3}{2}}}{4}, 0), (\tfrac{3}{4\sqrt{2}}, -\tfrac{1}{4\sqrt{6}}, -\tfrac{1}{2\sqrt{3}}), (-\tfrac{1}{4\sqrt{2}}, \tfrac{\sqrt{\frac{3}{2}}}{4}, 0) \right\}, \\
\mathbf{x}^{(2)} &= \left\{ (-\tfrac{\sqrt{\frac{3}{2}}}{4}, \tfrac{5}{12\sqrt{2}}, -\tfrac{1}{6}), (\tfrac{5}{4\sqrt{6}}, \tfrac{5}{12\sqrt{2}}, \tfrac{1}{3}), (\tfrac{1}{4\sqrt{6}}, -\tfrac{7}{12\sqrt{2}}, -\tfrac{1}{6}), (-\tfrac{\sqrt{\frac{3}{2}}}{4}, -\tfrac{1}{4\sqrt{2}}, 0) \right\}, \\
\mathbf{x}^{(3)} &= \left\{ (0, \tfrac{1}{3}, \tfrac{1}{3\sqrt{2}}), (-\tfrac{1}{2\sqrt{3}}, -\tfrac{1}{6}, \tfrac{1}{3\sqrt{2}}), (\tfrac{1}{2\sqrt{3}}, -\tfrac{1}{6}, \tfrac{1}{3\sqrt{2}}), (0, 0, -\tfrac{1}{\sqrt{2}}) \right\}, \\
\mathbf{x}^{(4)} &= \left\{ (-\tfrac{\sqrt{3}}{4}, \tfrac{1}{12}, \tfrac{1}{3\sqrt{2}}), (\tfrac{1}{4\sqrt{3}}, \tfrac{1}{12}, -\tfrac{\sqrt{2}}{3}), (-\tfrac{1}{4\sqrt{3}}, -\tfrac{5}{12}, \tfrac{1}{3\sqrt{2}}), (\tfrac{\sqrt{3}}{4}, \tfrac{1}{4}, 0) \right\}, \\
\mathbf{x}^{(5)} &= \left\{ (\tfrac{1}{4}, \tfrac{1}{4\sqrt{3}}, \tfrac{1}{\sqrt{6}}), (\tfrac{1}{4}, -\tfrac{\sqrt{3}}{4}, 0), (-\tfrac{1}{4}, -\tfrac{1}{4\sqrt{3}}, -\tfrac{1}{\sqrt{6}}), (-\tfrac{1}{4}, \tfrac{\sqrt{3}}{4}, 0) \right\}, \\
\mathbf{x}^{(6)} &= \left\{ (0, \tfrac{\sqrt{2}}{3}, -\tfrac{1}{6}), (-\tfrac{1}{\sqrt{6}}, -\tfrac{1}{3\sqrt{2}}, -\tfrac{1}{6}), (\tfrac{1}{\sqrt{6}}, -\tfrac{1}{3\sqrt{2}}, -\tfrac{1}{6}), (0, 0, \tfrac{1}{2}) \right\}.
\end{aligned}
\tag{A.7}
$$

Correspondingly, the deformation from the body's equilibrium configuration by the μ-th normal mode is given in shape space by $\tilde{q}^{\mu} = \tilde{q}_0^{\mu} + \lambda x^{\mu}$, where the equilibrium configuration is represented by the point $\tilde{q}_0^{\mu} = (0, 0, 0, 0, 0, \sqrt{\frac{3}{2}})$ and x^{μ} represents the μ-th normal mode (see Fig. 2.5). (x_1, x_2, x_3) is a triplet, (x_4, x_5) a doublet, and x_6 is the breathing mode, with frequencies $\omega = \sqrt{2}, 1, 2$, respectively. We remark that only the modes in the doublet and the breathing mode are commensurable.

The moment of inertia tensor corresponding to the equilibrium configuration is diagonal $\mathsf{M} = \mathsf{I}$, and the Coriolis tensor $\mathbf{B}_{\mu\nu}$ is non-zero in each component

$$
(B_1)_{\mu\nu} = \begin{pmatrix}
0 & 0 & 0 & 0 & 1 & 0 \\
0 & 0 & -1 & 1 & 0 & 0 \\
0 & 1 & 0 & -\sqrt{2} & 0 & 0 \\
0 & -1 & \sqrt{2} & 0 & 0 & 0 \\
-1 & 0 & 0 & 0 & 0 & 0 \\
0 & 0 & 0 & 0 & 0 & 0
\end{pmatrix}, \tag{A.8}
$$

$$
(B_2)_{\mu\nu} = \begin{pmatrix}
0 & 0 & 1 & 1 & 0 & 0 \\
0 & 0 & 0 & 0 & -1 & 0 \\
-1 & 0 & 0 & 0 & -\sqrt{2} & 0 \\
-1 & 0 & 0 & 0 & 0 & 0 \\
0 & 1 & \sqrt{2} & 0 & 0 & 0 \\
0 & 0 & 0 & 0 & 0 & 0
\end{pmatrix}, \tag{A.9}
$$

$$(B_3)_{\mu\nu} = \begin{pmatrix} 0 & -1 & 0 & -\sqrt{2} & 0 & 0 \\ 1 & 0 & 0 & 0 & -\sqrt{2} & 0 \\ 0 & 0 & 0 & 0 & 0 & 0 \\ \sqrt{2} & 0 & 0 & 0 & 0 & 0 \\ 0 & \sqrt{2} & 0 & 0 & 0 & 0 \\ 0 & 0 & 0 & 0 & 0 & 0 \end{pmatrix} . \tag{A.10}$$

From the form of the previous matrices it can be deduced that in the $\mathbf{L}_s = 0$ case: shape deformations involving the breathing mode plus another normal, or involving only the normal modes (x_4, x_5) cannot generate a rotation of the body – the latter being a general result that applies to any n-body system whose equilibrium shape has at least three different planes of symmetry (see the last part of 2.4). On the other hand, combinations of any mode of a doublet (x_4, x_5) with any one of the triplet (x_1, x_2, x_3) cannot give rise to finite cyclic trajectories in shape space and, therefore, the inquiry on the generation of a corresponding rotation is meaningless from the physical point of view.

Appendix B

Isotropic wavefunctions on $SO(3)$

In this appendix, we give a brief discussion of the wavefunction in $SO(3)$ which do not depend of the rotation axis' angles (Θ, Φ), which we call *isotropic wavefunctions* on $SO(3)$.

For a spin representation l, a general wavefunction on $SO(3)$ $\Psi(\eta; \Theta, Phi)$ of the state is given by (we omit the l index)

$$\Psi(\eta; \Theta, \Phi) = \sum_{mk} c_{mk} D_{mk}(\eta; \Theta, \Phi)\,. \tag{B.1}$$

The condition of isotropic wavefunction is equivalent to ask that $\Psi(\mathsf{R})$ be invariant under rotations of the coordinate system,

$$\Psi(\mathsf{R}) = \Psi(\mathsf{U}\mathsf{R}\mathsf{U}^{-1})\,, \qquad \forall\ U \in SO(3)\,. \tag{B.2}$$

Well-known functions with this property are the characters $\chi^l(\mathsf{R})$ of the irrep of the rotation group [94]

$$\chi^l(\eta) = \chi^l(\mathsf{R}) = \sum_{m=-l}^{m} D^{(l)}_{mm}(\mathsf{R})\,. \tag{B.3}$$

We prove that they are the only functions with the isotropic property. First, we expand the eq. (B.2)

$$\sum_{m,k} c_{mk} D_{mk}(\mathsf{R}) = \sum_{m,k,m',m''} c_{mk} D_{mm'}(\mathsf{U}) D_{m'm''}(\mathsf{R}) D_{m''k}(\mathsf{U}^{-1})\,, \tag{B.4}$$

where we obtain

$$c_{m_0k_0} = \sum_{m,k} c_{mk} D_{mm_0}(\mathsf{U}) D_{k_0k}(\mathsf{U}^{-1})\,, \tag{B.5}$$

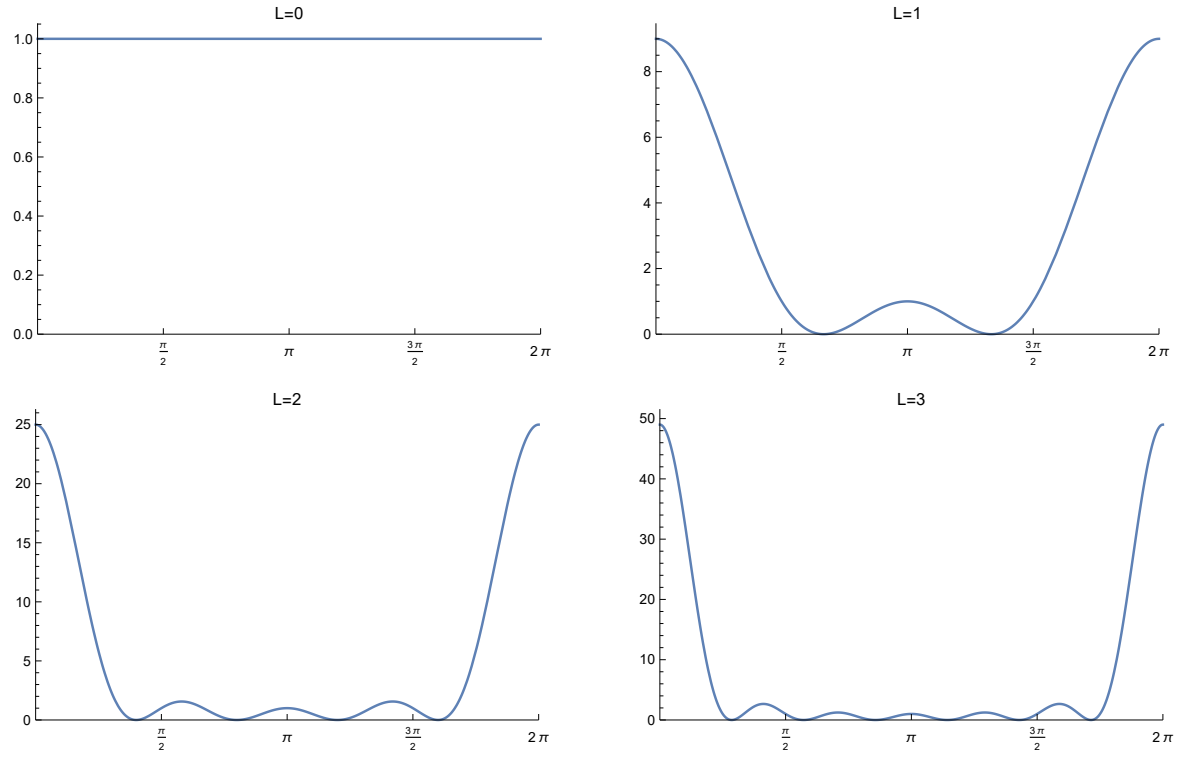

Figure B.1: The plot of $|\chi^l(\eta)|^2$ for $l = 0, 1, 2, 3$.

and the only way the last equation satisfies for every $\mathsf{U} \in SO(3)$ is with the relation

$$\sum_{m''} D_{mm''}(\mathsf{U}) D_{m''m'}(\mathsf{U}^{-1}) = \delta_{mm'} \,, \tag{B.6}$$

this relation imposes to the coeffcients the condition $c_{mk} = \delta_{mk} c$, which is the same expansion found in the wavefunction $\Psi(\eta)$.

The characters $\chi^l(\eta)$ have an easy expression [94]

$$\chi^l(\eta) = \frac{\sin[(2l+1)\frac{\eta}{2}]}{\sin\frac{\eta}{2}} \,. \tag{B.7}$$

We plot the probability density for the isotropic states $|\Psi(\mathsf{R})|^2$ for $l = 0, 1, 2, 3$ in the figure B.1. While bigger is the quantum number l, the state is more localized in the origin and then it more localized in one orientation. Let us remember that a rotation $\eta > \pi$ in the $\hat{\mathbf{n}}$ direction is equivalent to a rotation in the antipodal direction for an angle $\eta - \pi$.

Appendix C

$(\hat{\mathbf{n}} \cdot \mathbf{S})^k$ and $(\mathbf{B} \cdot \mathbf{S})^k$ expanded in tensor operators

In the 4-body model, we used the scalar operators $(\hat{\mathbf{n}} \cdot \mathbf{S})^k$ or $(\mathbf{B} \cdot \mathbf{S})^k$ for any positive value of k, where $\hat{\mathbf{n}}$ is the unit vector defined by the angles (θ, φ), and $\mathbf{B}$ and $\mathbf{S}$ are angular momentum operators of different Hilbert spaces, with spin b and s, respectively. For the rotational invariance, their expressions must be of the form

$$(\hat{\mathbf{n}} \cdot \mathbf{S})^k = \sum_{\sigma=0}^{2s} A_\sigma^{(k)}(s) \sum_{\mu=-\sigma}^{\sigma} Y_{\sigma\mu}^*(\theta,\, \varphi) T_{\sigma\mu}^{(s)}\,, \tag{C.1}$$

$$(\mathbf{B} \cdot \mathbf{S})^k = \sum_{\sigma=0}^{2j} \alpha_\sigma^{(k)}(b, s) \sum_{\mu=-\sigma}^{\sigma} T_{\sigma\mu}^{(b)\dagger} \otimes T_{\sigma\mu}^{(s)}\,, \tag{C.2}$$

where $j = \min(b, s)$, and $A_\sigma^{(k)}(s)$ and $\alpha_\sigma^{(k)}(b, s)$ are functions of s y b. In what follows we deduce recursive expressions to $A_\sigma^{(k)}(s)$ and $\alpha_\sigma^{(k)}(b, s)$. First, we consider $(\hat{\mathbf{n}} \cdot \mathbf{S})^k$. Let us start with $k = 0$ so that (
$uvn \cdot \mathbf{S})^0 = \mathbb{1} = A_0^{(0)} Y_{0,0}^*(\theta, \varphi) T_{00}$, and then, $A_0^{(0)}(s) = \sqrt{4\pi(2s+1)}$. For $k = 1$,
$uvn \cdot \mathbf{S} = A_1^{(1)} \sum_\mu Y_{1\mu}^*(\theta, \varphi) T_{1\mu}$ and, when it is evaluated at $(\theta, \varphi) = (0, 0)$, we find

$$\mathbf{S}_3 = A(s) Y_{1\mu}^*(0, 0) T_{1\mu} = \frac{A(s)}{2} \sqrt{\frac{3}{\pi}} T_{10}\,. \tag{C.3}$$

Using the explicit expression of T_{10} (1.37), we obtain

$$A(s) = A_1^{(1)}(s) = \frac{2}{3} \sqrt{s(s+1)(2s+1)\pi}\,. \tag{C.4}$$

With the expression of $\hat{\mathbf{n}}\cdot\mathbf{S}$ it is straightforward to conclude that $A_\sigma^{(k)}(s)=0$ for $\sigma>k$. Besides, due to the parity of $T_{\mu\nu}$, σ and k must have the same parity. The last two results are valid even when we substitute $\hat{\mathbf{n}}$ for a vector operator.

Now, for $A_\sigma^{(k)}(s)$ with $k>1$, we calculate the product of $(\hat{\mathbf{n}}\cdot\mathbf{S})$ with a general rotation invariant operator $\sum_\sigma B_\sigma \sum_\mu Y^*_{\sigma\mu}(\theta,\varphi)T_{\sigma\mu}$. The product of two invariant terms is invariant, and then the result has the same form $\sum_\sigma B'_\sigma \sum_\mu Y^*_{\sigma\mu}(\theta,\varphi)T_{\sigma\mu}$. Therefore the calculation is reduced to obtain B'_σ and can be expressed as

$$(\hat{\mathbf{n}}\cdot\mathbf{S})\left(\sum_\sigma B_\sigma\sum_\mu Y^*_{\sigma\mu}(\theta,\varphi)T_{\sigma\mu}\right)=\mathrm{M}[\hat{\mathbf{n}}\cdot\mathbf{S}]\begin{pmatrix}B_0\\B_1\\\vdots\\B_{2j}\end{pmatrix}=\begin{pmatrix}B'_0\\B'_1\\\vdots\\B'_{2j}\end{pmatrix}=\sum_\sigma B'_\sigma\sum_\mu Y^*_{\sigma\mu}(\theta,\varphi)T_{\sigma\mu}\,. \tag{C.5}$$

$\mathrm{M}[\hat{\mathbf{n}}\cdot\mathbf{S}]$ is a $(2s+1)$ square matrix whose indexes run from 0 to $2s$, and its elements are given by

$$\mathrm{M}[\hat{\mathbf{n}}\cdot\mathbf{S}]_{r'r}=A(s)\sum_{\mu,\nu}\mathrm{Tr}\left[Y^*_{1\mu}\,Y^*_{r\nu}\,Y_{r'0}\right]\mathrm{Tr}\left[T_{1\mu}\,T_{r\nu}\,T^\dagger_{r'0}\right]\,, \tag{C.6}$$

where we denote the integration of the spherical harmonics over the sphere by their trace and they are given by (see [1, 85])

$$\mathrm{Tr}\left[Y_{l_1m_1}Y_{l_2m_2}Y_{lm}\right]=\sqrt{\frac{(2l+1)(2l_1+1)(2l_2+1)}{4\pi}}\begin{pmatrix}l_1&l_2&l\\m_1&m_2&m\end{pmatrix}\begin{pmatrix}l_1&l_2&l\\0&0&0\end{pmatrix}\,, \tag{C.7}$$

$$\mathrm{Tr}\left[T_{l_1m_1}T_{l_2m_2}T_{lm}\right]=(-1)^{l_1+l_2+l-2s}\sqrt{(2l+1)(2l_1+1)(2l_2+1)}\begin{pmatrix}l_1&l_2&l\\m_1&m_2&m\end{pmatrix}\begin{Bmatrix}l_1&l_2&l\\s&s&s\end{Bmatrix}\,, \tag{C.8}$$

respectively. Using the previous expressions, after doing some algebra, we obtain

$$\mathrm{M}\left[\hat{\mathbf{n}}\cdot\mathbf{S}\right]_{r'r}=\frac{1}{2}\left(\frac{r}{2r-1}\sqrt{(2s+1-r)(2s+1+r)}\delta_{r',r-1}+\frac{r+1}{2r+3}\sqrt{(2s-r)(2s+2+r)}\delta_{r',r+1}\right)\,. \tag{C.9}$$

And finally, the expression for $A_\sigma^{(k)}(s)$ with $k>1$ is

$$A_\sigma^{(k)}(s)=A(s)\left(\mathrm{M}\left[\hat{\mathbf{n}}\cdot\mathbf{S}\right]^{k-1}\right)_{\sigma 1}\,. \tag{C.10}$$

It is important to remark that each component of $\mathrm{M}\left[\hat{\mathbf{n}}\cdot\mathbf{S}\right]$ is non negative, and then $A_\sigma^{(k)}(s)=0$ only if $\sigma>\min(k,2s)$, or σ and k have different parity. The first non zero coefficients $A_\sigma^{(k)}(s)$

are:

$$\begin{aligned}
A_0^{(0)}(s) &= \sqrt{4\pi(2s+1)}\,, \\
A_1^{(1)}(s) &= \tfrac{2}{3}\sqrt{s(s+1)(2s+1)\pi}\,, \\
A_0^{(2)}(s) &= \tfrac{2}{3}s(s+1)\sqrt{(2s+1)\pi}\,, \\
A_2^{(2)}(s) &= \tfrac{1}{15}\sqrt{(2s-1)(2s)(\dots)(2s+3)\pi}\,, \\
A_1^{(3)}(s) &= \tfrac{2}{15}(3s^2+3s-1)\sqrt{s(s+1)(2s+1)\pi}\,, \\
A_3^{(3)}(s) &= \tfrac{1}{70}\sqrt{(2s-2)(2s-1)(\dots)(2s+4)\pi}\,.
\end{aligned} \tag{C.11}$$

These relations are also obtained with the closed formula found in [25],

$$A_\sigma^{(k)}(s) = \sqrt{\frac{4\pi}{2s+1}}\, i^{k-\sigma}\partial_\phi^k \chi_\sigma^s(\phi)\Big|_{\phi=0} = \sqrt{\frac{4\pi}{2s+1}}\sum_{m=-s}^{s} m^k c_{sm,\sigma 0}^{sm}\,, \tag{C.12}$$

where $\chi_\sigma^s(\phi)$ are the generalized character of $SU(2)$ (see [94]).

Let us now consider the case when $\hat{\mathbf{n}}$ is substituted for an angular momentum operator $\mathbf{B}$ in the b spin states representation. The factor $\alpha_1^1(b,s)$ can be obtained by calculating the expectation value of $\mathbf{B}\cdot\mathbf{S}$ with the state $|b^b\rangle\otimes|s^s\rangle$ and using the formula,

$$\langle j^j|T_{KQ}^j|j^j\rangle = \delta_{Q,0}\sqrt{2K+1}\begin{pmatrix} j & K & j \\ -j & 0 & j\end{pmatrix} = \delta_{Q,0}(2j)!\sqrt{\frac{2K+1}{(2j-K)!(2j+1+K)!}}\,, \tag{C.13}$$

and then

$$\alpha(b,s) := \alpha_1^1(b,s) = \frac{1}{12}\sqrt{2b(2b+1)(2b+2)}\sqrt{2s(2s+1)(2s+2)}\,. \tag{C.14}$$

For $\alpha_\sigma^{(k)}(b,s)$ with $k>1$, we use the same procedure than before for $(\hat{\mathbf{n}}\cdot\mathbf{S})^k$. In this case, the equation (C.6) changes to

$$\mathrm{M}\left[\mathbf{B}\cdot\mathbf{S}\right]_{r'r} = \alpha(b,s)\sum_{\mu,\nu}\mathrm{Tr}\left[T_{1\mu}^{b\dagger}T_{r\nu}^{b\dagger}T_{r'0}^{b}\right]\mathrm{Tr}\left[T_{1\mu}^{s}T_{r\nu}^{s}T_{r'0}^{s\dagger}\right]\,, \tag{C.15}$$

and it can be deduced that

$$\begin{aligned}
\mathrm{M}\left[\mathbf{B}\cdot\mathbf{S}\right]_{r'r} &= \tfrac{1}{4}\Big(\delta_{r',r-1}\tfrac{r}{2r-1}\sqrt{(2b-r+1)(2b+r+1)(2s-r+1)(2s+r+1)} \\
&\quad + \delta_{r',r+1}\tfrac{r+1}{2r+3}\sqrt{(2b-r)(2b+r+2)(2s-r)(2s+r+2)}\Big)\,.
\end{aligned} \tag{C.16}$$

The α factors are calculated in the same form that in (C.10)

$$\alpha_\sigma^{(k)}(b,s) = \alpha(b,s)\left(\mathrm{M}\left[\mathbf{B}\cdot\mathbf{S}\right]^{k-1}\right)_{\sigma 1}\,. \tag{C.17}$$

We write the first terms of $\alpha_\sigma^{(k)}(b,s)$

$$\begin{aligned}
\alpha_0^{(0)}(b,s) &= \prod_{j=b,s}\sqrt{2j+1}\,,\\
\alpha_1^{(1)}(b,s) &= \tfrac{1}{3}\prod_{j=b,s}\sqrt{j(j+1)(2j+1)}\,,\\
\alpha_0^{(2)}(b,s) &= \tfrac{1}{3}\prod_{j=b,s} j(j+1)\sqrt{(2j+1)}\,,\\
\alpha_2^{(2)}(b,s) &= \tfrac{1}{120}\prod_{j=b,s}\sqrt{(2j-1)(2j)(\dots)(2j+3)}\,,\\
\alpha_1^{(3)}(b,s) &= \tfrac{\alpha(b,s)}{5}(12(b)(b+1)(s)(s+1)-4(b(b+1)+s(s+1))+3)\,,\\
\alpha_3^{(3)}(b,s) &= \tfrac{1}{1120}\prod_{j=b,s}\sqrt{(2j-2)(2j-1)(\dots)(2j+4)}\,.
\end{aligned} \tag{C.18}$$

Appendix D

The auxiliar operator B and the relation between L

Let us consider a 3D isotropic harmonic oscillator, with Hamiltonian given by

$$H = \frac{1}{2}(p_1^2 + p_2^2 + p_3^2) + \frac{1}{2}(x_1^2 + x_2^2 + x_3^2), \tag{D.1}$$

and let us consider the set of states $|n, s^{m_s}\rangle$ labeled by the quantum numbers

$$\begin{aligned} N|n, s^{m_s}\rangle &= n|n, s^{m_s}\rangle\,, \\ \mathbf{S}^2|n, s^{m_s}\rangle &= s(s+1)|n, s^{m_s}\rangle\,, \\ S_3|n, s^{m_s}\rangle &= m_s|n, s^{m_s}\rangle\,, \end{aligned} \tag{D.2}$$

where $S_i = \epsilon_{ijk} x_j p_k$ and $[S_i, S_j] = i\epsilon_{ijk} S_k$. Let us further assume that this system is coupled to its angular momentum, as in the Hamiltonian (15),

$$H = \sqrt{2}N + \frac{\lambda^2}{2}\left(\mathbf{L} + \frac{1}{2}\mathbf{S}\right)^2 = \sqrt{2}N + \frac{\lambda^2}{2}\left(\mathbf{L}^2 + \mathbf{L}\cdot\mathbf{S} + \frac{1}{4}\mathbf{S}^2\right)\,, \tag{D.3}$$

where $\mathbf{L}$ is the total angular momentum in the body frame. The eigenstates $|m, l^k\rangle$ of the orientation part satisfy

$$\begin{aligned} \mathbf{L}^2|m, l^k\rangle &= l(l+1)|m, l^k\rangle\,, \\ L_z|m, l^k\rangle &= k|m, l^k\rangle\,, \\ L_{sz}|m, l^k\rangle &= m|m, l^k\rangle\,, \end{aligned} \tag{D.4}$$

where

$$[L_i, L_j] = -i\epsilon_{ijk} L_k\,, \qquad [L_{si}, L_{sj}] = i\epsilon_{ijk} L_{sk}\,. \tag{D.5}$$

The subindex s means that the vector is referred to the space (fixed) frame. A basis (that we call the decoupled basis) of the Hilbert space is formed by $|n, m, s^{m_s}, l^k\rangle$, which are not eigenstates of (D.3).

The ladder operators of the angular momentum in the body frame are

$$L_\pm = L_x \mp iL_y \,, \tag{D.6}$$

by the commutation relations of its components. Also, because of that, $\mathbf{L}$ cannot be coupled with $\mathbf{S}$ in the usual way [14]. We use the auxiliar operator $\mathbf{B} = -\mathbf{L}$ and its eigenstates $|l^{m_b}\rangle_b$ where

$$\begin{aligned} \mathbf{B}^2|b^{m_b}\rangle_b &= b(b+1)|b^{m_b}\rangle_b \,. \\ B_3|b^{m_b}\rangle_b &= m_b|b^{m_b}\rangle_b \,. \end{aligned} \tag{D.7}$$

To obtain the relation between the states $|b^{m_b}\rangle_b$ and $|l^k\rangle$, we see that

$$\begin{aligned} l(l+1)|l^k\rangle &= \mathbf{L}^2|l^k\rangle &&= \mathbf{B}^2|l^k\rangle \\ -k|l^k\rangle &= -L_3|l^k\rangle &&= B_3|l^k\rangle \,. \end{aligned} \tag{D.8}$$

Then $|l^k\rangle = F|l^{-k}\rangle_b$, with F a constant of unit norm. Now, if we consider $|l^l\rangle = |l^{-l}\rangle_b$, by applying $L_- = -B_+$, we obtain

$$|l^{l-1}\rangle = -|l^{-l+1}\rangle_b \,, \tag{D.9}$$

and the general relation turns out to be

$$|l^k\rangle = (-1)^{l-k}|l^{-k}\rangle_b \,. \tag{D.10}$$

Introducing the operator $\mathbf{J} = \mathbf{B} + \mathbf{S}$, we find

$$\mathbf{B}\cdot\mathbf{S} = -\mathbf{L}\cdot\mathbf{S} = \frac{1}{2}(\mathbf{J}^2 - \mathbf{L}^2 - \mathbf{S}^2) \,. \tag{D.11}$$

so that Eq. (D.3) yields

$$H = \sqrt{2}N + \frac{\lambda^2}{4}\left(3\mathbf{L}^2 + \frac{3}{2}\mathbf{S}^2 - \mathbf{J}^2\right) . \tag{D.12}$$

The eigenstates of which are given by the basis $|n, m, s, l, j^{m_j}\rangle$, where we couple the basis $|s^{m_s}\rangle$ and $|l^k\rangle_b$.

It is convenient to express T^b_{KQ} in terms of T^l_{KQ}

$$\begin{aligned}
T^b_{KQ} &= \sum_{m,m'} (-1)^{l-m}\sqrt{2K+1}\begin{pmatrix} l & K & l \\ -m & Q & m' \end{pmatrix} |l^m\rangle_b\langle l^{m'}|_b \\
&= \sum_{m,m'} (-1)^{l+m'}\sqrt{2K+1}\begin{pmatrix} l & K & l \\ -m & Q & m' \end{pmatrix} |l^{-m}\rangle\langle l^{-m'}| \\
&= \sum_{m,m'} (-1)^{l-m'}\sqrt{2K+1}\begin{pmatrix} l & K & l \\ m & Q & -m' \end{pmatrix} |l^m\rangle\langle l^{m'}| \qquad \text{(D.13)} \\
&= (-1)^{K-Q}\sum_{m,m'} (-1)^{l-m}\sqrt{2K+1}\begin{pmatrix} l & K & l \\ -m & -Q & m' \end{pmatrix} |l^m\rangle\langle l^{m'}| \\
&= (-1)^{K-Q}T^l_{K,-Q} \\
&= (-1)^K T^{l\dagger}_{KQ}\,.
\end{aligned}$$

For example,

$$\langle l^k|T^b_{KQ}|l^{k'}\rangle = (-1)^{l-k'}\sqrt{2K+1}\begin{pmatrix} l & K & l \\ k & Q & -k' \end{pmatrix}\delta_{Q,k'-k}\,. \qquad \text{(D.14)}$$

Appendix E

Eigenbasis of the 3D isotropic harmonic oscillator

For the shape's wavefunction, we use the analogy with the 3D isotropic harmonic oscillator, where we use two complete sets of mutually compatible operators $\{N, \mathbf{S}^2, S_z\}$ and $\{N_+, N_-, N_3\}$, where each one is associated with a basis, $|n, s, m_s\rangle$ and $|n_+ n_- n_3\rangle$, respectively, and where n and s must have the same parity. In this appendix, we give a list of the necessary tools to do a basis's transformation and expose the procedure for $n = 0, 1, 2$.

The application of the $\{S_\pm, S_3, \mathbf{S}^2\}$ operators in the states $|n, s, m_s\rangle$ are

$$\begin{aligned} \mathbf{S}^2|n,s,m_s\rangle &= s(s+1)|n,s,m_s\rangle\,, \\ S_\pm|n,s,m_s\rangle &= \sqrt{(s\mp m_s)(s\pm m_s+1)}|n,s,m_s\pm 1\rangle \\ S_3|n,s,m_s\rangle &= m_s|n,s,m_s\rangle\,. \end{aligned} \tag{E.1}$$

These operators to be applied in the basis $|n_+, n_-, n_3\rangle$ we use the eqs (44)

$$\begin{aligned} \mathbf{S}^2 &= N(N+1) - 4N_+N_- - N_3(N_3-1) - 2(a_3^\dagger a_3^\dagger a_+ a_- + a_-^\dagger a_+^\dagger a_3 a_3) \\ &= (N_+ - N_-)^2 + (2N_3+1)(N_+ + N_- + 1) - 1 - 2(a_3^\dagger a_3^\dagger a_+ a_- + a_-^\dagger a_+^\dagger a_3 a_3)\,, \\ S_+ &= \sqrt{2}\left(a_3^\dagger a_- - a_+^\dagger a_3\right)\,, \\ S_- &= \sqrt{2}\left(a_-^\dagger a_3 - a_3^\dagger a_+\right)\,, \\ S_3 &= N_+ - N_-\,, \end{aligned} \tag{E.2}$$

It's easy to check that $|n, s = n, m_s = n\rangle = |n_+ = n, 0_-, 0_3\rangle$ and $|n, s = n, m_s = -n\rangle = |n_+, n_- = n, 0_3\rangle$, where the numerical values of the states in the basis $|n, s, m_s\rangle$ are indexed with

the labels n, s, m, respectively, and for the basis $|N_+, N_-, N_3\rangle$ with the labels $+, -, 3$.

The case $n = 0$ is trivial,

$$|0_n, 0_s, 0_m\rangle = |0_+, 0_-, 0_3\rangle \,. \tag{E.3}$$

Now, for $n = 1$, we have only $s = 1$ and $m_s = 0, \pm 1$. We use the ladder operators to the state with highest projection S_z, and we obtain

$$\begin{aligned} |1_n, 1_s, 1_m\rangle &= |1_+, 0_-, 0_-\rangle \,, \\ |1_n, 1_s, 0_m\rangle &= -|0_+, 0_-, 1_3\rangle \,, \\ |1_n, 1_s, -1_m\rangle &= -|0_+, 1_-, 0_3\rangle \,. \end{aligned} \tag{E.4}$$

As a final example, we do the case n=2, where the available in $|nsm_s\rangle$ basis are $|2, 0_s, 0_m\rangle$ and $|2_n, 2_s, m_s\rangle$ with $m_s = 0, \pm 1, \pm 2$, while in the $|n_+, n_-, n_3\rangle$ are $\{|2_+, 0_-, 0_3\rangle\,,\ |0_+, 2_-, 0_3\rangle, |0_+, 0_-, 2_3\rangle, |0_+, 1_-, 1_3\rangle, |1$ We apply S_- to $|2_n, 2_s, 2_m\rangle = |2_+, 0_-, 0_3\rangle$.

$$\begin{aligned} |2_n, 2_s, 2_m\rangle &= |2_+, 0_-, 0_3\rangle \,, \\ |2_n, 2_s, 1_m\rangle &= -|1_+, 0_-, 1_3\rangle \,, \\ |2_n, 2_s, 0_m\rangle &= \sqrt{\tfrac{2}{3}}|0_+, 0_-, 2_3\rangle - \sqrt{\tfrac{1}{3}}|1_+, 1_-, 0_3\rangle, \\ |2_n, 2_s, -1_m\rangle &= |0_+, 1_-, 1_3\rangle \,, \\ |2_n, 2_s, -2_m\rangle &= |0_+, 2_-, 0_3\rangle \,. \end{aligned} \tag{E.5}$$

Finally, we obtain the state $|2_n, 2_s, 0_m\rangle$ asking the orthogonality with $|2_n, 0_s, 0_m\rangle$,

$$|2_n, 0_s, 0_m\rangle = \sqrt{\tfrac{1}{3}}|0_+, 0_-, 2_3\rangle + \sqrt{\tfrac{2}{3}}|1_+, 1_-, 0_3\rangle \,. \tag{E.6}$$

Appendix F

The equivalence of the Majorana polynomial of a k-plane

In this appendix, we prove that the Majorana polynomial $p_\Pi(z)$ of a k-plane Π, with basis $\mathscr{B} = \{|\psi_j\rangle\}_{j=1}^k$ only depends of z and not of $\bar{z}$. Moreover, we obtain that $p_\Pi(z)$ is proportional to the Wronskian of $\mathscr{B}$ (theorem 19). Let us remember that $p_\Pi(\zeta)$ is equal to

$$p_\Pi(z) \equiv \langle \Pi_{-n}, \Pi \rangle = \frac{\det\langle \Psi_{-n}|\Psi\rangle}{\sqrt{\det\langle \Psi_{-n}|\Psi_{-n}\rangle}\sqrt{\det\langle \Psi|\Psi\rangle}}\,, \tag{F.1}$$

where Π_n is the coherent k-plane in the direction n with associated complex number z,

$$|\Psi_n\rangle = \text{span}\{|n,s\rangle, |n,s-1\rangle, \ldots, |n,s-k+1\rangle\}\,, \tag{F.2}$$

with $|n,m\rangle$ such that $n\cdot S|n,m\rangle = m|n,m\rangle$. Also, $\langle\Psi_1|\Psi_2\rangle$, is the matrix with entries $\langle\Psi_1|\Psi_2\rangle_{ij} = \langle\psi_{1i}|\psi_{2j}\rangle$ with respect to a bases of Π_1 and Π_2. As we will show below, the equation (F.1) is, in principle, a polynomial of z and $z^A = -1/\bar{z}$ (the antipodal point of n), and with a higher degree than $(2s+1-k)k$. However, we obtained that the variables of z^A vanish. First, we will write the entry $\langle\psi_{1\mu}|\psi_{2\nu}\rangle$ as a polynomial.

The inner product of two states as a polynomial

A state of spin 1/2 oriented in the direction $n(\theta,\phi)$ can be written as $|\hat{n}\rangle = \cos(\theta/2)\,(|+\rangle + z|-\rangle)$, where $z = \tan(\theta/2)e^{i\phi}$. Now, the inner product with two spin 1/2 states has the next form

$$\langle\hat{n}_2|\hat{n}_1\rangle = \cos(\theta_2/2)\cos(\theta_1/2)\,(1+\bar{z}_2 z_1) = \cos(\theta_2/2)\cos(\theta_1/2)\bar{z}_2\left(z_1 - z_2^A\right) = L_{z_2}R_{z_1}\left(z_1 - z_2^A\right)\,, \tag{F.3}$$

where $L_{z_2} = \cos(\theta_2/2)\bar{z}_2$ and $R_{z_1} = \cos(\theta_1/2)$. The generalization of the inner product of two states given by a tensor product of $N = 2s$ spin 1/2 states (in particular the totally symmetric states) is straightforward. Let $|\phi_1\rangle = |c_1\rangle \otimes |c_2\rangle \otimes \cdots \otimes |c_n\rangle$ and $|\phi\rangle = |n_1\rangle \otimes |n_2\rangle \otimes \cdots \otimes |n_N\rangle$, then

$$\langle\phi|\phi_1\rangle = Q \prod_{j=1}^{N} (\gamma_j - z_j^A)\,, \tag{F.4}$$

with γ_j and z_j the stereographic projection of c_j and n_j, respectively. The proportionality factor Q is

$$Q = \prod_{j=1}^{N} L_{z_j} R_{\gamma_j}\,. \tag{F.5}$$

It is important to remark that is factorizable to each direction of the constituents states. Let us denote the equation (F.4) with a polynomial of several variables, where the variables is given by the antipodal directions of the state $|\phi\rangle$,

$$P_{\phi_1}(z_1, z_2, \ldots, z_N) := \prod_{j=1}^{N} (\gamma_j - z_j) \propto \langle\phi^A|\phi_1\rangle\,, \tag{F.6}$$

Observation 1. If one of the states has the same constituents spin 1/2 states but with another order, the proportionality factor is the same. If $|\phi_1'\rangle = |c_{1P(1)}\rangle \otimes |c_{1P(2)}\rangle \otimes \cdots \otimes |c_{1P(n)}\rangle$, then

$$\langle\phi|\phi_1'\rangle = Q \prod_{j=1}^{N} (\gamma_{P(j)} - z_j^A)\,, \tag{F.7}$$

or in terms of polynomials

$$P_{\phi_1'}(z_1, z_2, \ldots, z_N) = P_{\phi_1}(z_{P^{-1}(1)}, z_{P^{-1}(2)}, \ldots, z_{P^{-1}(N)}) \tag{F.8}$$

Observation 2. If the state is a totally symmetric state $|\psi\rangle = |c_1, \ldots c_N\rangle$, then

$$\langle\phi|\psi\rangle = Q N_\psi \sum_P \prod_{j=1}^{N} \left(\gamma_{P(j)} - z_j^A\right)\,, \tag{F.9}$$

with N_ψ a normalization constant. In terms of a polynomial, if the state $|\phi\rangle$ is a tensor product state with the same constituent states of $|\psi\rangle$, then

$$P_\psi(z_1\ \ldots, z_N) = \sum_P P_\phi(z_{P(1)}\ \ldots, z_{P(N)}) \propto \langle\phi^A|\psi\rangle\,, \tag{F.10}$$

Observation 3. The inner product of two totally symmetric states $|\psi\rangle$, $|\psi_1\rangle$ is equal to the product of one totally symmetric state $|\psi_1\rangle$ and a tensor product state $|\phi\rangle$ with the same constituents 1/2 spin states of $|\psi\rangle$. With this, the polynomial is proportional to several inner products between states

$$\langle\psi^A|\psi_1\rangle = \langle\phi^A|\psi_1\rangle \propto P_{\psi_1}(z_1\ \ldots, z_N) = P_{\psi_1}(z_{P(1)}\ \ldots, z_{P(N)})\,, \tag{F.11}$$

with $|\psi\rangle = |n_1, \ldots, n_N\rangle$ and $|\phi\rangle = |n_1\rangle \otimes \cdots \otimes |n_N\rangle$, and the order of the variables $z_1, \ldots, z_N$ doesn't affect. Therefore, for each state of spin s, $|\psi\rangle$, we can associate a polynomial of N variables $(z_1, \ldots, z_N)$, which is proportional to the inner product $\langle\phi^A|\psi\rangle$, where $|\phi\rangle$ is the spin s state with constellation given by the complex numbers z_j and $|\phi^A\rangle$ is the antipodal state of $|\phi\rangle$. In particular, if we put the same variable z in each entry of the polynomial, we recover the Majorana polynomial,

$$\langle -n, s|\psi\rangle \propto P_\psi(z, \ldots, z)\,, \tag{F.12}$$

For instance, we also put the polynomial of the inner product of a generic state $|\psi\rangle$ with $|n, m = s - k\rangle$,

$$\langle -n, m|\psi\rangle \propto P_\psi(\underbrace{z, \ldots, z}_{s+m}, \underbrace{z^A, \ldots, z^A}_{s-m})\,. \tag{F.13}$$

To simplify the last expression we define

$$P_\psi(z^{(s+m)}, z^{A(s-m)}) := P_\psi(\underbrace{z, \ldots, z}_{s+m}, \underbrace{z^A, \ldots, z^A}_{s-m})\,, \tag{F.14}$$

Observation 4

$$P_\psi(z^{(2s-1)}, z^{A(1)}) = P_\psi(z^{(2s)}, z^{A(0)}) + (z - z^A)P'_\psi(z^{(2s)}, z^{A(0)})\,, \tag{F.15}$$

where $P'_\psi(z^{(2s)}, z^{A(0)})$ is the derivative of $P_\psi(z^{(2s)}, z^{A(0)})$ with respect to z. There is a similar result for $P_\psi(z^{(s+m)}, z^{A(s-m)})$,

$$P_\psi(z^{(s+m)}, z^{A(s-m)}) = \sum_{k=0}^{m}(z - z^A)^k P^{(k)}_\psi(z^{(2s)}, z^{A(0)})\,, \tag{F.16}$$

The polynomial of the equation (F.1)

As a summary of the last subsection, we have that the inner product of two spin s states is $\langle\phi|\psi\rangle = N_\psi N_\phi P_\psi(z_1, \ldots, z_N)$, where $|\phi\rangle = |z_1\,, \ldots\,, z_N\rangle$ and N_ψ and N_ϕ are constants. Now,

the equation (F.1) is proportional to

$$P_z(\Pi) \propto \det\langle \Pi_{-z}|\Pi\rangle \propto \begin{vmatrix} \langle n,s|\psi_0\rangle & \langle n,s-1|\psi_0\rangle & \dots & \langle n,s-(k-1)|\psi_0\rangle \\ \langle n,s|\psi_1\rangle & \langle n,s-1|\psi_1\rangle & \dots & \langle n,s-(k-1)|\psi_1\rangle \\ \vdots & \vdots & \vdots & \vdots \\ \langle n,s|\psi_{k-1}\rangle & \langle n,s-1|\psi_{k-1}\rangle & \dots & \langle n,s-(k-1)|\psi_{k-1}\rangle \end{vmatrix}, \quad \text{(F.17)}$$

Each column and row has a common factor (N_ψ), and therefore the equation is proportional to

$$P_z(\Pi) \propto \begin{vmatrix} P_{\psi_0}(z^{2s}, z^{A(0)}) & P_{\psi_0}(z^{2s-1}, z^{A(1)}) & \dots & P_{\psi_0}(z^{2s-(k-1)}, z^{A(k-1)}) \\ P_{\psi_1}(z^{2s}, z^{A(0)}) & P_{\psi_1}(z^{2s-1}, z^{A(1)}) & \dots & P_{\psi_1}(z^{2s-(k-1)}, z^{A(k-1)}) \\ \vdots & \vdots & \vdots & \vdots \\ P_{\psi_{k-1}}(z^{2s}, z^{A(0)}) & P_{\psi_{k-1}}(z^{2s-1}, z^{A(1)}) & \dots & P_{\psi_{k-1}}(z^{2s-(k-1)}, z^{A(k-1)}) \end{vmatrix}. \quad \text{(F.18)}$$

The proportionality factor has terms related to normalization factors, or factors which involve irregularities of the coordinates (as $\cos\theta_j/2$). Then, the zeros of $P_z(\Pi)$ are described to the last equation, which gives us a polynomial of two variables, z and z^A of order $2sk - \frac{(k-1)k}{2}$ and $\frac{(k-1)k}{2}$, respectively. Using the equation (F.18), the last determinant can be rewritten as

$$\begin{aligned} P_z(\Pi) \propto & \begin{vmatrix} P_{\psi_0}(z^{2s}, z^{A(0)}) & (z-z^A)P^{(1)}_{\psi_0}(z^{2s}, z^{A(0)}) & \dots & (z-z^A)^{k-1}P^{(k-1)}_{\psi_0}(z^{2s}, z^{A(0)}) \\ P_{\psi_1}(z^{2s}, z^{A(0)}) & (z-z^A)P^{(1)}_{\psi_1}(z^{2s}, z^{A(0)}) & \dots & (z-z^A)^{k-1}P^{(k-1)}_{\psi_1}(z^{2s}, z^{A(0)}) \\ \vdots & \vdots & \vdots & \vdots \\ P_{\psi_{k-1}}(z^{2s}, z^{A(0)}) & (z-z^A)P^{(1)}_{\psi_{k-1}}(z^{2s}, z^{A(0)}) & \dots & (z-z^A)^{k-1}P^{(k-1)}_{\psi_{k-1}}(z^{2s}, z^{A(0)}) \end{vmatrix}. \\ =& (z-z^A)^{(k-1)k/2} \begin{vmatrix} P_{\psi_0}(z^{2s}, z^{A(0)}) & P^{(1)}_{\psi_0}(z^{2s}, z^{A(0)}) & \dots & P^{(k-1)}_{\psi_0}(z^{2s}, z^{A(0)}) \\ P_{\psi_1}(z^{2s}, z^{A(0)}) & P^{(1)}_{\psi_1}(z^{2s}, z^{A(0)}) & \dots & P^{(k-1)}_{\psi_1}(z^{2s}, z^{A(0)}) \\ \vdots & \vdots & \vdots & \vdots \\ P_{\psi_{k-1}}(z^{2s}, z^{A(0)}) & P^{(1)}_{\psi_{k-1}}(z^{2s}, z^{A(0)}) & \dots & P^{(k-1)}_{\psi_{k-1}}(z^{2s}, z^{A(0)}) \end{vmatrix}. \\ =& (z-z^A)^{(k-1)k/2} W\,, \end{aligned} \quad \text{(F.19)}$$

with W the Wronskian of the Majorana polynomials of the states $|\psi_0\rangle, \dots, |\psi_{k-1}\rangle$. By the degree of the polynomial of $P_z(\Pi)$, the Wronskian is a polynomial of z of degree at most of $2sk-(k-1)k = (2s+1-k)k$. Therefore, every k-plane has an associated polynomial of degree $(2s+1-k)k$.

Bibliography

[1] G. S. Agarwal. Relation between atomic coherent-state representation, state multipoles, and generalized phase-space distributions. *Phys. Rev. A*, 24:2889, 1981.

[2] Y. Aharonov and J. Anandan. Phase change during a cyclic quantum evolution. *Phys. Rev. Lett.*, 58:1593, 1987.

[3] J. P. Amiet and S. Weigert. Coherent states and the reconstruction of pure spin states. *Journal of Optics B: Quantum and Semiclassical Optics*, 1(5):L5, 1999.

[4] J. Anandan. Non-adiabatic non-abelian geometric phase. *Phys. Lett. A*, 133(4–5):171–175, 1988.

[5] J. Anandan. A geometric approach to quantum mechanics. *Foundations of Physics*, 21(11):1265–1284, 1991.

[6] A. Ashtekar and T. Schilling. Geometrical Formulation of Quantum Mechanics. In A. Harvey, editor, *On Einstein's Path*, pages 23–65. Springer, 1999.

[7] M. Aulbach, D. Markham, and M. Murao. The maximally entangled symmetric state in terms of the geometric measure. *New J. Phys.*, 12:073025, 2010.

[8] H. Bacry. Orbits of the rotation group on spin states. *J. Math. Phys.*, 15:1686, 1974.

[9] D. Baguette, T. Bastin, and J. Martin. Multiqubit symmetric states with maximally mixed one-qubit reductions. *Phys. Rev. A*, 90:032314, 2014.

[10] W. Ballmann. *Lectures on Kähler Manifolds*. Cambridge University Press, 2007.

[11] I. Bengtsson and K. Życzkowski. *Geometry of Quantum States (2nd Ed.).* Cambridge Univesrity Press, 2017.

[12] M. V. Berry. Quantal phase factors accompanying adiabatic changes. *Proc. R. Soc. Lond. A*, 392:45–57, 1984.

[13] M. V. Berry and M. Wilkinson. Diabolical points in the spectra of triangles. *Proc. R. Soc. Lond. A*, 392:15–43, 1984.

[14] L. C. Biedenharn and J. D. Louck. *Angular momentum in quantum physics.* Cambridge University Press, 1981.

[15] R. Bijker and F. Iachello. Cluster states in nuclei as representations of a $u(\nu + 1)$ group. *Phys. Rev. C*, 61:067305, 2000.

[16] R. Bijker and F. Iachello. *Phys. Rev. Lett.*, 112:152501, 2014.

[17] G. Björk, M. Grassl, P. de la Hoz, G. Leuchs, and L. L. Sánchez-Soto. Stars of the quantum universe: extremal constellations on the Poincaré sphere. *Phys. Scr.*, 90:108008, 2015.

[18] F. *et al* Bouchard. Quantum metrology at the limit with extremal majorana constellations. *Optica*, 4(12), 2017.

[19] D. C. Brody and L. P. Hughston. Geometric quantum mechanics. *J. Geom. Phys.*, 38:19, 2000.

[20] P. Bruno. Quantum geometric phase in majorana's stellar representation: Mapping onto a many-body aharonov-bohm phase. *Phys. Rev. Lett.*, 108:240402, 2012.

[21] Brody D C, Gustavsson A C T, and Hughston L P. Entanglement of three-qubit geometry. *J. Phys. Conf. Ser.*, 67:010244, 2007.

[22] L. Cambell and W. Garnett. *The Life of James Clerk Maxwell.* Adamant Media Corporation, 2001.

[23] L. Chen, M. Aulbach, and M. Hajdušek. Comparison of different definitions of the geometric measure of entanglement. *Phys. Rev. A*, 89:042305, 2014.

[24] C. Chryssomalakos and H. Hernández-Coronado. Optimal quantum rotosensors. *Phys. Rev. A.*, 95:052125, 2017.

[25] P. de la Hoz, A. B. Klimov, Y.-H. Kim, C. Müller, Ch. Marquardt, G. Leuchs, and L. L. Sánchez-Soto. Multipolar hierarchy of efficient quantum polarization measures. *Phys. Rev. A*, 88:063803, 2013.

[26] J D Dollard and C N Friedman. *Product Integration with Application to Differential Equations.* Cambridge Press, 1984.

[27] W. Dür, G. Vidal, and J. I. Cirac. Three qubits can be entangled in two inequivalent ways. *Phys Rev A*, 62:062314, 2000.

[28] A. Eremenko and A. Gabrielov. Degrees of real wronski maps. *Discrete Comput. Geom.*, 28:331–347, 2002.

[29] R. Ohmann et al. Supramolecular rotor and translator at work: On-surface movement of single atoms. *ACS Nano*, 9(8):8394–8400, 2015.

[30] U. G. E. Perera et al. Controlled clockwise and anticlockwise rotational switching of a molecular motor. *Nat. Nanotechnol.*, 8:46–51, 2013.

[31] Y. Zhang et al. Simultaneous and coordinated switching of all molecular rotors in a network. *Nat. Nanotechnol.*, 11:706–712, 2016.

[32] P. Mathonet etal. Entanglement equivalence of n-qubit symmetric states. *Phys. Rev. A*, 81:052315, 2010.

[33] M H Freedman, A Kitaev, M J Larsen, and Zhenghan Wang. Topological quantum computing. *Bull. Am. Math. Soc.*, 20:31–38, 2001.

[34] W. Ganczarek, M. Ku, and K. Życzkowski. Barycentric measure of quantum entanglement. *Phys. Rev. A*, 85(3):032314, 2012.

[35] J.-P. Gazeau. *Coherent States in Quantum Physics.* Wiley-VCH Press, 2009.

[36] H. Georgi. *Lie Algebras in Particle Physics.* The Benjamin/Cummings Publishing Company, 1982.

[37] R. M. Gingrinch. Properties of entanglement monotones for three-qubit pure states. *Phys. Rev. A*, 65:052302, 2002.

[38] O. Giraud, D. Braun, D. Baguette, T. Bastin, and J. Martin. Tensor representation of spin states. *Phys Rev Lett*, 114:080401, 2015.

[39] A. Guichardet. On rotation and vibration motions of molecules. *Ann. Inst. H. Poincaré, Phys. Theor.*, 40/3:329–342, 1984.

[40] B. C. Hall. *Lie Groups, Lie Algebras, and Representations: An Elementary Introduction.* Graduate Texts in Mathematics, Springer, 2nd ed. edition.

[41] M. Halpern. Field-strength and dual variable formulations of gauge theory. *Phys. Rev. D*, 19/2:517–530, 1979.

[42] G. Herzberg and H. C. Longuet-Higgins. Intersection of potential energy surfaces in polyatomic molecules. *Discuss. Faraday Soc.*, 35:77–82, 1963.

[43] H. Heydari. Geometrical structure of entangled states and the secant variety. *Quantum Inf. Process.*, 7(1):43, 2008.

[44] F. Holweck, J.-G. Luque, and J.-Y. Thibon. Geometric descriptions of entangled states by auxiliary varieties. *J. Math. Phys.*, 53:102203, 2012.

[45] R. Hubener, M. Kleinmann, T.-C. Wei, C. González-Guillén, and O. Gühne. Geometric measure of entanglement for symmetric states. *Phys. Rev. A*, 80:032324, 2009.

[46] Bengtsson I, Brännlund J, and Życzkowski K. $\mathbb{C}P^n$, or, entanglement illustrated. *Int. J. Mod. Phys. A*, 17:4675, 2002.

[47] T. Iwai. A representation of the Guichardet connection in the Aharonov-Anandan connection. *Phys. Lett. A*, 162:289–293, 1992.

[48] E. Deumens J. A. Morales and Y. Öhrn. On rotational coherent states in molecular quantum dynamics. *J. Math. Phys.*, 40(2).

[49] T. R. Kane and M. P. Scher. A dynamical explanation of the falling cat phenomenon. *Int. J. Solids Struct.*, 5:663–670, 1969.

[50] H. A. Kastrup. Quantization of the canonically conjugate pair angle and orbital angular momentum. *Phys. Rev. A*, 73:052104, 2006.

[51] H. A. Kastrup. Wigner functions for the pair angle and orbital angular momentum. *Phys. Rev. A*, 94:062113, 2016.

[52] H. A. Kastrup. Wigner functions for angle and orbital angular momentum: Operators and dynamics. *Phys. Rev. A*, 95:052111, 2017.

[53] S. Kobayashi and K. Nomizu. *Foundations of Differential Geometry II*. J. Wiley, 1969.

[54] G. S. Kottas, L. I. Clarke, D. Horinek, and Josef Michl. Artificial molecular rotors. *Chem. Rev.*, 105:1281–1376, 2005.

[55] M. Kuś and K. Życzkowski. Geometry of entangled states. *Phys. Rev. A*, 63:032307, 2001.

[56] A. R. Kuzmak. Quantum state geometry and entanglement of two spins with anisotropic interaction in evolution. *J. Geom. Phys.*, 116:81–89, 2017.

[57] A. R. Kuzmak and V. M. Tkachuk. Geometry of a two-spin quantum state in evolution. *J. Phys. A*, 49:045301, 2016.

[58] L. D. Landau and E. M. Lifshitz. *Quantum Mechanics*. Pergamon Press, 1981. Third edition.

[59] S. Lang. Old and new conjectured diophantine inequalities. *Bulletin of the American Mathematical Society*, 23(1):37–75, 1990.

[60] R. G. Littlejohn, K. A. Mitchell, M. Reinsch, V. Aquilanti, and S. Cavalli. Body frames and frame singularities for three-atom systems. *Phys. Rev. A*, 58/5:3705–3717, 1998.

[61] R. G. Littlejohn, K. A. Mitchell, M. Reinsch, V. Aquilanti, and S. Cavalli. Internal spaces, kinematic rotations, and body frames for four-atom systems. *Phys. Rev. A*, 58/5:3718–3738, 1998.

[62] R. G. Littlejohn and M. Reinsch. Internal or shape coordinates in the n-body problem. *Phys. Rev. A*, 52(3):2035–2051, 1995.

[63] R. G. Littlejohn and M. Reinsch. Gauge fields in the separation of rotations and internal motions in the n-body problem. *Rev. Mod. Phys.*, 69/1:213–275, 1997.

[64] R.G. Littlejohn and K. A. Mitchell. Gauge theory of small vibrations in polyatomic molecules. In Paul Newton, Philip Holmes, and Alan Weinstein, editors, *Geometry, Mechanics, and Dynamics*, pages 407–428. Springer New York, 2002.

[65] Y Liu, A Roy, and M Stone. Non-abelian berry transport, spin coherent states, and majorana points. *J. Phys. A: Math. Theor.*, 45:135304, 2012.

[66] E Majorana. Atomi orientati in campo magnetico variabile. *Nuovo Cimento*, 9:43, 1932.

[67] A. Mandilara, T. Coudreau, A. Keller, and P. Milman. Entanglement classification of pure symmetric states via spin coherent states. *Phys Rev A*, 90:050302, 2014.

[68] D. J. Marín-Lámbarri, R. Bijker, M. Freer, M. Gai, T. Kokalova, D. J. Parker, and C. Wheldon. Evidence for triangular d_{3h} symmetry in ^{12}C. *Phys. Rev. Lett.*, 113:012502, 2014.

[69] J. Martin, O. Giraud, P. A. Braun, D. Braun, and T. Bastin. Multiqubit symmetric states with high geometric entanglement. *Phys. Rev. A*, 81:062347, 2010.

[70] R. C. Mason. *Diophantine equations over function fields*, volume 96 of *London Math. Soc. Lecture Notes Series*. Cambidge University Press, 1984.

[71] R. C. Mason. Equations over function fields. In H. Jager, editor, *Number Theory, Noordwijkerhout 1983*, volume 1068 of *Lecture Notes in Mathematics*, pages 149–157. Springer, 1984.

[72] C. A. Mead. The geometric phase in molecular systems. *Rev. Mod.Phys.*, 64/1:51–85, 1992.

[73] C. A. Mead and D. G. Truhlar. On the determination of born-oppenheimer nuclear motion wave functions including complications due to conical intersections and identical nuclei. *J. Chem. Phys.*, 70:2284–2296, 1979.

[74] A. Miyake. Classification of multipartite entangled states by multidimensional determinants. *Phys. Rev. A*, 67:012108, 2003.

[75] R. Montgomery. Gauge theory of the falling cat. *Fields Inst. Commun.*, 1:193–218, 1993.

[76] R. Montgomery. The geometric phase of the three-body problem. *Nonlinearity*, 9:1341–1360, 1996.

[77] D. J. Moore. Non-adiabatic berry phase for periodic hamiltonians. *J. Phys. A*, 23:2049–2054, 1990.

[78] R. Mosseri and R. Dandoloff. Geometry of entangled states, Bloch spheres and Hopf fibrations. *J. Phys. A*, 34:10243, 2001.

[79] N. Mukunda and R. Simon. Quantum kinematic approach to the geometric phase. i. general formalism. *Ann. Phys.*, 228(2):205–268, 1993.

[80] R Pereira and C Paul-Paddock. Anticoherent subspaces. *Jour. Math. Phys.*, 58:062107, 2017.

[81] A. Perelomov. *Generalized Coherent States and Their Applications*. Springer Verlag, 1986.

[82] J. M. Radcliffe. Some properties of coherent spin states. *J. Phys. A: Gen. Phys.*, 4:313–324, 1971.

[83] P. Ribeiro, J. Vidal, and R Mosseri. Exact spectrum of the lipkin-meshkov-glick model in the thermodynamic limit and finite-size corrections. *Phys. Rev. E*, 78:021106, 2008.

[84] J. M. Robbins and M. V. Berry. A geometric phase for m=0 spins. *J. Phys. A*, 27:L435–L438, 1994.

[85] J. J. Sakurai. *Modern Quantum Mechanics (Revised Edition)*. Addison-Wesley, 1994.

[86] J. Samuel and R. Bhandari. General setting for berry's phase. *Phys. Rev. Lett.*, 60:2339, 1988.

[87] M. Sanz, I. L. Egusquiza, R. Di Candia, H. Saberi, L. Lamata, and E. Solano. Entanglement classification with matrix product states. *Scientific Reports*, 6:30188, 2016.

[88] I Scherbak. Gaudin's model and the generating function of the wronski map. *arXiv:math/0309002*.

[89] T. Schilling. *Geometry of Quantum Mechanics*. PhD thesis, The Pennsylvania State University, 1996.

[90] A. Shapere and F. Wilczek. Gauge kinematics of deformable bodies. *Am. J. Phys.*, 57:514–518, 1989.

[91] B. Simon. Holonomy, the quantum adiabatic theorem, and berry's phase. *Phys. Rev. Lett.*, 51:2167, 1983.

[92] A. Tachibana and T. Iwai. Complete molecular hamiltonian based on the born-oppenheimer adiabatic approximation. *Phys. Rev. A*, 33/4:2262–2269, 1986.

[93] L. R. Turner. Inverse of the Vandermonde matrix with applications. *Nasa Technical Note D-3547*, 1966.

[94] D.A. Varshalovich, A.N. Moskalev, and V.K. Khersonskii. *Quantum Theory of Angular Momentum*. World Scientific, 1988.

[95] T. Wei and P. M. Goldbart. Geometric measure of entanglement and applications to bipartite and multipartite quantum states. *Phys. Rev. A*, 68:042307, 2003.

[96] F Wilczek and A Zee. Appearance of gauge structure in simple dynamical systems. *Phys. Rev. Lett.*, 52:2111–2114, 1984.

[97] F. Zak. *Tangents and Secants of Algebraic Varieties*, volume 127. AMS Translations of mathematical monographs, 1993.

[98] P Zanardi and M Rasetti. Holonomic quantum computing. *Phys. Lett. A*, A264:94–99, 1999.

[99] J. Zimba. Anticoherent spin states via the Majorana representation. *EJTP*, 3(10):143–156, 2006.